Metal Abundances and Ionization in QSO Intrinsic Absorbers

Fred Hamann
Center for Astrophysics and Space Sciences
University of California, San Diego; La Jolla, CA 92093-0111
Internet: fhamann@ucsd.edu

ABSTRACT

This paper provides a general reference for deriving the ionizations and metal abundances for absorption-line clouds in photoionization equilibrium with a QSO spectrum. The results include a quantitative assessment of the theoretical uncertainties and firm lower limits on the metallicities when no ionization constraints are available. The calculations applied to the best available column densities for QSO intrinsic absorbers support previous studies; there is strong evidence for super-solar metallicities in broad absorption line (BAL) and at least some "associated" ($z_a \approx z_e$) absorption regions. Even in cases where the level of ionization is unknown (for example, when only H I and C IV lines are measured), firm lower limits on the metal abundances (C/H) imply $Z \gtrsim Z_\odot$ for typical BALs and some $z_a \approx z_e$ absorbers. These results support the independent evidence for high metallicities in QSO broad emission-line regions. I argue that high gas-phase abundances, up to $\sim$10 $Z_\odot$, can be expected in QSOs due to the normal enrichment by stars in the cores of young, massive ($\gtrsim 10^{11}$ $M_\odot$) galaxies.

The measured column densities in intrinsic absorbers also indicate that the gas is usually optically thin in the H I Lyman continuum out to energies above at least the C IV and N V ionization edges (i.e. $\gtrsim$100 eV). The column density ratios often require a range of ionization states in the same absorber. Neighboring $z_a \approx z_e$ systems (having similar redshifts and often blended spectroscopically) also usually require different ionizations or metal abundances. If the abundances are similar in neighboring systems, their ionization parameters must sometimes differ by more than an order of magnitude, requiring a significant range of densities and/or distances from the ionizing QSO. These result, and the overall levels of ionization, are not consistent with single-zone models of the UV line and X-ray continuum ("warm") absorbers.

Subject headings: Galaxies: abundances — Galaxy evolution — Quasars: absorption lines — Quasars: general

1. INTRODUCTION

Metal absorption lines in QSO spectra are important probes of galactic evolution and star formation at redshifts up to $z \sim 5$. Most studies have emphasized the cosmologically intervening systems, with redshifts much less than the QSO emission redshift ($z_a \ll z_e$), as probes of extended structures such as galactic halos and (perhaps) the disks of young spiral galaxies. However, if QSOs reside in galactic nuclei, there is also the possibility of probing galactic nuclear environments by measuring absorption (and emission) lines that form physically close to the QSOs. Such "intrinsic" features could yield information about galactic nuclear evolution that is not available by other means.

Intrinsic absorbers include the broad absorption lines (BALs) and any of the so-called associated ($z_a \approx z_e$) metal line systems that are physically related to QSOs or active galactic nuclei (AGNs). BALs are understood as forming in high velocity outflows that reach up to $\sim 0.1c$ within $\sim$1 kpc of radio-quiet QSOs (Turnshek 1988; Weymann *et al.* 1985 and 1991; Stocke *et al.* 1992; Hamann, Korista & Morris 1993; Barlow *et al.* 1992; Barlow 1993). The $z_a \approx z_e$ systems have much narrower lines and could have a variety of origins (Weymann *et al.* 1979). The standard definition of $z_a \approx z_e$ lines in QSOs has been that they appear within several thousand km s^{-1} of the emission redshift and are less than a few hundred km s^{-1} wide (cf. Weymann *et al.* 1979; Foltz *et al.* 1988; Anderson *et al.* 1987). Some $z_a \approx z_e$ systems meeting these criteria might reside in external galaxies, like intervening $z_a \ll z_e$ absorbers, while others are physically close to the QSOs. Direct evidence for a close physical relationship has come from time-variable line strengths. For example, in two QSOs, UM 675 ($z_e = 2.15$; Hamann *et al.* 1995a) and Q2343+125 ($z_e = 2.515$; Hamann, Barlow & Junkkarinen 1996a), the variability timescales imply minimum space densities above several times 10^3 cm^{-3} and maximum distances of $\sim$1 kpc from the ionizing continuum source. More dramatic time-variability, requiring larger densities and smaller distances, appears to be common in the absorption lines of Seyfert 1 galaxies (Ulrich 1988; Voit, Shull & Begelman 1987; Shull & Sachs 1993; Kriss *et al.* 1995; Koratkar *et al.* 1996; Maran *et al.* 1996). Further evidence for the intrinsic nature of $z_a \approx z_e$ lines in QSOs has come, ofr example, from observations of (1) partial coverage of the background emission source(s) (well resolved, optically thick lines with too-shallow absorption troughs; Wampler, Bergeron & Petitjean 1993; Petitjean, Rauch & Carswell 1994; Hamann, Barlow & Junkkarinen 1996; Hamann *et al.* 1997a and 1997b; Barlow *et al.* 1996), and (2) smooth and relatively broad line profiles (up to a few hundred km s^{-1} FWHM) that are markedly different from the narrow, often multi-component intervening systems (Blades 1988; Hamann *et al.* 1997a and 1997b; Barlow *et al.* 1996).

Some recent studies also indicate that intrinsic absorbers are generically metal rich, with metallicities often above solar (Wampler *et al.* 1993; Møller, Jakobsen & Perryman 1994; Petitjean *et al.* 1994; Savaglio *et al.* 1994; Hamann *et al.* 1995a and 1997b; Tripp *et al.* 1996; Turnshek *et al.* 1996; Korista *et al.* 1996). These high metallicities are

significantly larger than the intervening systems (where typically $Z \lesssim 0.1$ $Z_\odot$; Bergeron 1988; Pettini *et al.* 1994), but they are consistent with recent estimates of $Z \gtrsim Z_\odot$ in the broad emission line regions of QSOs (Hamann & Ferland 1992 and 1993; Ferland *et al.* 1996; Hamann & Korista 1996). Testing the high-Z results is important because of the possible implications for chemical enrichment and galaxy/structure formation in the early universe (Hamann & Ferland 1993; §5.1 below).

Here I present a general theoretical reference for deriving ionizations and metal abundances in intrinsic absorbers, with a quantitative assessment of the uncertainties. I assume the column densities are accurately measured (or constrained) from the absorption line data. Accurate column densities are already available for a few bright QSOs, but the spectroscopy now underway with the Keck 10 m telescope and soon to follow from new 8 m class telescopes – providing resolutions comparable to the thermal line widths – will yield accurate column densities for a large number of sources. These improvements in the data warrant a more thorough examination of the theoretical uncertainties. The work presented here builds on previous studies such as Bergeron & Stasińska (1986), Chaffee *et al.* (1986), Steidel (1990) and Petitjean, Bergeron & Puget (1992).

The abundance of any metal relative to hydrogen can be derived from the equation,

$$\left[\frac{\mathrm{M}}{\mathrm{H}}\right] \;=\; \log\left(\frac{N(\mathrm{M}_i)}{N(\mathrm{HI})}\right) \;+\; \log\left(\frac{f(\mathrm{HI})}{f(\mathrm{M}_i)}\right) \;+\; \log\left(\frac{\mathrm{H}}{\mathrm{M}}\right)_\odot \qquad (1)$$

where $(\mathrm{H/M})_\odot$ is the solar abundance ratio, and N and f are respectively the column densities and ionization fractions of H I and the metal M in ion state i. Table 1 lists several solar abundance ratios from Grevesse & Anders (1989) for convenience. This paper will focus on the ionization corrections, $f(\mathrm{HI})/f(\mathrm{M}_i)$. The equality holds in Eqn. 1 only if the ionization correction applies in an average sense to the entire absorbing region. However, the correction factors – in this and all previous studies – derive from one-zone calculations. Actual absorbers can have multiple absorbing zones and a range of ionization states in the same system. (I will argue in §§4 and 5.2 that this is, in fact, often the case.) The H I line(s) can form partly, or exclusively, in regions that do not overlap with a given M_i, and the column density of H I in the M_i zone can be much less than the measured value of $N(\mathrm{HI})$. Therefore, $f(\mathrm{HI})/f(\mathrm{M}_i)$ ratios that are appropriate for particular M_i zones yield only lower limits to [M/H].

Relative abundances among the metals can also be potent diagnostics of the enrichment mechanism(s) and overall metallicity. For example, the recent reports of extremely high phosphorus abundances in BALQSOs, $[\mathrm{P/C}] \gtrsim 1.8$ (Turnshek 1988; Junkkarinen *et al.* 1995), if confirmed, would clearly signify some form of non-standard enrichment (Shields 1996). The abundance of nitrogen relative to other metals, e.g. oxygen, can provide an independent measure of the overall metallicity because, for standard galactic enrichment, N/O is expected to pass from sub-solar to super-solar as the overall metallicity increases beyond solar (Wheeler, Sneden & Truran; Hamann & Ferland 1993). This behavior is

due to "secondary" CNO processing in stellar envelopes, which causes the N abundance to grow like $\sim Z^2$ instead of Z – at least at high metallicities (see Hamann & Ferland 1993; Vila-Costas & Edmunds 1993). Relative metal abundances can be derived from the following analog to Eqn. 1,

$$\left[\frac{a}{b}\right] \;=\; \log\left(\frac{N(a_i)}{N(b_j)}\right) \;+\; \log\left(\frac{f(b_j)}{f(a_i)}\right) \;+\; \log\left(\frac{b}{a}\right)_{\odot} \qquad (2)$$

where a_i and b_j represent metals a and b in ionization stages i and j, respectively.

Abundance ratios derived from Eqns. 1 and 2 can be very uncertain if one is forced to invoke large (and uncertain) ionization corrections. For example, metallicity estimates for intrinsic absorbers often require large correction factors to compare H I to the multiply-ionized metals. If the absorbing clouds are photoionized by the QSO/AGN continuum, the uncertainties are due mainly to the unknown shape and intensity of the ionizing spectrum at UV through soft X-ray wavelengths. The recent work by Korista *et al.* (1996) on the BALQSO 0226–104 demonstrates the importance of spectral shape considerations. Here I explore a wide range of spectral shapes consistent with observations. I then use the results to analyze (or reanalyze) some of the best published data and test the robustness of recent high-metallicity estimates. I will show that there is strong evidence for super-solar metallicities, even in some cases where the level of ionization is unknown.

Section 2 describes the calculations and assumptions. Section 3 presents an array of results in the form of diagnostic diagrams. Section 4 applies the results to several well-measured $z_a \approx z_e$ and BAL systems. Section 5 provides a summary and a brief discussion of the implications.

2. CALCULATIONS AND ASSUMPTIONS

I assume the absorbing gas is photoionized by the continuous radiation from the QSO/AGN, and I use the computer code CLOUDY (version 90.01; Ferland 1996) to calculate equilibrium ionization fractions under various conditions. The calculations assume static, plane parallel, constant density clouds illuminated on one face. The radiative intensity is specified by the ionization parameter U – defined as the dimensionless ratio of $\lambda \leq 912$ Å photon to hydrogen space densities at the illuminated face of the clouds. The hydrogen space density is fixed at $n_e = 10^8$ cm^{-3} in all cases, although previous model experiments show that the ionization at a given U is essentially the same for densities between 10^{-2} and 10^{11} cm^{-3} (Hamann *et al.* 1995a). I assume there is no dust extinction in the absorption line regions or along the line of sight between the absorbers and the continuum source.

2.1. Ionizing Continuum Shapes

Spectra of QSOs and AGNs at optical through UV wavelengths can be characterized by a power law ($F_\nu \propto \nu^\alpha$) with typical indices of $\alpha \approx -0.3$ to -0.7 (cf. Sanders *et al.* 1989; O'Brian, Gondhalekar & Wilson 1989; Sargent, Steidel & Boksenberg 1989; Francis *et al.* 1991). The flux must decline more sharply between the UV and soft X-rays in order to account for the observed UV to X-ray flux ratios. (In particular, the measured values of the power law index α_{ox} (defined below) are typically more negative than α across the optical-UV; see Wilkes *et al.* 1994; Avni, Worrall & Morgan 1995.) However, the poor or altogether lacking constraints on QSO/AGN spectra at these important energies (between roughly 10 and 500 eV, where the ionization thresholds of important ions appear) imply that there are unavoidable uncertainties in most [M/H] determinations (particularly those requiring a comparison between H I and multiply-ionized metals).

I use four formulations, which I call A, B, C and PL, to explore a wide range of continuum shapes consistent with QSO/AGN observations. PL is a single power law with a freely varied slope. A, B and C (described mathematically in the Appendix) are segmented power laws with two free parameters describing the spectral shape between the UV and soft X-rays. The first parameter is α_{ox}, which is the two-point power law index ($F_\nu \propto \nu^{\alpha_{ox}}$) between 2500 Å and 2 keV. The definition of α_{ox} can be written,

$$\frac{F_\nu(2\mathrm{keV})}{F_\nu(2500\text{Å})} = 403.3^{\alpha_{ox}} \tag{3}$$

Note that this definition avoids the implicit minus sign used in most previous work (Zamorani *et al.* 1981). The second free parameter is the characteristic temperature T_c (for continuum A) or energy E_c (for B and C) where the UV spectrum gives way to a steeper decline toward the X-rays. Figure 1 plots the A, B and C continua for a range of these parameters. The figure also shows for comparison (dotted lines) the generic AGN spectrum derived by Mathews & Ferland (1987, hereafter MF87), with an added change in slope at 0.125 eV ($\sim$10 μm) to decrease the long wavelength flux. Hereafter I will use the notation A(log T_c, α_{ox}), B(log E_c, α_{ox}) and C(log E_c, α_{ox}), with T_c in K and E_c in eV, to indicate the continuum type (A, B, or C) and the specific parameters used. For example, the bold solid curves in Figure 1 represent the fiducial cases A(5.7,−1.6), B(1.4,−1.6) and C(1.4,−1.6).

The bottom right-hand panel in Figure 1 (D) shows the MF87 and fiducial A, B and C continua after transmission through a column of highly ionized gas – having ionization parameter $U = 15$, total column density log $N_H = 22.5$ cm^{-2}, and solar elemental abundances. The transmitted spectra show absorption in soft X-rays due mainly to bound-free transitions of O VII and O VIII at $\sim$0.8 keV. This type of absorption is characteristic of the so-called "warm" absorbers that appear to be common in Seyfert galaxy spectra (Halpern 1984; Nandra & Pounds 1994; George *et al.* 1996). The correlated presence of X-ray warm absorbers and $z_a \approx z_e$ UV line absorbers in the majority of Seyferts and a few QSOs (Mathur 1994; Mathur *et al.* 1994; Mathur *et al.* 1995a and 1995b; George

et al. 1995; Kriss *et al.* 1995; Maran *et al.* 1996; Kriss *et al.* 1996a and 1996b; Crenshaw 1996) suggests that warm absorbers might lie along the line-of-sight between the continuum source and the UV absorption-line gas. This absorbing geometry also appears in some recent dynamical models of BAL and $z_a \approx z_e$ outflows (Murray *et al.* 1995). I will refer to the transmitted spectra in Fig. 1D as AT, BT and CT, with the shape parameters in parenthesis as before.

2.2. Continuum Optical Depths

If the line-absorbing gas is optically thin in the UV through soft X-ray continuum, there will be a single ionization state throughout with the fractions $f(\mathrm{M}_i)$ and ratios $f(\mathrm{HI})/f(\mathrm{M}_i)$ for a given space density depending only on the shape and intensity of the ionizing spectrum. There is no dependence on the column density and very little dependence on the metallicity, as long as both remain low enough to preserve the low continuum optical depths[1]. Most measurements of the column densities (§4 below) in $z_a \approx z_e$ systems and non-Mg II BALs[2] indicate that the continuum optical depths are, in fact, negligibly low. To my knowledge, there are no observations of Lyman limit absorption in (established) intrinsic systems, and the H I column densities derived from the Lyman series lines are usually well below the threshold for optical depth unity at the Lyman edge (i.e. $\log\ N(\mathrm{HI}) < 17.2$ cm^{-2}). The column densities derived from the metal lines are also well below the limits for optically thick absorption at their bound-free edges. (For the most abundant metals, C, N, O and Ne, the $\tau \approx 1$ limits range from $17.5 \lesssim \log\ N(\mathrm{M}_i) \lesssim 16.9$ cm^{-2} for neutral atoms to >18.0 cm^{-2} for highly ionized species; Osterbrock 1989.) Previous photoionization calculations applied to BALs (Weymann *et al.* 1985) show that the continuum optical depths might approach unity at the He II Lyman limit (228 Å). Numerical experiments performed here (§3.3 below) with a variety of continuum shapes confirm that optical depths near unity at the He II edge can occur in clouds with $\log\ N(\mathrm{HI}) \approx 16.5$ cm^{-2}, which is roughly the maximum H I column allowed by most observations. However, even in this extreme case, the marginal He II opacities have no significant effect on the line-of-sight-averaged ionization fractions.

Therefore, unless stated otherwise, the calculations below assume the absorbing gas is optically thin in the continuum at all wavelengths. They also assume that the lines themselves are not significant sources of continuous opacity, even though Korista *et al.*

---

[1]Numerical experiments show that the $f(\mathrm{HI})/f(\mathrm{M}_i)$ ratios for all ions considered here are the same within ∼0.1 dex for $0.01 \le Z \le 10$ Z$_\odot$ and $-3.5 \le \log U \le 1.5$ in optically thin clouds (with the metals scaled in solar proportions). The only deviations larger than this are ∼0.3 and ∼0.2 dex depressions in the ratios involving Si III and Si IV, respectively, at the high Z and low U extremes. I therefore use $Z = 1$ Z$_\odot$ for all calculations in the remainder of this paper.

[2]I do not consider the minority class of BALs having low ionization lines such as Mg II λ2795, because they could have significant optical depths at the H I Lyman edge (Voit, Weymann & Korista 1993).

(1996) noted that the shielding of continuum radiation by BALs might progressively soften the continuum (weaken the far-UV flux) farther from the QSO. I will briefly discuss the effects of larger continuum optical depths in §3.3.

3. RESULTS

The results in this section provide a general reference for deriving ionizations and metal abundances from Eqns. 1 and 2. Applications will be discussed in §4 below. The figures and tables all use the notation C2 for C II, C3 for C III, C4 for C IV, etc., to save space.

3.1. Fully Optically Thin Clouds

Calculations for fully optically thin clouds are widely applicable to intrinsic systems. Figure 2 shows the ionization fractions $f(\mathrm{M}_i)$ and $f(\mathrm{HI})$ at various ionization parameters U for incident spectra given by MF87, single power laws (PL) with $\alpha = -1.0$ and -1.5, and each of the fiducial continua A, B and C from Figure 1. The different continuum shapes can produce significantly different results, even for these nominal cases. For example, the sharp break in continuum B at energy E_c (see Figure 1) produces smaller ionization corrections in C IV and N V compared to the A, C and MF87 continua, while the PL continua produce much larger ionization corrections for highly ionized elements.

Figure 3 shows how different values of T_c and α_{ox} in continuum A affect the ionization fractions, and Figure 4 shows analogous behavior for different E_c and α_{ox} values in continuum C. The results for continuum B (not shown) are similar. One general result is that, for a given level of ionization (i.e. for fixed column density ratios of, for example, C III/C IV or N III/N V), the ionization corrections are larger for larger values of T_c and E_c. This is because the increased far-UV flux shifts the $f(\mathrm{M}_i)$ curves toward lower U where $f(\mathrm{HI})$ is larger. Therefore, adopting continuum shapes with large T_c or E_c leads to larger derived metallicities. For example, a given observed ratio of $N(\mathrm{C\ III})/N(\mathrm{C\ IV}) = 1$ column densities yields $\sim$0.8 dex larger [C/H] for the largest compared to the smallest T_c and E_c values in Figures 3a and 4a. Larger (less negative) values of α_{ox} also favor larger ionization corrections and thus larger metal abundances.

If the measured column densities provide no constraints on the ionization, or if they indicate a range of ionizations, it might be reasonable to assume that each line forms near the peak in its $f(\mathrm{M}_i)$ curve (cf. Hamann *et al.* 1995a). This assumption, in any case, yields conservatively low estimates of [M/H] for moderately ionized metals like C IV and N V because their ionization corrections are nearly minimized at the $f(\mathrm{M}_i)$ peaks (see below). Figures 5 and 6 plot the normalized corrections, $\log(f(\mathrm{HI})/f(\mathrm{M}_i)) + \log(\mathrm{H/M})_\odot$, evaluated at the $f(\mathrm{M}_i)$ peaks for a wide range of continuum A and C shapes. As expected, the

correction factors for highly ionized species are very sensitive to the continuum shape. The corrections are larger for large values of T_c, E_c and α_{ox}, leading to larger derived [M/H] in these cases.

Figure 7 shows that the correction factors for a given continuum shape all reach minimum values at finite U. These minima occur near (but at slightly larger U than) the peaks in the $f(\mathrm{M}_i)$ curves (compare Figs. 2 and 7). Figures 8 and 9 plot the normalized minimum ionization corrections (the quantity $\log(f(\mathrm{HI})/f(\mathrm{M}_i)) + \log(\mathrm{M/H})_\odot$ evaluated at the minimum of $f(\mathrm{HI})/f(\mathrm{M}_i)$) for various continuum A and C shapes. These minimum correction factors can be used with Eqn. 1 to place firm lower limits on [M/H].

Figure 10 shows the normalized ionization corrections needed to derive the relative metal abundances N/C, N/O and P/C from several ionic ratios involving these elements. The quantity plotted for each ionic ratio corresponds to the last two terms in Eqn. 2. The results utilize the same calculations as Figs. 2 -4, for optically thin clouds photoionized by different A and C continuum shapes.

Ideally, one would derive relative metal abundances from ions with similar ionization potentials so that (1) the measured lines form as much as possible in the same gas and (2) the ionization correction is small and insensitive to the uncertain spectral shape and intensity. Figure 10 shows that, among the more readily measured column densities, N III/C III provides the most reliable indicator of the relative nitrogen abundance. The figure also shows that there is a minimum ionization correction for P V/C IV, which can be used to place firm lower limits on the P/C abundance.

3.2. Fully Optically Thin Clouds Shielded by a Warm Absorber

If an X-ray warm absorber lies between the line-absorbing clouds and the QSO/AGN continuum source, the incident spectra could resemble the curves plotted in Figure 1D. The left-hand panel in Figure 11 shows the ionization fractions in optically thin clouds irradiated by the transmitted continuum CT(1.4,−1.6). (The ionization state of the warm absorber and its possible contribution to the UV absorption lines are discussed in §§3.3 and 5.2 below.) The intervening warm absorber depresses the flux incident on the UV-line clouds at soft X-ray wavelengths and thus alters the ionization fractions for highly ionized species such as Mg X, Ne VIII, O VIII, O VII and, to a lesser extent, O VI. However, the intervening warm absorber does not substantially alter the $f(\mathrm{HI})/f(\mathrm{M}_i)$ ratios for lower ionization metals, including C IV and N V. Therefore, one could still use the results from §3.1 for most abundance determinations.

3.3. Marginally Optically Thick/Warm Absorber Clouds

Another possibility is that the UV lines form within the X-ray warm absorber itself (Mathur *et al.* 1994; Mathur 1994; Mathur *et al.* 1995a and 1995b). Column densities derived from observed UV absorption lines generally require low continuum optical depths at the ionization thresholds of H I and the low- to moderate-ionization metals (up to at least the C IV and N V; §2.2 and §4 below). But the data do not directly constrain the opacities due to He I and He II, and they do not rule out significant opacities in the soft X-rays due to highly ionized metals. (The measured low Ne VIII column density in the QSO UM 675 is a notable exception; see Hamann *et al.* (1995a) and §5.2 below.) If the line-forming gas has significant continuum opacities anywhere across the UV through soft X-ray spectrum, there can result a range of ionization states in one-zone environments with the amount of low-ionization material depending on the total column density. This one-zone, multi-state situation can yield very different ionization corrections from the fully optically thin cases described above.

The right-hand side of Figure 11 shows the mean ionization fractions for clouds having roughly the maximum continuum optical depths allowed by observations (§2.2). The specific parameters for this calculation are an optical depth at the H I Lyman limit of $\tau_{LL} \leq 0.2$ (or equivalently log $N(\mathrm{HI}) \leq 16.5$ cm^{-2}), a total hydrogen column density of log $N_H \leq 22.0$ cm^{-2}, and solar abundances. The upper limit on τ_{LL} keeps the clouds from becoming "cold" absorbers at low U, which would contradict the low column densities measured for H I and the low- to moderate-ionization metals (§2.2). The $\tau_{LL} \leq 0.2$ requirement is enforced by truncating the total column density at log $N_H < 22.0$ cm^{-2} if necessary. These low-U clouds are not warm absorbers. They have low optical depths at all wavelengths, except at the He II Lyman limit where they reach optical depths up to unity. At high ionizations (log $U \gtrsim 0.0$), the full column of log $N_H = 22.0$ cm^{-2} is realized and the clouds become warm absorbers with considerable soft X-ray opacity. These high-U calculations encompass the warm absorber models described by Mathur and collaborators.

The ionization fractions in Figure 11 differ from the fully optically thin results only for the highly ionized metals in high-U clouds, i.e. in the warm absorber regime (compare to Fig. 2b). The H I and low- to moderately-ionized metals are unaffected by the finite column densities because the gas is still required to be optically thin at most UV through far-UV wavelengths. Therefore, as in §3.2, one can still use the fully optically thin results to derive abundances from these ions.

3.4. Two Minor Cautions

Before applying the results above to actual data, I note two minor points of caution. First, the ionization state of the gas could be out of equilibrium with the radiation field

if the intensities vary significantly on timescales comparable to, or shorter than, the recombination times. Krolik & Kriss (1995) showed that non-equilibrium effects can occur in low density gas, $n_e \lesssim 10^6$ cm^{-3}, near rapidly varying Seyfert 1 galaxies. I have ignored this complication because the spectral variations in luminous QSOs should have much lower amplitudes than the Seyferts (Christiani *et al.* 1996), and because the densities in at least the BAL regions should be higher than $\sim 10^6$ cm^{-3} (Turnshek 1988; Weymann *et al.* 1985; Barlow *et al.* 1992; Barlow 1993). Furthermore, if the ionization does lag behind changes in the continuum flux, the ionization state at any epoch represents an average over the recent spectral variations (see Krolik & Kriss 1995 for discussion). Therefore the calculations here can be interpreted as averages over the spectral and ionization fluctuations.

Second, some of the highest ionization clouds depicted in the figures above are unstable to changes in the gas pressure. Instabilities can occur for gas temperatures $T_e > 10^5$ K (cf. Field 1965; Gehrels & Williams 1993), but the ranges in U for instability depend on the shape of the ionizing spectrum. For an incident MF87 continuum, the gas is unstable for $1.5 \lesssim \log\ U \lesssim 1.8$ and $2.2 \lesssim \log\ U \lesssim 2.5$ (Hamann *et al.* 1995b; see also Kallman & Mushotzky 1985; Netzer 1990; Marshall *et al.* 1993; and Krolik & Kriss 1995). The temperatures and ionizations inferred generally for BAL and $z_a \approx z_e$ regions are well below these unstable regimes (also Netzer 1996).

4. APPLICATIONS: METAL ABUNDANCES IN QSOs

Here I use the calculations for optically thin, unshielded clouds (§3.1) to estimate [M/H] from the best published column densities for BAL and $z_a \approx z_e$ systems. I consider a range of continuum shapes consistent with the observations of each QSO and use those ranges to derive theoretical uncertainties. Table 2 lists the sources, their emission redshifts, the type of absorption system (BAL or $z_a \approx z_e$), and the adopted spectral parameters for continua A and C. Usually no observational constraints are available on the far-UV continua. I therefore adopt $\log T_c = 5.7^{+0.3}_{-0.5}$ for continuum A and $\log E_c = 1.4^{+0.5}_{-0.3}$ for continuum C, unless noted otherwise below. Values of T_c and E_c outside of these ranges are unlikely because they would violate most QSO/AGN observations at UV and X-ray wavelengths. (The resulting spectra would either decline to steeply toward higher energies across the optical-UV [small T_c and E_c] or rise too steeply toward lower energies in X-rays, producing too-large soft X-ray excesses [large T_c and E_c]; see §2.1 and the Appendix for references to observations). If no measurements of α_{ox} are available, I use the redshifts and optical magnitudes (from Hewitt & Burbidge 1993) to estimate α_{ox} from the luminosity–α_{ox} relation given by Wilkes *et al.* (1994, their equations 6 and 12; see also Avni *et al.* 1995). In those cases, I adopt uncertainties of ± 0.2 for α_{ox} based on the measured scatter among QSOs of a given luminosity (Avni *et al.* 1995).

The abundance results are summarized in Table 3 and in the notes on individual

systems below. For each system, Table 3 lists the absorption redshift, the velocity (Δv in km s^{-1}) relative to the emission redshift (for $z_a \approx z_e$ systems only), the measured column densities in H I (log N(HI) in cm^{-2}) and each metal ion (log N), and three pairs of [M/H] and U results. The first two [M/H]–U pairs are the best estimates of these quantities for clouds ionized by continua A and C respectively, with U defined whenever possible by column density ratios such as C II/C III/C IV, N III/N V, Al II/Al III or Si II/Si III/Si IV. When no firm constraints on U are available, or when different constraints yield significantly different U values, I assume the lines form at the peaks in their $f(\mathrm{M}_i)$ curves and derive [M/H] from Figures 5 and 6. This assumption is invoked for the majority of systems in the table, as indicated by a 'p' in the third column. It yields conservatively low [M/H] values for moderately ionized metals like C IV and N V because the ionization corrections are near their minima at the $f(\mathrm{M}_i)$ peaks (e.g. compare Figs. 5 and 8 in §3.1). Even in cases where U is well-constrained by one or more column density ratio, the [M/H] in Table 3 are probably often underestimates, particularly for C IV, N V and more highly ionized species, because only some of the measure H I will reside with each metal ion in multi-phase absorbers (§1 and §5.1 below).

The last [M/H]–U pair in Table 3 indicates the absolute minimum metal abundance, $[\mathrm{M/H}]_{min}$, and corresponding U_{min} for ionization by continuum C (from Figure 9). The results for continuum A (not listed) are similar. These minimum abundances apply for *any* single- or multi-phase medium photoionized by continuum C (see §3.1). The uncertainties listed for all of the [M/H]–U pairs show the range of values allowed by the range of continuum shapes in Table 2. The uncertainties in the measured column densities (when available from the literature) are also listed in Table 3 (in column 1), but they are not included in the [M/H]–U estimates. Please see the references cited below for more information on the measurement uncertainties.

4.1. Notes on Individual $z_a \approx z_e$ Systems

4.1.1. Q 0000−263

Bechtold *et al.* (1994) derive $\alpha_{ox} \approx -1.85$ for this QSO based on UV and X-ray observations separated by three months. The figures in Bechtold *et al.* reveal an unusually steep UV spectrum with $\alpha_{uv} \sim -1.6$ to -2.0 between roughly ∼2400 and ∼900 Å in the rest frame. I therefore adopt low values of T_c and E_c, with uncertainties that encompass the wide range of shapes still permitted in the far-UV. The column densities in Table 3 are from Savaglio *et al.* (1994). The ratio of Si III/Si IV columns defines the ionization parameter in the two highest redshift systems. There is strong evidence for [M/H] $\gtrsim 0.0$ in three of the eleven systems: $z_a = 4.1270$, 4.1323 and 4.1334.

4.1.2. UM 675

The UV continuum is observed to turn down sharply blueward of the Lyα emission line ($\sim$1200 Å; Beaver *et al.* 1991). However, it is not clear that this spectral shape is intrinsic to the QSO or that it continues beyond the shortest observed rest-frame wavelength of $\sim$520 Å. Lyons *et al.* (1996) show that the intrinsic UV continuum can, in fact, be interpreted as a simple power law with $\alpha_{uv} \sim -1$ modified by many blended, intervening Lyα absorption lines (the so-called Lyman "valley"; Møller & Jakobsen 1990). Here I adopt somewhat low values of T_c and E_c consistent with the observed spectrum, but with uncertainties that encompass the usual range of possible intrinsic shapes. The column densities (from Hamann *et al.* 1995a) require a range of ionizations (i.e. more than one U value). It is clear from Table 3 that the H I forms mostly in the lower ionization gas e.g. with C III, C IV and N III. As a result, the [M/H] values derived assuming each ion forms at the peak in its $f(\mathrm{M}_i)$ curve are greatly underestimated for highly ionized species such as O VI and Ne VIII.

The $z_a \approx z_e$ system in this QSO is of particular interest because its time-variability places the absorbers within a few hundred pc of the continuum source (Hamann *et al.* 1995a). In agreement with Hamann *et al.* (1995a), Table 3 provides strong evidence for [C/H] $\gtrsim 0.0$ and [N/C] $\gtrsim 0.8$. Note that the revised column densities derived for this source by Hamann *et al.* (1997b), which make an uncertain correction for the partial coverage of the background light source, would imply larger M/H ratios by factors of $\sim$2.

4.1.3. PKS 0424−131

Wilkes *et al.* (1994) derive $\alpha_{ox} \approx -1.60$ based on non-simultaneous UV and X-ray observations. I assign an uncertainty of ± 0.1 due to the possible variability and measurement/fitting uncertainties. The column densities are from Petitjean *et al.* (1994), who take explicit account of the partial coverage of the background emission source(s) when necessary.

$z_a = 2.100$. The ratios of C II/C IV and Si II/Si III/Si IV column densities suggest that there is a range of ionizations in this system. The [M/H] values for the low-ionization metals indicate metallicities $0.0 \lesssim$ [M/H] $\lesssim 1.0$ for the maximum H I column listed in Table 3. Line fits by Petitjean *et al.* indicate that the H I column could actually be a factor of $\sim$10 lower, which would imply commensurately higher metallicities.

$z_a = 2.133$. The C IV and N V column densities apply to the sum of two line components fit by Petitjean *et al.* (1994). The H I column might arise from either or both of the two systems.

$z_a = 2.173$. The ionization parameter for this systems was estimated from the Si III/Si

IV column density ratio.

4.1.4. PKS 0450−132

York *et al.* (1991) give a B magnitude of 17.5, which yields $\alpha_{ox} \approx -1.7$ following Wilkes *et al.* (1994). The column densities are from Petitjean *et al.* (1994), where again partial coverage is taken into account when necessary. The two systems listed in Table 3 are just single components in multi-component blends. The H I columns are upper limits based on line fitting.

$z_a = 2.1050$. The ionization parameter adopted for this system is an average of two similar values derived from the C II/C IV and Si II/Si IV column density ratios. The results in Table 3 indicate that most the H I forms with the low ionization metals. The [M/H] values for those ions imply $0.0 \lesssim$ [M/H] $\lesssim 0.5$ for the maximum H I column density. Line fitting by Petitjean *et al.* (1994) shows that the H I column could actually be a few times lower, which would imply commensurately larger metallicities.

$z_a = 2.2302$. The ionization parameter follows from the Si III/Si IV column density ratio. The [M/H] values for the Si ions imply metallicities of order solar or higher, assuming the maximum H I column density. Petitjean *et al.* (1994) indicate that the actual H I column could be a factor of ∼10 lower, which would again imply larger [M/H].

4.1.5. HS 1946+769

Bechtold *et al.* (1994) derive $\alpha_{ox} \approx -1.93$ based on UV and X-ray observations made three months apart. The UV continuum for $\lambda_{rest} > 740$ Å is discussed by Kuhn *et al.* (1995), but the far-UV continuum is not constrained. The column densities are from Tripp *et al.* (1996). Those listed for $z_a = 3.0496$ are Tripp *et al.*'s best estimates for one component of a severely blended, multi-component system (from their Table 5). The upper limit on the H I column comes from the lack of Lyman limit absorption ($\tau_{LL} < 0.2$) associated with this system (see also Fan & Tytler 1994). I estimate U for the $z_a = 3.0496$ system from the ratio of Al II/Al III column densities. The resulting ionization is consistent with the measured Si III/Si IV ratio, and with the limits on Si II/Si IV, C II/C IV and N V/C IV (for reasonable N/C abundances). Note that all of the [M/H] values listed for this system are only lower limits, because the H I column density is an upper limit and in some cases the metal columns are lower limits (e.g. C IV, Si III and Si IV). The results are consistent with Tripp *et al.* (1996).

4.1.6. Q 2116−358

The column densities are from Wampler *et al.* (1993). Table 3 does not include the associated system at $z_a = 2.318434$ because its H I column density is poorly known. Wampler *et al.* estimate log $N(\mathrm{HI}) \lesssim 17.6$ cm^{-2}, which implies $\tau_{LL} \lesssim 2.5$ at the Lyman limit. For the other four systems near $z_a \approx 2.318$ (Table 3), the column density ratios of different ions of C and Si imply a range of U values – sometimes spanning more than an order of magnitude in the same system. I therefore assume all of the ions form at the peaks in their $f(\mathrm{M}_i)$ curves. Wampler *et al.* describe evidence for partial coverage in several of the systems, but it is not clear that they took that into account in deriving the column densities. If the column densities are accurate, there is strong evidence for [M/H] $\gtrsim 0.0$ in all nine systems and for [M/H] $\gtrsim 1.0$ in a few.

It should be noted that the (probably) large H I column in the system at $z_a = 2.318434$ could significantly lower the Lyman continuum flux incident upon any clouds farther from the QSO. I did not take this into account in Table 3, but the net effect on more distant clouds would be to shift the $f(\mathrm{M}_i)$ curves to the left in Figures 2 -4 and thus *increase* the $f(\mathrm{HI})/f(\mathrm{M}_i)$ ratios and the derived metal abundances by factors up to ∼10.

4.1.7. PG 2302+029

The lines in this unusual system are dominated by a single broad component with FWHM ∼ 3000 to 5000 km s^{-1} and centroids displaced by −56,000 km s^{-1} from the emission redshift (Jannuzi *et al.* 1996). The absorbers could be ultra-high velocity ejecta from the QSO, possibly related to the BAL phenomenon, or intervening gas distributed on cosmologically significant scales, perhaps in a foreground cluster of galaxies. I include this system here assuming that the clouds, whatever their location, are optically thin in the continuum and in photoionization equilibrium with a QSO spectrum.

The near-UV spectrum of the QSO is somewhat steep, with $\alpha \approx -1.25$ for $\lambda_{rest} > 1216$ Å (O'Brian *et al.* 1988). I therefore adopt low fiducial values of T_c and E_c. The column densities in Table 3 follow from the equivalent widths in Jannuzi *et al.* (1996) assuming the lines have negligible optical depths. The upper limit on the H I column is based on my own estimate of $\lesssim$4 Å for the Lyα equivalent width. The derived minimum C/H ratio is not much below solar, consistent with absorption near the QSO. However, Jannuzi *et al.* point out that the measured column densities are consistent with much lower metallicities if the gas is collisionally ionized (compare, for example, Figs. 3 and 5 in Hamann *et al.* 1995a). Therefore, the metallicity results in Table 3 cannot be used to determine the intrinsic *vs.* intervening origin of the lines.

4.2. Notes on Individual BAL Systems

4.2.1. Q 0226−104

Constraints on the continuum shape are discussed by Korista *et al.* (1996). The spectrum steepens sharply at rest wavelengths below ∼1200 Å, but it is not clear that this shape is intrinsic to the QSO or that it continues across the entire far-UV spectrum. I therefore adopt slightly low values of T_c and E_c to be consistent with the observed spectral shape, but with uncertainties that encompass the usual range of shapes. I adopt Korista *et al.*'s estimate of $\alpha_{ox} \approx -1.7$ from the relations in Wilkes *et al.* (1994).

The wide range of column densities measured for this source – from combined ground-based and Hubble Space Telescope observations (Korista *et al.* 1992 and 1996) – provide the best constraints available on the ionization and abundances in a BALQSO. Korista *et al.* (1996) note that the column densities measured from the ground (H I, C IV, N V and Si IV) are typical of BALQSOs, and therefore the derived abundances and ionizations might also be typical. The results in Table 3 are consistent with the previous studies of this source (Korista *et al.* 1996; Turnshek *et al.* 1996), indicating a range of ionizations with super-solar metallicities and N relatively more enhanced.

4.2.2. Q1246−057 and RS 23

The column densities are from Junkkarinen, Burbidge & Smith (1987). These two sources were chosen from Junkkarinen *et al.'s* sample of six BALQSOs because their absorption troughs are less confused with the emission lines – making the column densities more reliable. Super-solar metallicities are required for both objects, even though the level of ionization is unknown.

4.2.3. Mean BALQSO

The column densities were measured by Hamann *et al.* (1993) from the mean spectrum of 36 BALQSOs having weak or absent low ionization lines (Weymann *et al.* 1991). Super-solar metallicities are again required for this average BALQSO.

5. SUMMARY AND DISCUSSION

The figures in §3 provide a general reference for estimating the ionization and metal abundances in clouds that are photoionized by a QSO/AGN. The poor or altogether lacking constraints on the UV through soft X-ray spectra of QSOs/AGNs imply that

there are unavoidable uncertainties in the ionization corrections and derived abundances. Nonetheless, the calculations applied to the best measured column densities for QSO intrinsic absorbers (from the literature) provide strong evidence for super-solar metallicities in BALs and at least some $z_a \approx z_e$ systems. Even when the continuum shape is uncertain and the level of ionization is unknown (for example, when only H I and C IV lines are detected), firm lower limits on the ionization corrections imply [M/H] > 0.0 for typical BALs and some $z_a \approx z_e$ systems. Conversely, none of the 32 systems considered here require $Z < \mathrm{Z}_\odot$. These results support the previous claims for typically high metallicities in QSO intrinsic absorbers (§1). They also support the independent evidence for high metallicities in QSOs based on the broad emission lines (Hamann & Ferland 1992 and 1993; Hamann & Korista 1996; Ferland *et al.* 1996).

The measured column densities for intrinsic absorbers indicate that the absorbing gas is usually optically thin in the H I Lyman continuum out to energies beyond at least the C IV and N V ionization edges (at 64 eV and 98 eV, respectively). Column density ratios such as C II/C III/C IV, N III/N V and Si II/Si III/Si IV often imply a range of ionization states in the same system. Neighboring $z_a \approx z_e$ systems (having similar redshifts and often blended spectroscopically) also typically have different ionizations or abundances. If the abundances are similar in neighboring systems, their ionization parameters must sometimes differ by more than an order of magnitude. To achieve different ionization states in optically thin gas, the absorbers (at the same or similar redshifts) must span a significant range of densities or distances from the ionizing QSO.

5.1. High Metallicities at High Redshift

The general result for solar or higher metallicities in QSOs is consistent with normal galaxy evolution. Vigorous star formation in the cores of massive galaxies can produce gas-phase metallicities well above solar within a few billion years of the initial collapse (cf. Arimoto & Yoshii 1987; Köppen & Arimoto 1990). High metal abundances are a signature of *massive* galaxies because only they can retain their gas long enough against the building thermal pressures from supernova explosions. The enriched nuclear gas might ultimately be ejected from the galaxy or consumed by the black hole, but the evidence for evolution to high Z remains today in the stars. For example, the stars in the central bulge of our own Galaxy have a broad distribution of metallicities, with a mean of $\sim$1 $\mathrm{Z}_\odot$ and a maximum of $\sim$3 $\mathrm{Z}_\odot$ (McWilliam & Rich 1994; Rich 1995 – private comm.). If the gas is well-mixed during the evolution, its final metallicity will equal that of the most metal rich stars (i.e. $\sim$3 $\mathrm{Z}_\odot$). Simple closed-box (or, equivalently, rapid infall) models of the chemical enrichment (Tinsley 1980; Searle & Zinn 1972), which fit the stellar Z-distribution in the bulge very well (Rich 1990), also predict final gas-phase metallicities of $\sim$3 $\mathrm{Z}_\odot$ (assuming $\sim$95% conversion of the original gas into stars). The same calculations applied to the higher mean stellar metallicities of $\sim$2 to 3 $\mathrm{Z}_\odot$ observed in the cores of elliptical galaxies and some nearby

spirals (cf. Bica 1988; Bica, Arimoto & Alloin 1988; Bica, Alloin & Schmidt 1990; Gorgas, Efstathiou & Aragón Salamanca 1990; Worthey, Faber & Jesús Gonzalez 1992; Jablonka, Alloin & Bica 1992; Kennicutt & Garnett 1996) imply even higher gas-phase abundances of ∼6 to 9 $Z_\odot$. These simple estimates are supported by more sophisticated simulations of the enrichment (cf. Hamann & Ferland 1993 and references therein). Therefore, super-solar metallicities can be *expected* in QSO environments as long as (1) the gas is processed in the cores of massive ($\gtrsim 10^{11}$ $M_\odot$) galaxies (or at least in dense condensations that become the cores of massive galaxies), and (2) the enrichment timescales are shorter than the time needed for QSOs to "turn on" or become observable (e.g. less than a few Gyr for QSOs at redshifts $\gtrsim$4; Hamann & Ferland 1993).

In addition to this normal stellar enrichment, other processes peculiar to black-hole/accretion-disk environments might contribute to, or even dominate, QSO abundances (Artymowicz, Lin & Wampler 1993; Shields 1996). Metallicities above ∼10 $Z_\odot$ are problematic for standard enrichment models unless the initial mass functions strongly favor massive stars. The results in §4 indicate that $Z \gtrsim 10$ $Z_\odot$ occurs in typical BAL and some $z_a \approx z_e$ regions. Possibly an additional source of metals is required, or possibly the gas does not derive from a well-mixed interstellar medium. The extremely high phosphorus abundances of [P/C] $\gtrsim$ 1.8 reported for a few BALQSOs (Turnshek 1988; Junkkarinen *et al.* 1995) have led to speculation that BALs form in a special environment, such as dwarf novae ejecta (Shields 1996). The high [P/C] values are in any case not compatible with the normal stellar enrichment of a well-mixed interstellar medium. These results should be tested in other objects. Presently, there is no evidence for large P/C ratios in $z_a \approx z_e$ absorbers or in the broad emission-line regions.

5.2. Intrinsic UV Absorbers as X-ray Warm Absorbers?

There is no evidence from the data discussed here that the line-absorbing clouds also produce continuous X-ray absorption. Bound-free absorption in soft X-rays due to highly ionized metals, mainly O VII and O VIII, occurs in many Seyfert galaxies and at least some QSOs (e.g. Nandra & Pounds 1994; George *et al.* 1996 and references therein). Mathur (1994), Mathur *et al.* (1994), Mathur *et al.* (1995a) and Green & Mathur (1996) argued that BALs and $z_a \approx z_e$ lines form in the same gas as the X-ray warm absorbers. In their models, the ions producing the common UV lines are minor constituents in highly ionized gas with $\log U \gtrsim -0.5$. These one-zone models predict strong trends for larger column densities in more highly ionized species (see also Netzer 1996 and Shields & Hamann 1996). For example, a modest ionization of $\log U = 0.0$ produces logarithmic column density ratios of C II/C III/C IV, N III/N V, O III/O VI and Si II/Si III/Si IV equal to $-5.8/-2.1/0.0$, -3.3, -3.9, and $<-5.2/-2.1/0.0$, respectively, in a nominal warm absorber (§3.3, Fig. 11). If the metals have solar relative abundances, the same calculation predicts logarithmic column density ratios such as Mg II/C IV < -9.1, Si IV/C IV $= -3.9$, N V/C IV $= +0.3$,

O VI/C IV = +1.7, Ne VIII/C IV = +0.1.

Although one-zone models are consistent with the combined UV and X-ray observations of several Seyfert galaxies and QSOs (see papers by Mathur *et al.* above; also Shields & Hamann 1996), the more reliable (e.g. higher spectral resolution) absorption-line data discussed here do not support a single-zone absorber. In particular, the strongs trends for much larger column densities in more highly ionized species are not present in the data. The measured column densities often indicate a range of ionizations, with most of the lines forming at $\log U \lesssim -1.0$. The significant presence of singly-ionized metals alone cannot be reconciled with a highly ionized, one-zone absorber when the gas is *known* to be optically thin in the H I Lyman continuum. In the one case where warm absorber-like ionizations are known to be present (via Ne VIII λ770,780 in the $z_a \approx z_e$ system of UM 675), the column density is roughly two orders of magnitude too small to be a warm absorber (Hamann *et al.* 1995a). The ensemble data for that system (Table 3) indicate that the gas is optically thin in the continuum at *all* UV through X-ray wavelengths.

Nonetheless, the detections of strong O VI λ1032,1038 and especially NeVIII λ770,780 are significant. Few observations so far have included these lines, but O VI, at least, appears to be common. There might often be *components* of UV absorbing regions that have high, warm absorber-like ionizations. Perhaps sometimes, and perhaps more often in Seyfert galaxies, the highly ionized components *are* warm absorbers. More efforts to combine X-ray observations with accurate UV-derived column densities across a range of ionizations, including O VI and Ne VIII, are needed to explore the relationship between the two absorbers further.

I am grateful to G. J. Ferland and K. T. Korista for their generous help with Ferland's CLOUDY software. Thanks to V. Junkkarinen and G. Shields for useful discussions and J. C. Shields, K. T. Korista and the referee P. Møller for helpful comments on this manuscript. This work was supported by NASA grants and AR-5292.02-93B, NAG 5-1630 and NAG 5-3234.

APPENDIX. Continuum Shape Details

The ionizing continua A, B and C are all consistent with generic QSO/AGN observations. They each portray a range of shapes at the crucial UV through soft X-ray wavelengths. Continuum A (Figure 1A) has the form,

$$F_\nu \propto \nu^{\alpha_{uv}} e^{-\frac{kT_{ir}}{h\nu}} e^{-\frac{h\nu}{kT_c}} + \Gamma \nu^{\alpha_x} e^{-\frac{kT_{c2}}{h\nu}} e^{-\frac{h\nu}{kT_x}} \quad (4)$$

which is the sum of two power laws, each having exponential cutoffs at high and low energies. I adopt a power law index in the near-infrared through UV, $\alpha_{uv} = -0.5$, consistent

with the wealth of QSO/AGN observations cited in §2.1. The infrared cutoff has a fixed characteristic temperature of $T_{ir} \approx 300$ K (equivalent to $\sim$10 μm), which eliminates free-free heating at high densities (Ferland *et al.* 1992). The important high energy UV cutoff, T_c, is freely varied; the range $5.0 \leq \log\ T_c \leq 6.0$ K is shown in Figure 1A. The relative strengths of the UV and X-ray continua are set by the constant Γ according to the definition of α_{ox} (Eqn. 3). The X-ray continuum has a power law index of $\alpha_x = -1.0$. This slope is typical of radio-quiet QSOs (Wilkes & Elvis 1987) and Seyfert galaxies (Nandra & Pounds 1994) at energies 2–10 keV. The energetically more important soft X-ray spectra are usually steeper than this below $\sim$0.5 to 1 keV (Wilkes & Elvis 1987; Turner & Pounds 1989; Wilkes *et al.* 1994; Walter *et al.* 1994; Gondhalekar *et al.* 1994; Fiore *et al.* 1994; Laor *et al.* 1994; Marshall, Fruscione & Carone 1995). Therefore, the choice of $\alpha_x = -1.0$ is probably also a good compromise for radio-loud QSOs, even though their 2–10 keV slopes are typically closer to -0.5 (Wilkes & Elvis 1987). The X-ray power law is suppressed at low energies by an exponential decline characterized by the temperature $T_{c2} = T_c/6$. At the highest energies, the X-ray flux declines with a characteristic temperature of $\log T_x = 9.0$ K. These cutoff temperatures are simply a mathematical convenience for producing a smooth, well behaved continuum overall.

Continuum B (Figure 1B) is a segmented power law with changes in the index at energies 0.125 eV, E_c, and E_{cx}. The power law indices between these energies are,

$$\begin{aligned} \alpha_{ir} &= +2.5 \qquad \text{for } 0 < h\nu \leq 0.125 \text{ eV} \\ \alpha_{uv} &= -0.5 \qquad \text{for } 0.125 \text{ eV} < h\nu \leq E_c \\ \alpha_c &= -3.5 \qquad \text{for } E_c < h\nu \leq E_{cx} \\ \alpha_x &= -1.0 \qquad \text{for } E_{cx} < h\nu < \infty \end{aligned} \tag{5}$$

The freely varied parameters are α_{ox} and E_c, with the value of E_{cx} determined from the definition of α_{ox} in Eqn. 3.

Continuum C (Figure 1C) is a broken power law like continuum B, but with $E_{cx} = 0.7$ keV fixed in all cases. This break in the spectral slope at 0.7 keV is consistent with observations of soft X-ray "excesses" (Wilkes & Elvis 1987; Wilkes *et al.* 1994; Walter *et al.* 1994; Fiore *et al.* 1994; Laor *et al.* 1994; Marshall *et al.* 1995). Continuum C differs from B in that it always includes a soft X-ray excess, and the slope α_c between E_c and E_{cx} depends on the adopted values of α_{ox} and E_c. For example in Figure 1C, α_c varies from -1.72 for C(0.9,$-$1.6) to -3.02 for C(1.9,$-$1.6).

REFERENCES

Anderson, S. F., Weymann, R. J., Foltz, C. B., & Chaffee Jr., F. H. 1987, AJ, 94, 278
Arimoto, N. & Yoshii, Y. 1987, A&A, 173, 23

Artymowicz, P., Lin, D. N. C., & Wampler, E. J. 1993, ApJ, 409, 592
Avni, Y., Worrall, D. M., & Morgan, W. A. 1995, ApJ, 454, 673
Baldwin, J. A., Ferland, G. J., Korista, K. T., Carswell, R. F., Hamann, F., Phillips, M. M., Verner, D., Wilkes, B., & Williams, R. E. 1996, ApJ, 461, 664
Barlow, T. A. 1993, *Ph.D. Dissertation*, University of California – San Diego
Barlow, T. A., *et al.* 1996, in prep.
Barlow, T. A., Junkkarinen, V. T., Burbidge, E. M., Weymann, R. J., Morris, S. L., & Korista, K. T. 1992, ApJ, 397, 81
Beaver, E. A., *et al.* 1991, ApJ, 377, L1
Bechtold, J., *et al.* 1994, AJ, 108, 374
Bergeron, J. 1988, in *QSO Absorption Lines: Probing the Universe*, eds. J.C. Blades, C. Norman, & D.A. Turnshek, (Cambridge: Cambridge Univ. Press), p. 127
Bergeron, J. & Stasińska, G. 1986, A&A, 169, 1
Bica, E. 1988, A&A, 195, 76
Bica, E., Alloin, D., & Schmidt 1990, A&A, 228, 23
Bica, E., Arimoto, N., & Alloin, D. 1988, A&A, 202, 8
Blades, J. C. 1988, in *QSO Absorption Lines: Probing the Universe*, eds. J.C. Blades, C. Norman, & D.A. Turnshek, (Cambridge: Cambridge Univ. Press), p. 147
Chaffee, F. H., Foltz, C. B., Bechtold, J., & Weymann, R. J. 1986, ApJ, 301, 116
Christiani, S., Trentini, S., La Franca, F., Aretxaga, I., Andreani, P., Vio, R., & Gemmo, A. 1996, A&A, in press
Crenshaw, D. M. 1996, in *Emission Lines in Active Galaxies*, eds. B.M. Peterson, F.-Z. Cheng and A.S. Wilson, (San Francisco: Astr. Soc. Pac.), in press
Fan, X.-M., & Tytler, D. 1994, ApJS, 94, 17
Ferland, G. J. 1996 "HAZY, a Brief Introduction to Cloudy", University of Kentucky, Department of Physics and Astronomy, Internal Report
Ferland, G. J., Peterson, B. M., Horne, K., Welsch, W. F., & Nahar, S. N. 1992, ApJ, 387, 95
Ferland, G. J., Baldwin, J. A., Korista, K. T., Hamann, F., Carswell, R. F., Phillips, M., Wilkes, B., & Williams, R. E. 1996, ApJ, 461, 683
Fiore, F., Elvis, M., McDowell, J., Siemiginowska, A., Wilkes, B., & Mathur, S. 1994, ApJ, 431, 515
Foltz, C. B., Chaffee Jr., Weymann, R. J., & Anderson, S. F. 1988, in *QSO Absorption Lines: Probing the Universe*, eds. J. C. Blades, D. A. Turnshek, & C. A. Norman (Cambridge: Cambridge Univ. Press), p. 53
Francis, P. J., Hewitt, P. C., Foltz, C. B., Chaffee, F. H., Weymann, R. J., & Morris, S. L. 1991, ApJ, 373, 465
George, I. M., Turner, T. J., & Netzer, H. 1995, ApJ, 438, L67
George, I. M., *et al.* 1996, in prep.
Gondhalekar, P. M., Kellet, B. J., Pounds, K., Mathews, L., & Quenby, J. J. 1994, MNRAS, 268, 973
Gorgas, J., Efstathiou G., & Aragón Salamanca, A. 1990, MNRAS, 245, 217

Green ,P. J., & Mathur, S. 1996, ApJ, 462, 637
Grevesse, N., & Anders, E. 1989, in *Cosmic Abundances of Matter*, AIP Conf. Proc. 183, ed. C. I. Waddington (New York:AIP), 1
Halpern, J. P. 1984, ApJ, 281, 90
Hamann, F., Barlow, T. A., Beaver, E. A., Burbidge, E. M., Cohen, R. D., Junkkarinen, V., & Lyons, R. 1995a, ApJ, 443, 606
Hamann, F., Barlow, T. A., & Junkkarinen, V. 1997a, ApJ, 478, 87
Hamann, F., Barlow, T. A., R. D., Junkkarinen, V., & Burbidge, E. M., 1997b, ApJ, 478, 80
Hamann, F., & Ferland, G. J. 1992, ApJL, 391, L53
Hamann, F., & Ferland, G. J. 1993, ApJ, 418, 11
Hamann, F., & Korista, K. T. 1996, ApJ, 464, 158
Hamann, F., Korista, K. T., & Morris, S. L. 1993, ApJ, 415, 541
Hamann, F., Shields, J. C., Ferland, G. J., & Korista, K. T. 1995b, ApJ, 454, 688
Hewitt, D. & Burbidge, G. 1993, ApJS, 87, 451
Jablonka, P., Alloin, D., & Bica, E. 1992, A&A, 260, 97
Jannuzi, B. T., *et al.* 1996, ApJ, 470, L11
Junkkarinen, V. T., Beaver, E. A., Burbidge, E. M., Cohen, R. C., Hamann, F., Lyons, R. W., & Barlow, T. A. 1995, BAAS, 27, 827
Junkkarinen, V. T., Burbidge, E. M., & Smith, H. E. 1987, ApJ, 317, 460
Kallman, T. R. & Mushotzky, R. 1985, ApJ, 292, 49
Kennicutt, R. C., and Garnett, D. R. 1996, ApJ, 456, 504
Köppen, J., & Arimoto, N. 1990, A&A, 240, 22
Koratkar, A., *et al.* 1996, ApJ, in press
Korista, K. T., Weymann, R. J., Morris, S. L., Kopko, M., Jr., Turnshek, D. A., Hartig, G. F., Foltz, C. B., Burbidge, E. M., & Junkkarinen, V. T. 1992, ApJ, 401, 529
Korista, K. T., Hamann, F., Ferguson, J., & Ferland, G. J. 1996, ApJ, 461, 641
Kriss, G. A., Davidson, A. F., Zheng, W., Kruk, J. W., & Espey, B. R. 1995, ApJ, 454, L7
Kriss, G., *et al.* 1996a, ApJ, in press
Kriss, G., *et al.* 1996b, ApJ, in press
Krolik, J., & Kriss, G. 1995, ApJ, 447, 512
Kuhn, O., Bechtold, J., Cutri, R. Elvis, M., & Rieke, M. 1995, ApJ, 438, 643
Laor, A., Fiore, F., Elvis, M., Wilkes, B. J., & McDowell, J. C. 1994, ApJ, 435, 611
Lyons, R., *et al.* 1996, in prep
Maran, S. P., *et al.* 1996, ApJ, 465, 733
Marshall, H. L., Fruscione, A., & Carone, T. E. 1995, ApJ, 439, 90
Marshall, F. E., *et al.* 1993, ApJ, 405, 168
Mathews, W. G., & Ferland, G. J. 1987, ApJ, 323,456
Mathur, S. 1994, ApJ, 431, L75
Mathur, S., Elvis, M., & Singh, K. P. 1995a, ApJ, 455, L9
Mathur, S., Elvis, M., & Wilkes, B. 1995b, ApJ, 452, 230
Mathur, S., Wilkes, B., Elvis, M., & Fiore, F. 1994, ApJ, 434, 493

McWilliam, A., & Rich, R. M. 1994, ApJS, 91, 749
Møller, P., & Jakobsen, P. 1990, A&A, 228, 299
Møller, P., Jakobsen, P., & Perryman, M. A. C., 1994, A&A, 287, 719
Murray, N., Chiang, J., Grossman, S. A., & Voit, G. M. 1995, ApJ, 451, 498
Nandra, K., & Pounds, K. A. 1994, MNRAS, 268, 405
Netzer, H. 1990, in *Active Galactic Nuclei* (Berlin:Springer-Verlag), 57
Netzer, H. 1996, ApJ, in press
O'Brian, P., Gondhalekar, P. M., & Wilson, R. 1988, MNRAS, 233, 801
Osterbrock, D. E. 1989, *Astrophysics of Gaseous Nebulae and Active Galactic Nuclei*, University Science Press, p. 88
Pettini, M., Smith, L. J., Hunstead, R. W., & King, D. L. 1994, ApJ, 426, 79
Petitjean, P., Bergeron, J. & Puget, J. L. 1992, A&A, 265, 375
Petitjean, P., Rauch, M., & Carswell, R. F. 1994, A&A, 291, 29
Rich, R. M. 1990, ApJ, 362, 604
Sanders, D. B., Phinney, E. S., Neugebauer, G., Soifer, B. T., & Matthews, K. 1989, ApJ, 347, 29
Sargent, W. L., Steidel, C. C., & Boksenberg, A. 1989, ApJS, 69, 703
Savaglio, S., D'Odorico, S., & Møller, P. 1994, A&A, 281, 331
Searle, L., & Sargent, W. L. W. 1972, ApJ, 173, 25
Shields, G. 1996, ApJL, in press
Shields, J. C., & Hamann, F. 1996, ApJ, submitted
Shull, J. M., & Sachs, E. R. 1993, 416, 536
Steidel, C. C. 1990, ApJS, 74, 37
Stocke, J., Morris, S., Weymann, R., and Foltz, C. 1992, ApJ, 396, 487
Tinsley, B. 1980, *Fund. of Cosmic Phys.*, 5, 287
Tripp, T. M., Lu, L., & Savage, B. D. 1996, ApJS, in press
Turner, T. J., & Pounds, K. A. 1989, MNRAS, 240, 833
Turnshek, D. A. 1988, *QSO Absorption Lines: Probing the Universe*, eds. J.C. Blades, C. Norman, & D.A. Turnshek, (Cambridge: Cambridge Univ. Press), p.17
Turnshek, D. A., Kopko, M., Monier, E., Noll, D., Espey, B., & Weymann, R. J. 1996, ApJ, 463, 110
Ulrich, M. H. 1988, MNRAS, 230, 121
Vila-Costas, M. B., & Edmunds, M. G. 1993, MNRAS, 265, 199
Voit, G. M., Shull, J. M., & Begelman, M. C. 1987, 316, 573
Voit, G. M., Weymann, R. J., & Korista, K. T. 1993, ApJ 413, 95
Walter, R., Orr, A., Courvoiser, T. J.-L., Fink, H. H., Makino, F., Otani, C., & Wamsteker, W. 1994, A&A, 285, 119
Wampler, E., J., Bergeron, J., & Petitjean, P. 1993, A&A, 273, 15
Weymann, R. J., Turnshek, D. A., & Christiansen, W. A. 1985, in *Astrophysics of Active Galaxies and Quasi-Stellar Objects*, ed. J. Miller, (Mill Valley, CA: University Science Books), 185
Weymann, R. J., Morris, S. L., Foltz, C. B., & Hewett, P. C. 1991, ApJ, 373, 23 (WMFH)

Weymann, R. J. Williams, R. E., Peterson, B. M., & Turnshek, D. A. 1979, ApJ, 218, 619
Wheeler, J. C., Sneden, C., and Truran, J. W., 1989, ARA&A, 27, 279
Wilkes, B. J., & Elvis, M. 1987, ApJ, 323, 243
Wilkes, B. J., Tananbaum, H., Worrall, D. M., Avni, Y., Oey, M. S., & Flanagan, J. 1994, ApJS, 92, 53
Worthey, G., Faber, S. M., & Jesús Gonzalez, J. 1992, ApJ, 398, 69
York, D. G., Yanny, B., Crotts, A., Carilli, C., Garrison, E., & Matheson, L. 1991, MNRAS, 250, 24
Zamorani, G., *et al.* 1981, ApJ, 245, 357

Figure Captions

Figure 1. Synthetic QSO spectra used in the calculations are shown normalized to unity at 2500 Å. Panels A, B and C show the continuum types A, B and C (see text §2.1). The solid curves illustrate a range of plausible shapes allowed by the free parameters α_{ox} plus log T_c (for continuum A) or α_{ox} plus log E_c (for B and C). The bold solid lines indicate the fiducial cases A(5.7,−1.6), B(1.4,−1.6) and C(1.4,−1.6). The dotted line labeled MF87 in each panel is the generic AGN spectrum from Mathews & Ferland (1987). Panel D shows the MF87 continuum and the fiducial cases for A, B and C after transmission through an X-ray warm absorber (§2.1). The transmitted spectra of types A, B and C are labeled AT, BT, and CT, respectively, in panel D.

Figure 2a. Ionization fractions, $f(\mathrm{M}_i)$ and f(HI), are shown for different ionization parameters, U, in clouds that are optically thin at all continuum wavelengths. The ionizing spectra are A(5.7,−1.6) – left window – and B(1.4,−1.6) – right window. The f(HI) values are shown across the top. The various $f(\mathrm{M}_i)$ curves are labeled at their peaks. The two dotted curves in the top panels are S4 (not labeled) and S6. The two dash-dot curves in those panels are Fe2 (not labeled) and Fe3. The two dash-dot curves in the middle panels are Al2 (not labeled) and Al3. The three dash-dot curves in the bottom panels are Si2, Si3 (not labeled) and Si4.

Figure 2b. C(1.4,−1.6) and MF87. See Fig. 2a.

Figure 2c. PL(−1.0) and PL(−1.5). See Fig. 2a.

Figure 3a. A(5.2,−1.6) and A(6.0,−1.6). See Fig. 2a.

Figure 3b. A(5.7,−1.3) and A(5.7,−1.9). See Fig. 2a.

Figure 4a. C(1.1,−1.6) and C(1.9,−1.6). See Fig. 2a.

Figure 4b. C(5.7,−1.3) and C(5.7,−1.9). See Fig. 2a.

Figure 5. Continuum A; contours of constant ionization correction normalized to solar, $\log(f(\mathrm{HI})/f(\mathrm{M}_i)) + \log(\mathrm{H/M})_\odot$, evaluated at the peaks in the $f(\mathrm{M}_i)$ curves are plotted for optically thin clouds photoionized by various continua with the parameters T_c and α_{ox} as shown. Each window applies to a different ion, labeled at the top. The dotted contours appear at increments of 0.1 dex, the thin solid contours appear every 0.25 dex and the bold contours every 1.0 dex. See §3.1.

Figure 6. Continuum C; normalized ionization corrections analogous to Fig. 5.

Figure 7. Ionization corrections normalized by solar abundances, $\log(f(\mathrm{HI})/f(\mathrm{M}_i)) + \log(\mathrm{H/M})_\odot$, for optically thin clouds are shown for different ionization parameters, U. The ionizing spectra are A(5.7,−1.6) at left and C(1.4,−1.6) right. The curves are labeled at their minima as in Fig. 2a.

Figure 8. Continuum A; minimum normalized ionization corrections, $\log(f(\mathrm{HI})/f(\mathrm{M}_i)) + \log(\mathrm{H/M})_\odot$, evaluated at the minima in the $f(\mathrm{HI})/f(\mathrm{M}_i)$ curves, are plotted for various ions in optically thin clouds. The format follows Fig. 5.

Figure 9. Continuum C; minimum normalized ionization corrections analogous to Fig. 8.

Figure 10a. Continuum A; normalized ionization corrections, $\log(f(b_j)/f(a_i)) + \log(b/a)_\odot$, for deriving relative metal abundances $[a/b]$ from Eqn. 2. The curve labeled N5/C4 gives the correction factor needed to derive [N/C] from the ratio of N V/C IV column densities, etc. The curve for P5/C4 is shifted downward by −3.0 for convenience. Each panel shows results for a different ionizing continuum shape.

Figure 10b. Continuum C; normalized ionization corrections for deriving relative metal abundances, analogous to Fig. 10a.

Figure 11. Ionization fractions for optically thin clouds ionized by continuum CT (transmitted through a warm absorber; left-hand panel), and for clouds with $\log\ N(\mathrm{HI}) \leq 16.5$ cm^{-2}, $\log\ N_H \leq 22.0$ cm^{-2}, solar abundances and ionized by the fiducial continuum C (right panel). The format follows Fig. 2a.

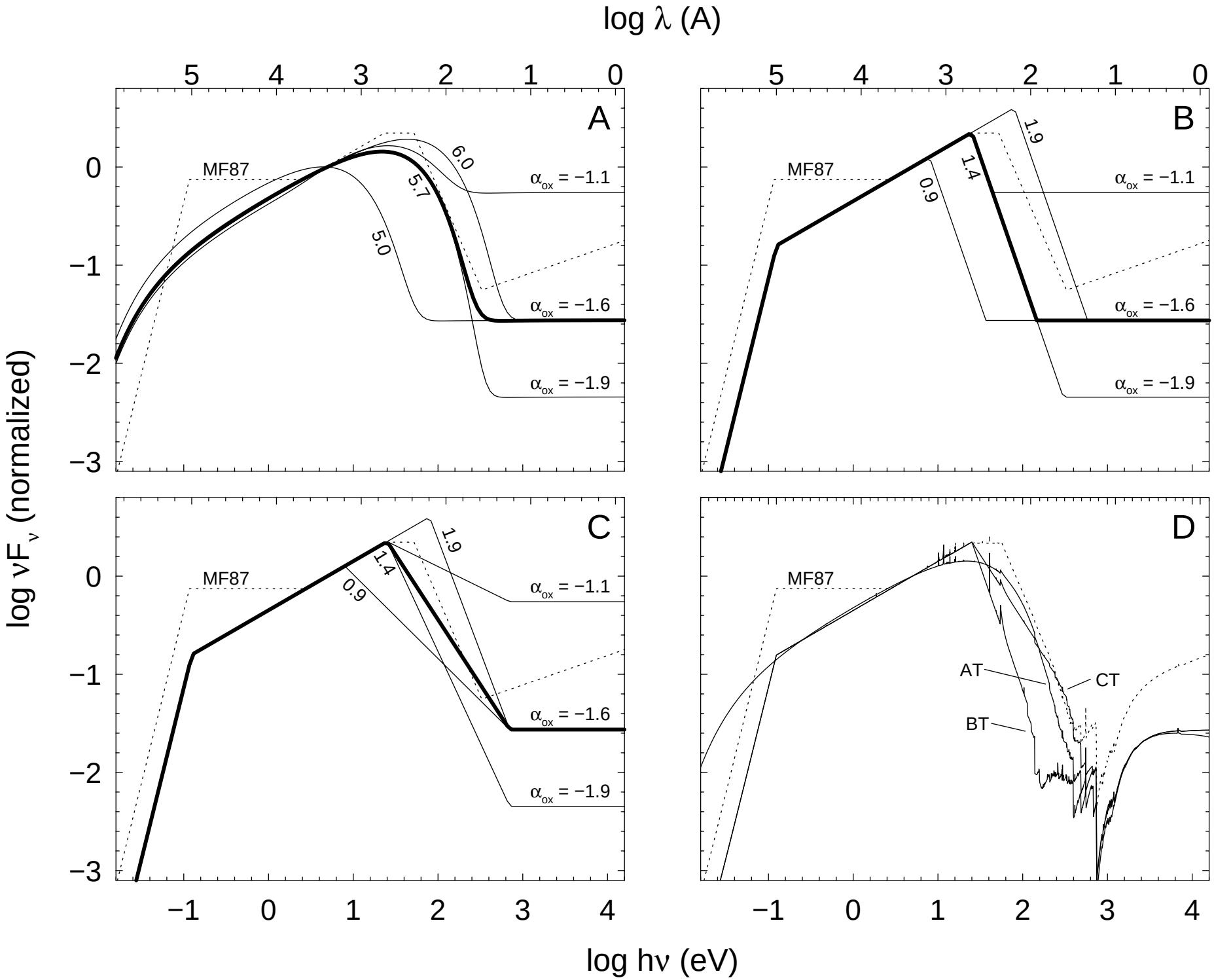
log λ (A)
log νF$_\nu$ (normalized)
log hν (eV)
A
B
C
D
MF87
α_{ox} = −1.1
α_{ox} = −1.6
α_{ox} = −1.9
6.0
5.7
5.0
1.9
1.4
0.9
AT
CT
BT

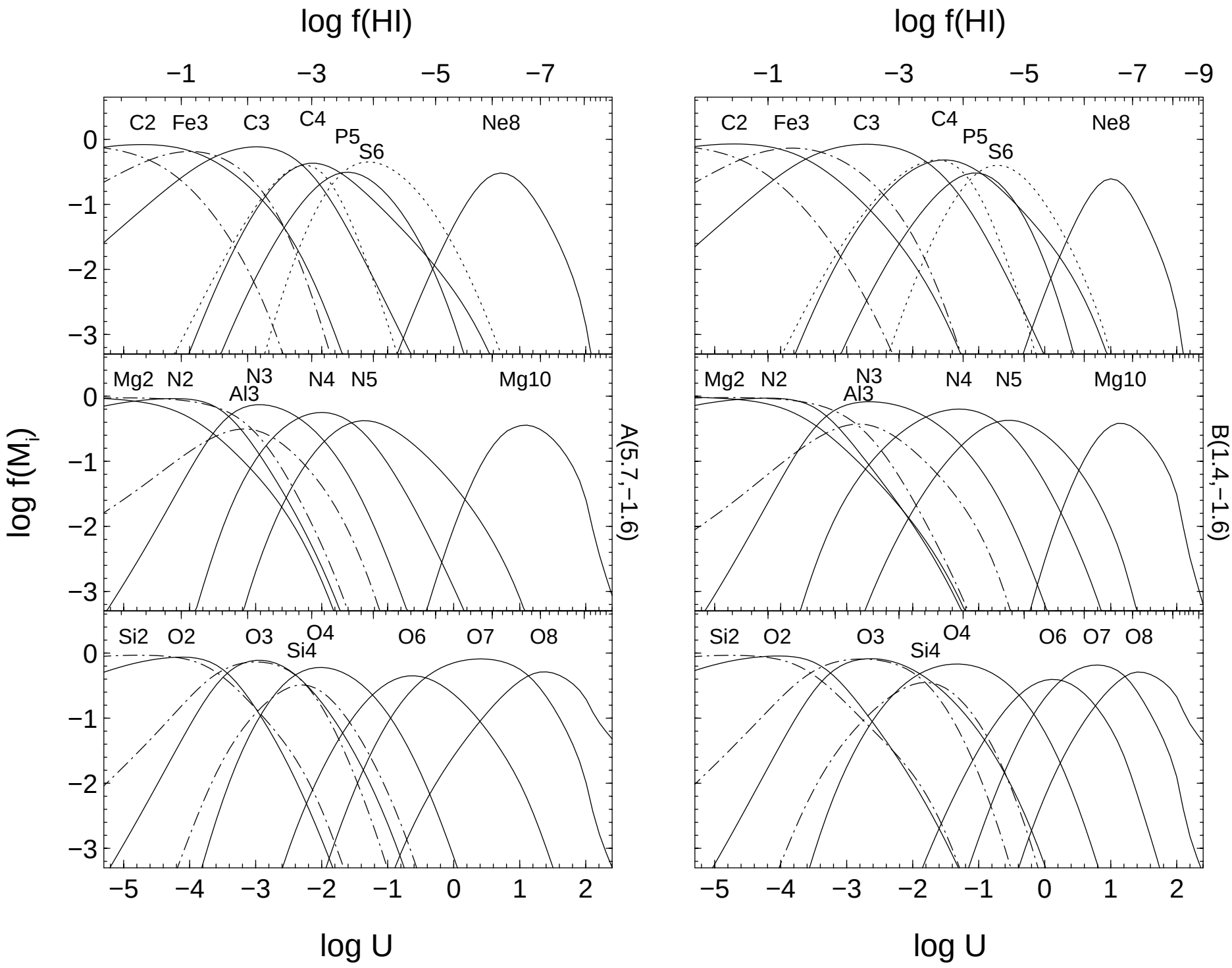
log f(HI)
−1
−3
−5
−7
−9
C2
Fe3
C3
C4
P5
S6
Ne8
Mg2
N2
N3
Al3
N4
N5
Mg10
Si2
O2
O3
Si4
O4
O6
O7
O8
log f(M_i)
A(5.7,−1.6)
B(1.4,−1.6)
log U

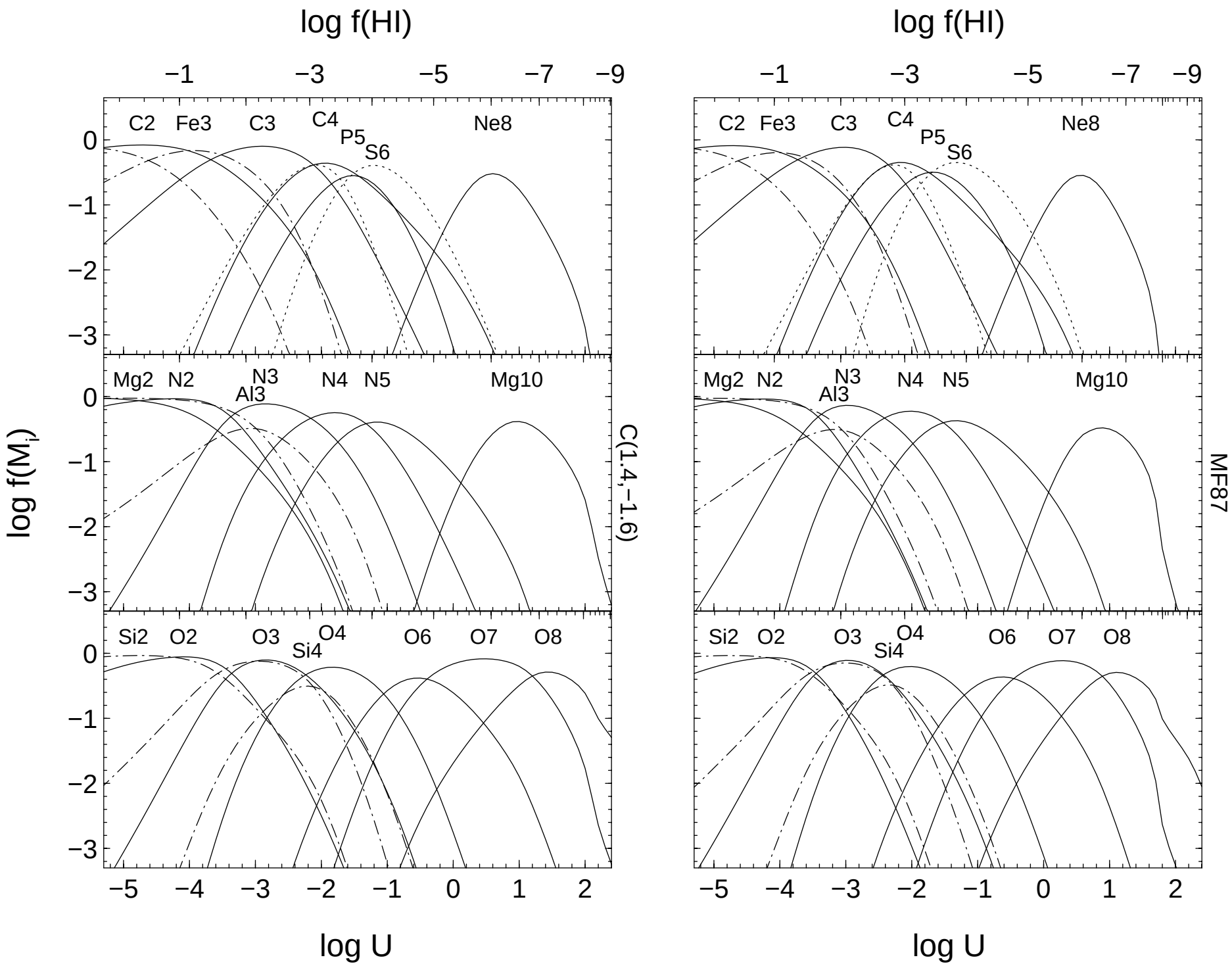
log f(HI)
−1
−3
−5
−7
−9
C2
Fe3
C3
C4
P5
S6
Ne8
Mg2
N2
Al3
N3
N4
N5
Mg10
Si2
O2
O3
Si4
O4
O6
O7
O8
log f(M_i)
C(1.4,−1.6)
MF87
log U
0
−1
−2
−3
−4
−5
1
2

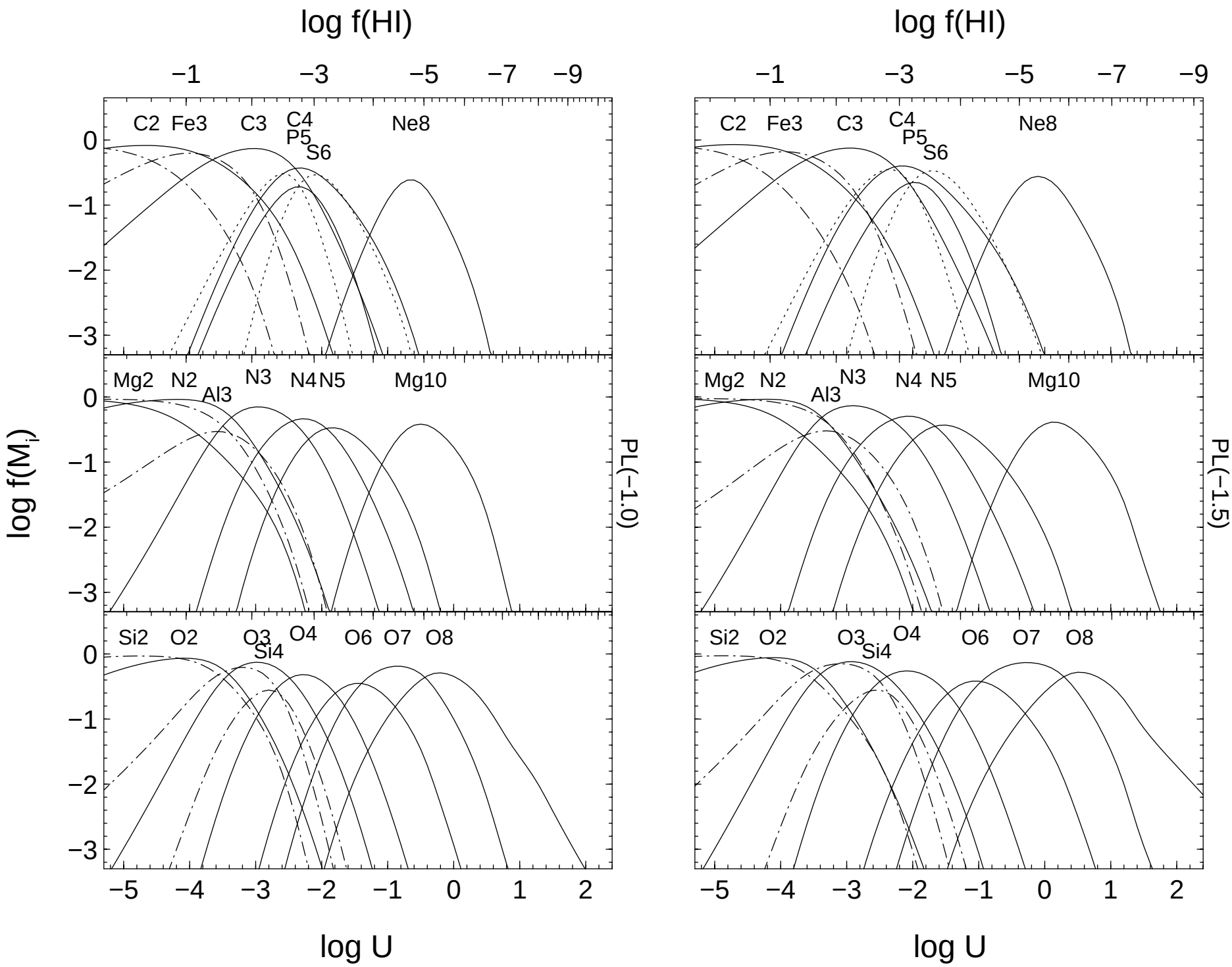
log f(HI)
−1
−3
−5
−7
−9
C2
Fe3
C3
C4
P5
S6
Ne8
Mg2
N2
Al3
N3
N4
N5
Mg10
Si2
O2
O3
Si4
O4
O6
O7
O8
log f(M_i)
PL(−1.0)
PL(−1.5)
0
−1
−2
−3
−5
−4
−3
−2
−1
0
1
2
log U

TABLE 1

Solar Abundances[a]

Ele.	$\log (H/M)_\odot$
C	3.44
N	3.95
O	3.07
Ne	3.91
Mg	4.42
Al	5.53
Si	4.45
S	4.79
P	6.43
Fe	4.33

[a]From Grevesse & Anders (1989).

TABLE 2

Sources and Adopted Continuum Shapes

Source	Type	z_e	A($\log T_c$, α_{ox})	C($\log E_c$, α_{ox})
Q 0000−263	$z_a \approx z_e$	4.11	$(5.3^{+0.7}_{-0.3}, -1.85\pm0.1)$	$(1.2^{+0.7}_{-0.3}, -1.85\pm0.1)$
UM 675	$z_a \approx z_e$	2.15	$(5.4^{+0.6}_{-0.2}, -1.7\pm0.2)$	$(1.3^{+0.6}_{-0.2}, -1.7\pm0.2)$
PKS 0424−131	$z_a \approx z_e$	2.17	$(5.7^{+0.3}_{-0.5}, -1.60\pm0.1)$	$(1.4^{+0.5}_{-0.3}, -1.60\pm0.1)$
Q 0450−132	$z_a \approx z_e$	2.25	$(5.7^{+0.3}_{-0.5}, -1.7\pm0.2)$	$(1.4^{+0.5}_{-0.3}, -1.7\pm0.2)$
HS 1946+769	$z_a \approx z_e$	3.05	$(5.7^{+0.3}_{-0.5}, -1.93\pm0.07)$	$(1.4^{+0.5}_{-0.3}, -1.93\pm0.07)$
Q 2116−358	$z_a \approx z_e$	2.34	$(5.7^{+0.3}_{-0.5}, -1.7\pm0.2)$	$(1.4^{+0.5}_{-0.3}, -1.7\pm0.2)$
PG 2302+029	?	1.05	$(5.4^{+0.6}_{-0.2}, -1.7\pm0.2)$	$(1.3^{+0.6}_{-0.2}, -1.7\pm0.2)$
Q 0226−104	BAL	2.26	$(5.4^{+0.6}_{-0.2}, -1.7\pm0.2)$	$(1.3^{+0.6}_{-0.2}, -1.7\pm0.2)$
Q 1246−057	BAL	2.22	$(5.7^{+0.3}_{-0.5}, -1.7\pm0.2)$	$(1.4^{+0.5}_{-0.3}, -1.7\pm0.2)$
RS 23	BAL	1.91	$(5.7^{+0.3}_{-0.5}, -1.7\pm0.2)$	$(1.4^{+0.5}_{-0.3}, -1.7\pm0.2)$
Mean BALQSO	BAL	$\sim$2	$(5.7^{+0.3}_{-0.5}, -1.7\pm0.2)$	$(1.4^{+0.5}_{-0.3}, -1.7\pm0.2)$

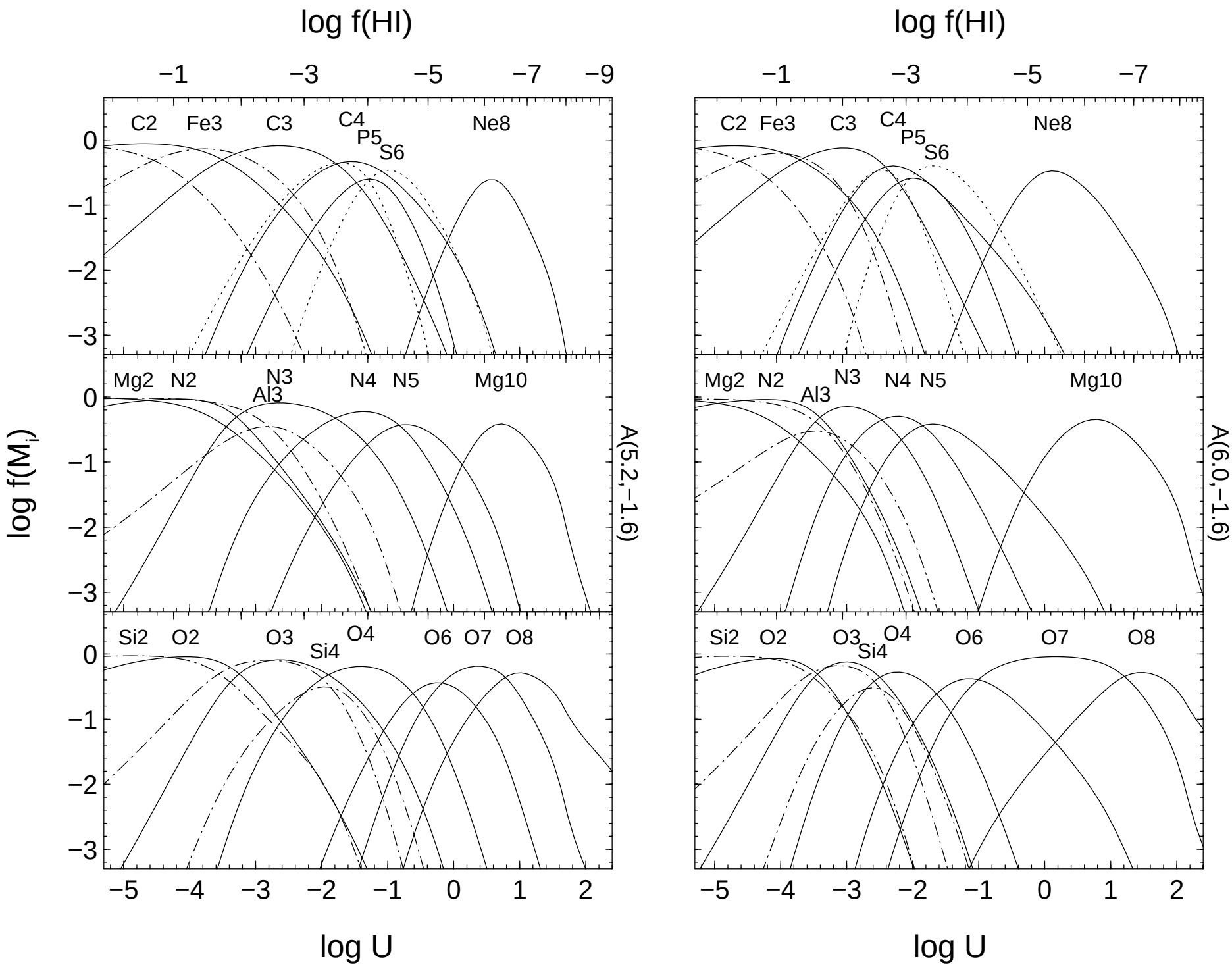
log f(HI)
−1
−3
−5
−7
−9
C2
Fe3
C3
C4
P5
S6
Ne8
Mg2
N2
Al3
N3
N4
N5
Mg10
Si2
O2
O3
Si4
O4
O6
O7
O8
log f(M_i)
A(5.2,−1.6)
A(6.0,−1.6)
0
−1
−2
−3
−5
−4
−3
−2
−1
0
1
2
log U

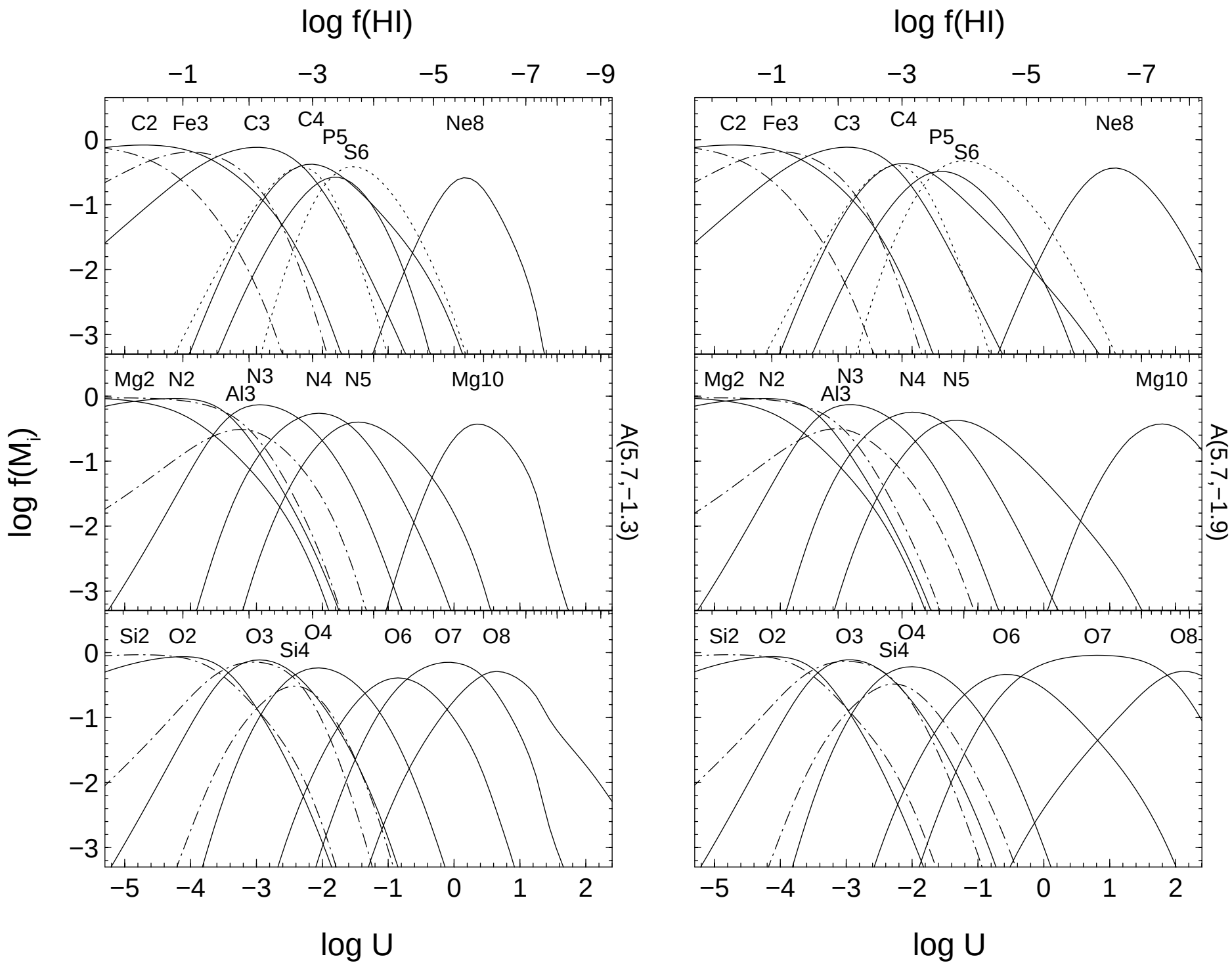
log f(HI)
−1
−3
−5
−7
−9
C2
Fe3
C3
C4
P5
S6
Ne8
Mg2
N2
Al3
N3
N4
N5
Mg10
Si2
O2
O3
Si4
O4
O6
O7
O8
log f(M_i)
A(5.7,−1.3)
A(5.7,−1.9)
log U
0
−1
−2
−3
−5
−4
1
2

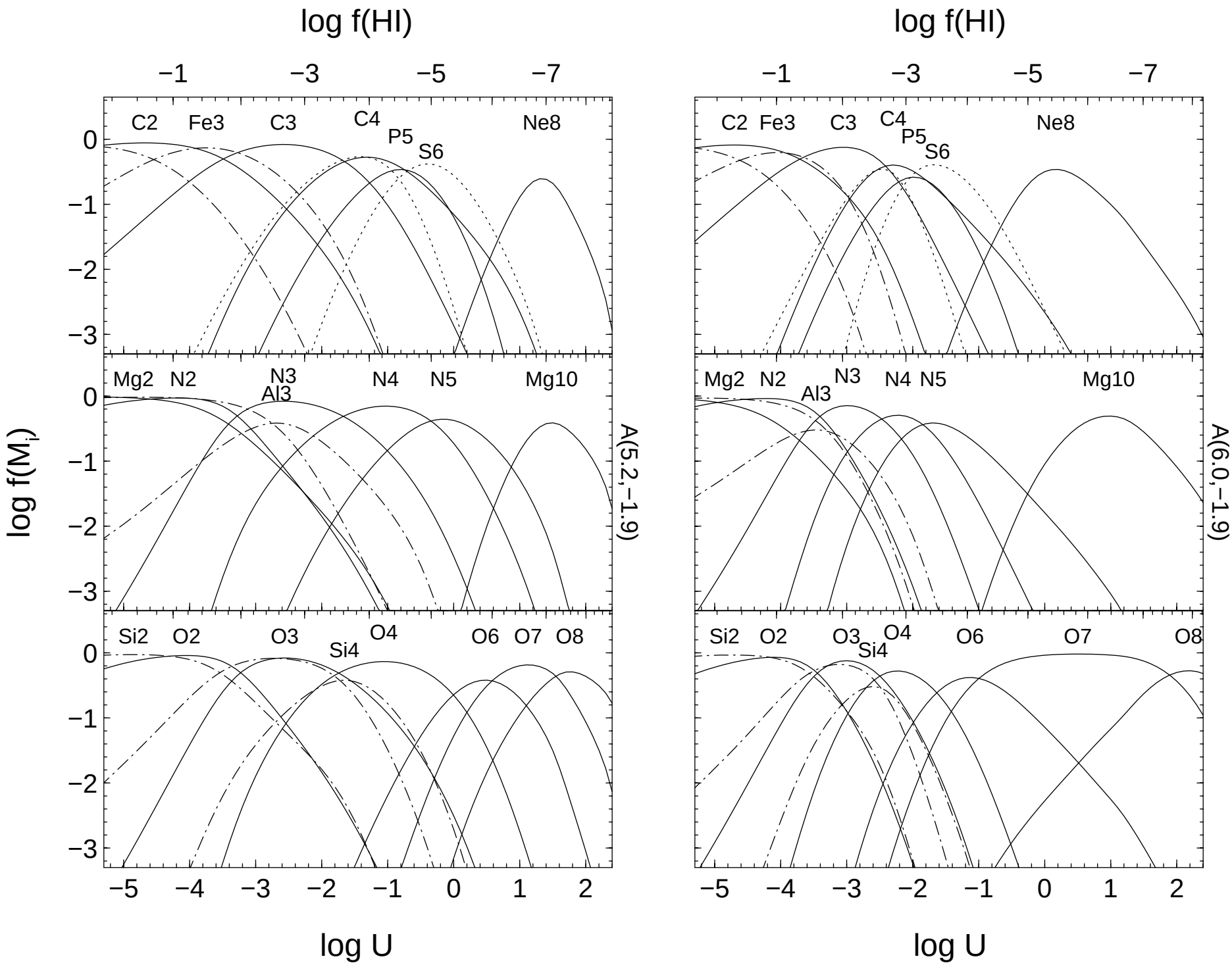
log f(HI)
−1
−3
−5
−7
C2
Fe3
C3
C4
P5
S6
Ne8
Mg2
N2
Al3
N3
N4
N5
Mg10
Si2
O2
O3
Si4
O4
O6
O7
O8
log f(M_i)
A(5.2,−1.9)
A(6.0,−1.9)
0
−1
−2
−3
−5
−4
1
2
log U

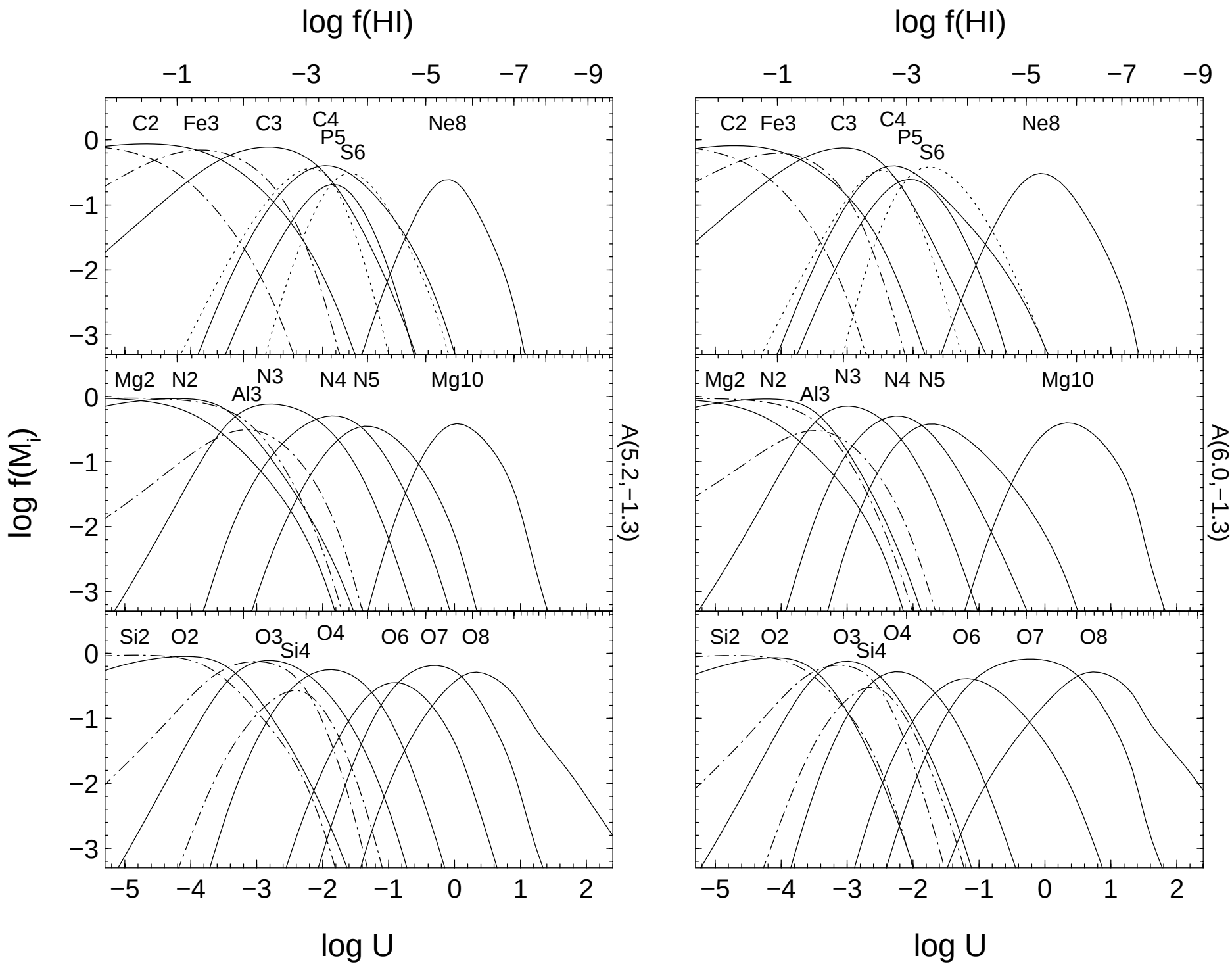
log f(HI)
−1
−3
−5
−7
−9
C2
Fe3
C3
C4
P5
S6
Ne8
Mg2
N2
Al3
N3
N4
N5
Mg10
Si2
O2
O3
Si4
O4
O6
O7
O8
log f(M_i)
A(5.2,−1.3)
A(6.0,−1.3)
0
−1
−2
−3
−5
−4
−3
−2
−1
0
1
2
log U

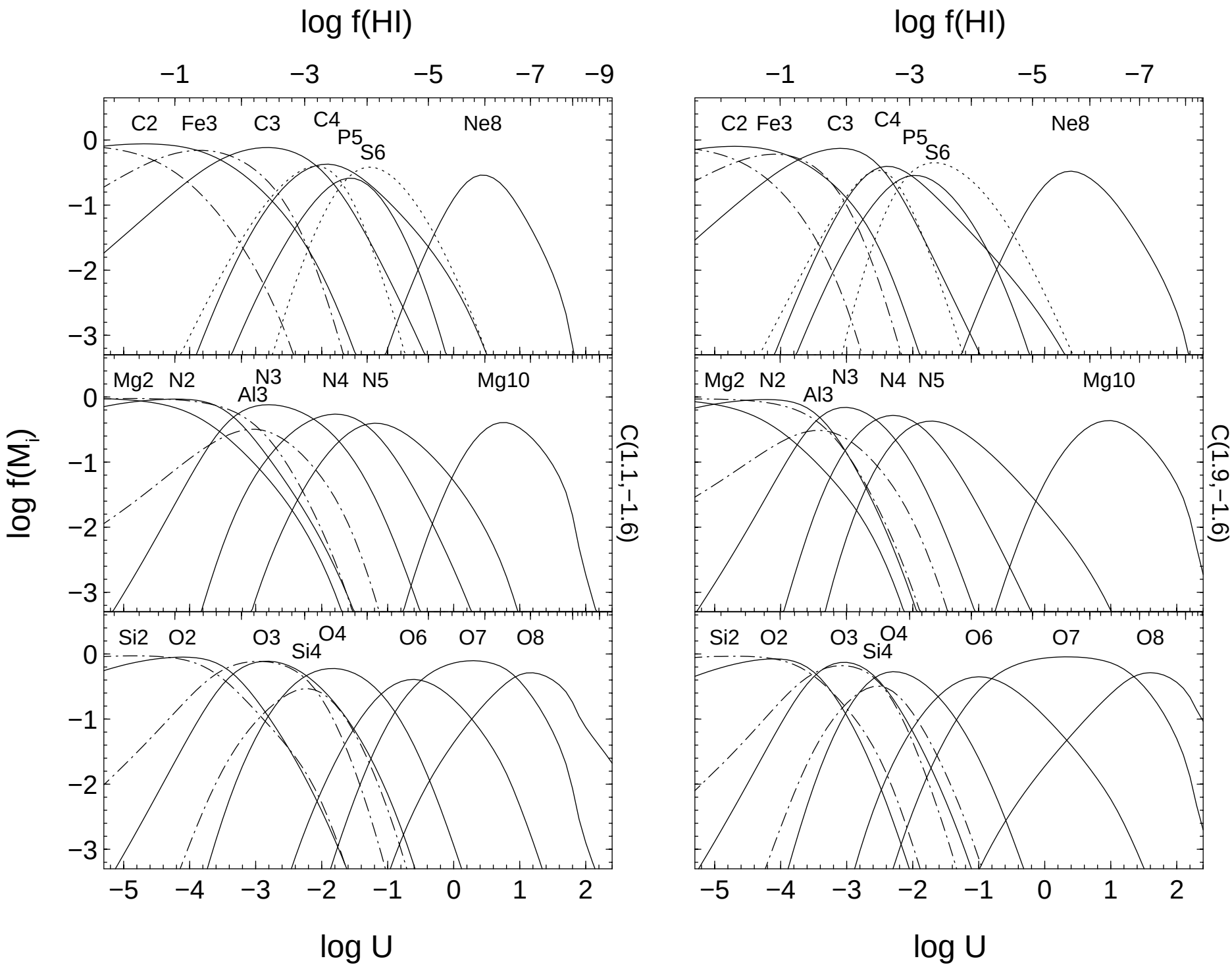
log f(HI)
−1
−3
−5
−7
−9
C2
Fe3
C3
C4
P5
S6
Ne8
Mg2
N2
Al3
N3
N4
N5
Mg10
Si2
O2
O3
Si4
O4
O6
O7
O8
log f(M_i)
C(1.1,−1.6)
C(1.9,−1.6)
log U
0
−1
−2
−3
−4
−5
1
2

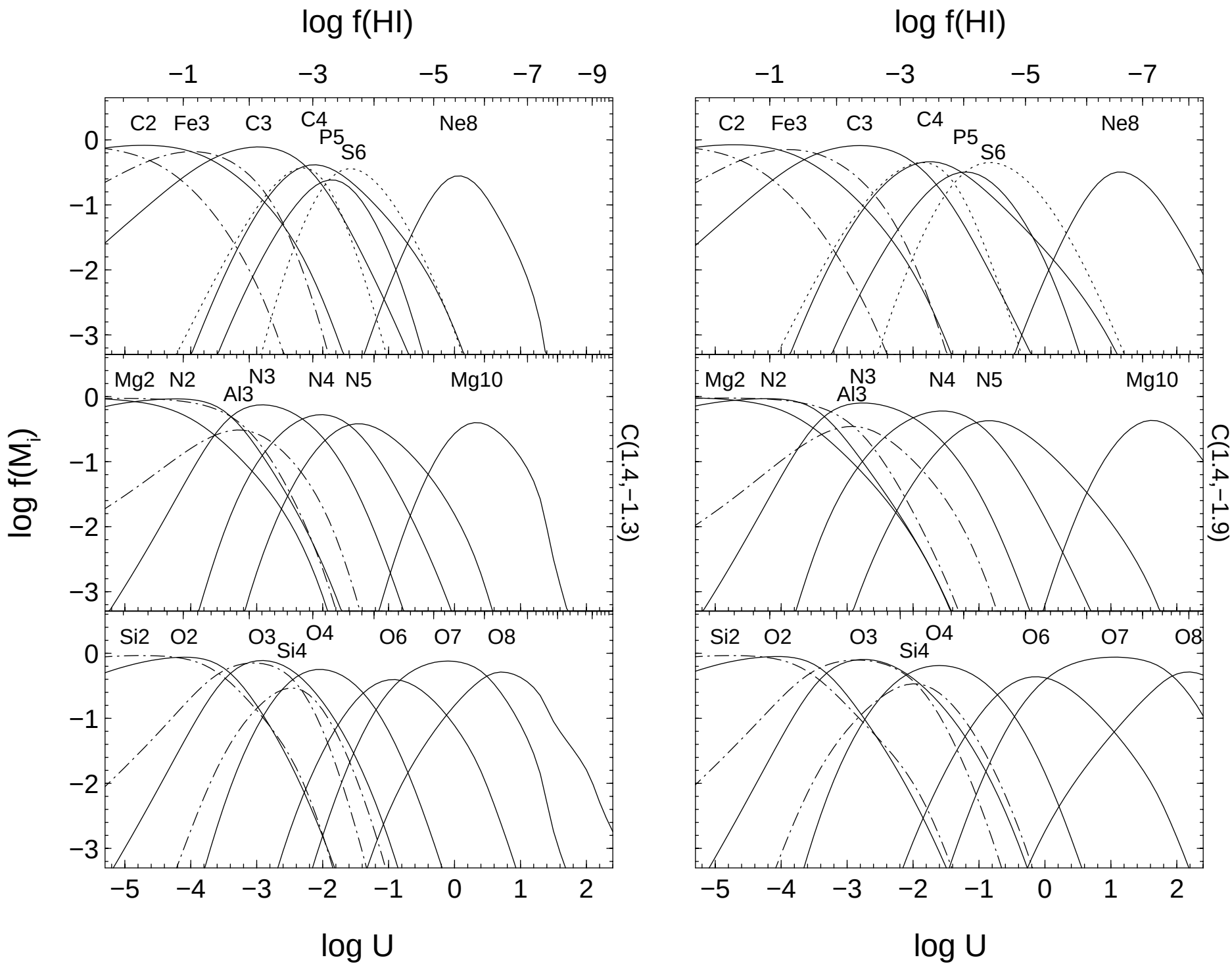
log f(HI)
−1
−3
−5
−7
−9
C2
Fe3
C3
C4
P5
S6
Ne8
Mg2
N2
Al3
N3
N4
N5
Mg10
Si2
O2
O3
Si4
O4
O6
O7
O8
log f(M_i)
C(1.4,−1.3)
C(1.4,−1.9)
0
−1
−2
−3
−5
−4
1
2
log U

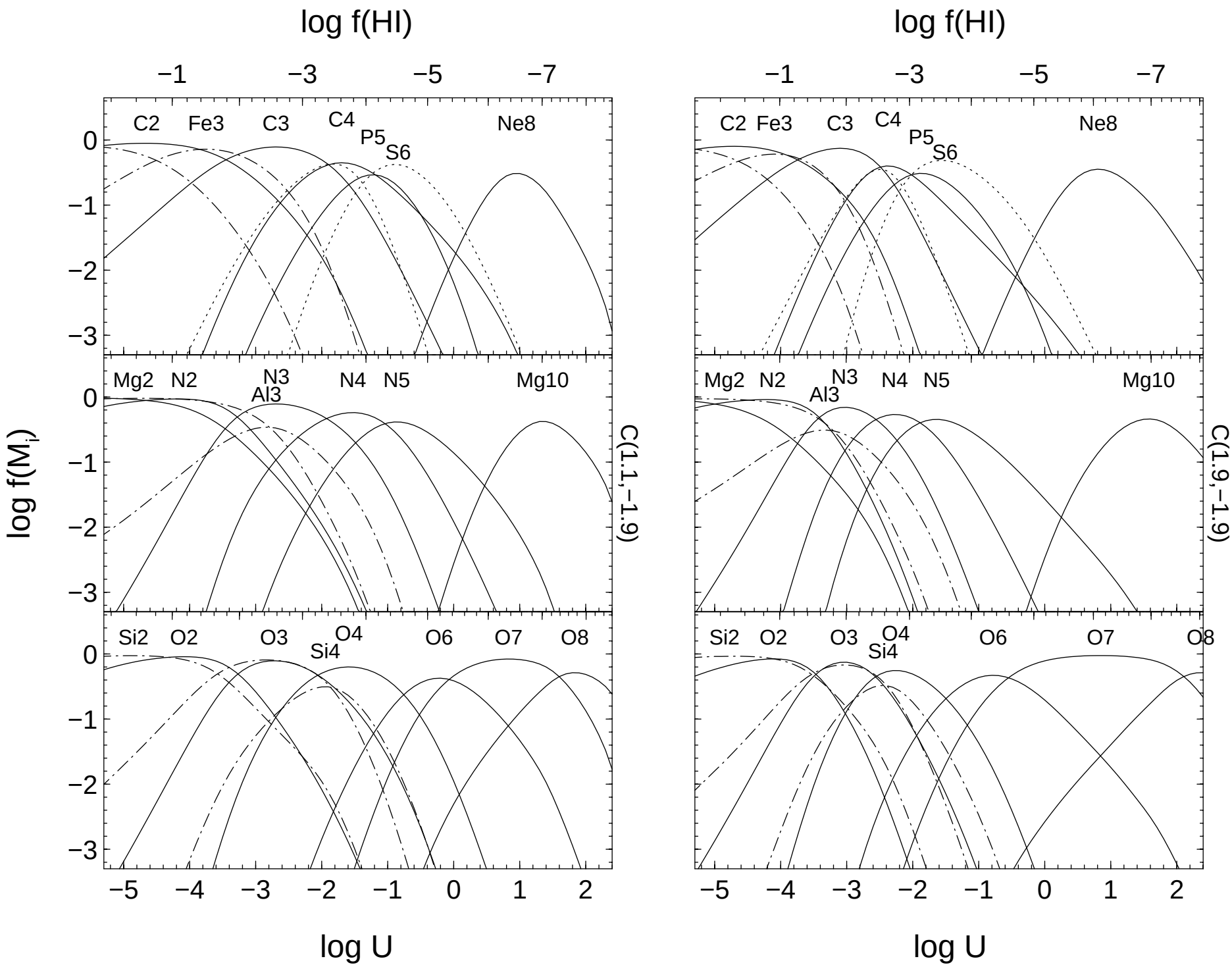
log f(HI)
−1
−3
−5
−7
C2
Fe3
C3
C4
P5
S6
Ne8
Mg2
N2
N3
Al3
N4
N5
Mg10
Si2
O2
O3
Si4
O4
O6
O7
O8
log f(M_i)
C(1.1,−1.9)
C(1.9,−1.9)
log U
0
−1
−2
−3
−4
−5
1
2

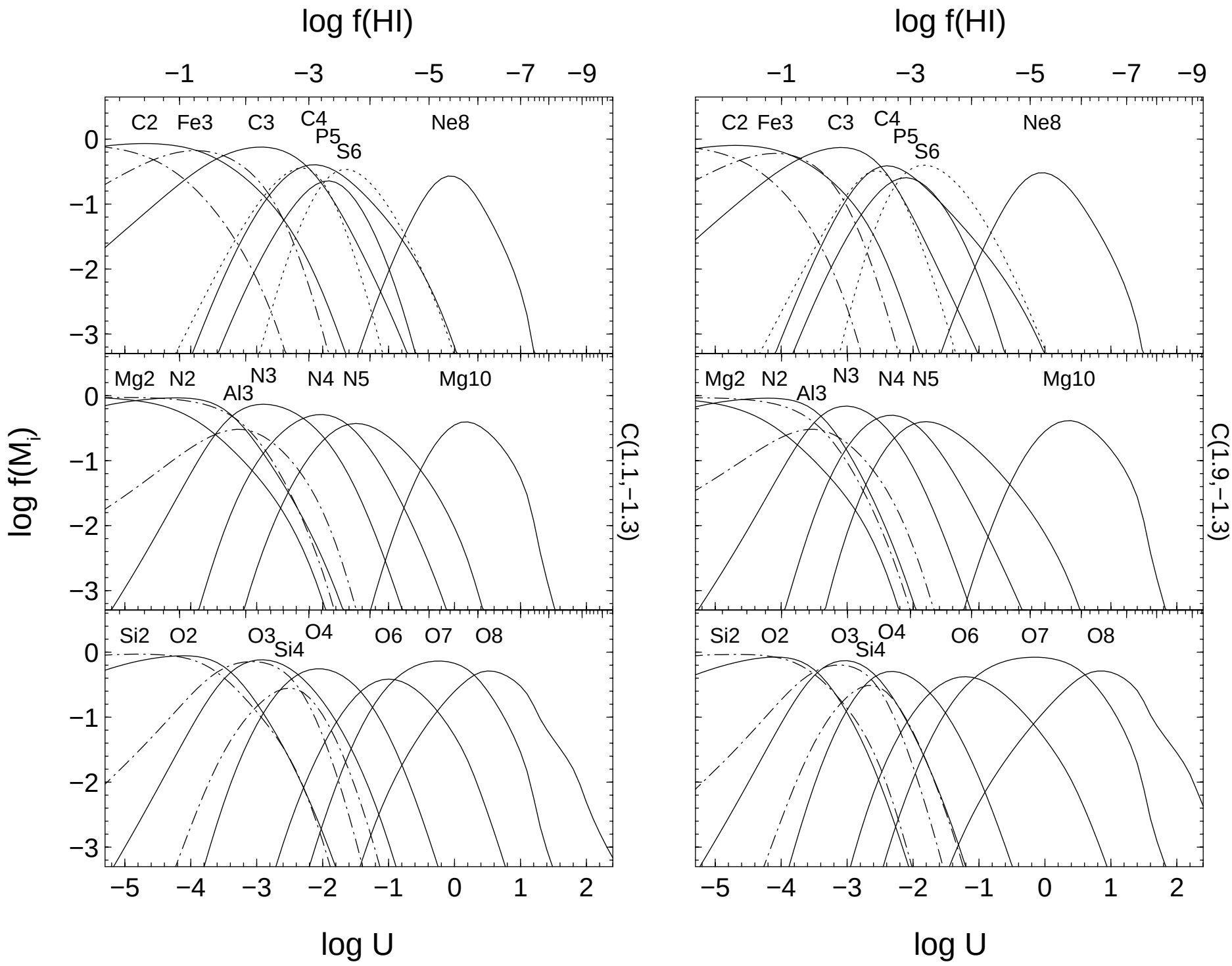
log f(HI)
−1
−3
−5
−7
−9
C2
Fe3
C3
C4
P5
S6
Ne8
Mg2
N2
Al3
N3
N4
N5
Mg10
Si2
O2
O3
Si4
O4
O6
O7
O8
log f(M_i)
C(1.1,−1.3)
C(1.9,−1.3)
0
−1
−2
−3
−5
−4
−3
−2
−1
0
1
2
log U

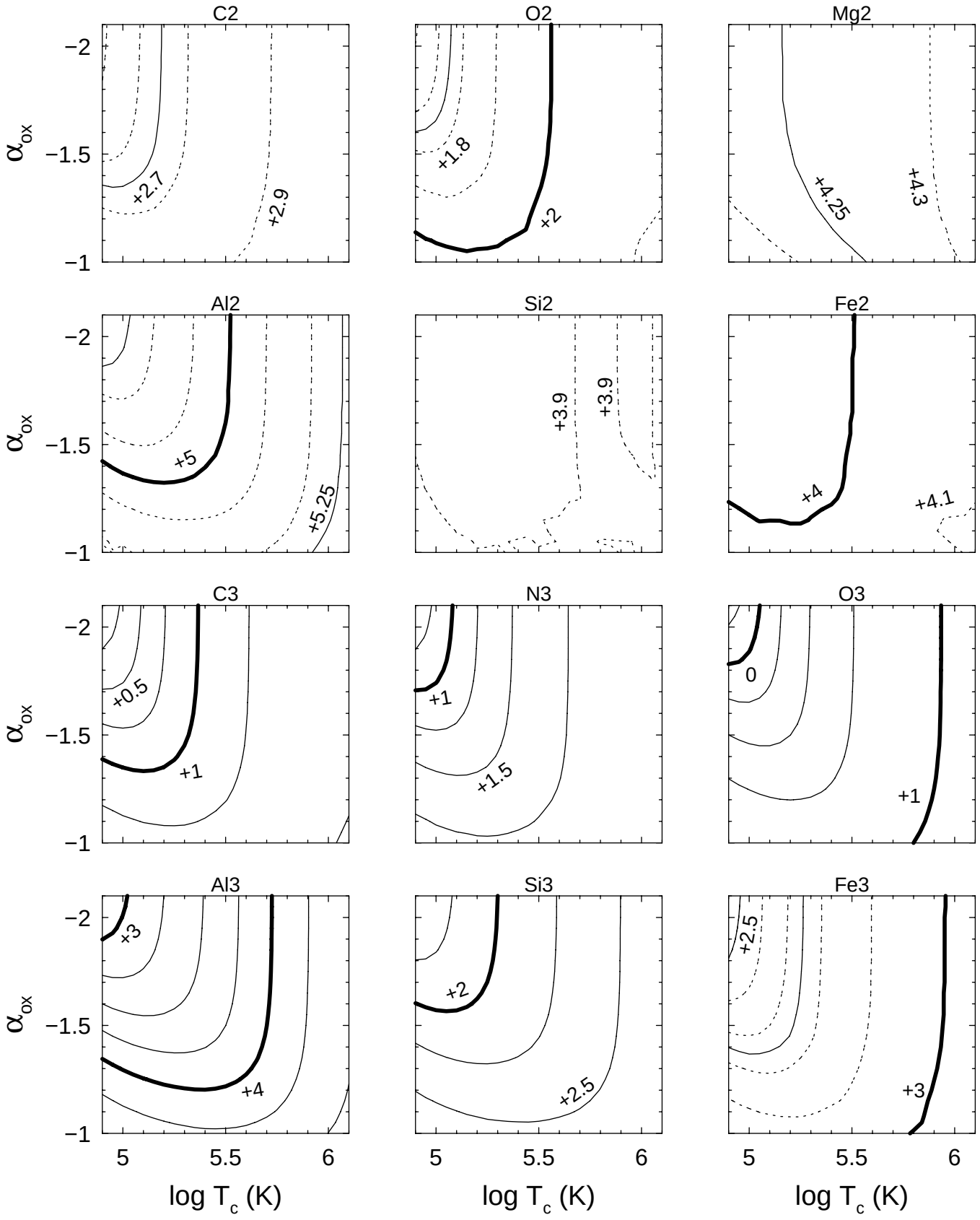
C2
+2.7
+2.9
O2
+1.8
+2
Mg2
+4.25
+4.3
Al2
+5
+5.25
Si2
+3.9
+3.9
Fe2
+4
+4.1
C3
+0.5
+1
N3
+1
+1.5
O3
0
+1
Al3
+3
+4
Si3
+2
+2.5
Fe3
+2.5
+3
−2
−1.5
−1
5
5.5
6
α_ox
log T_c (K)

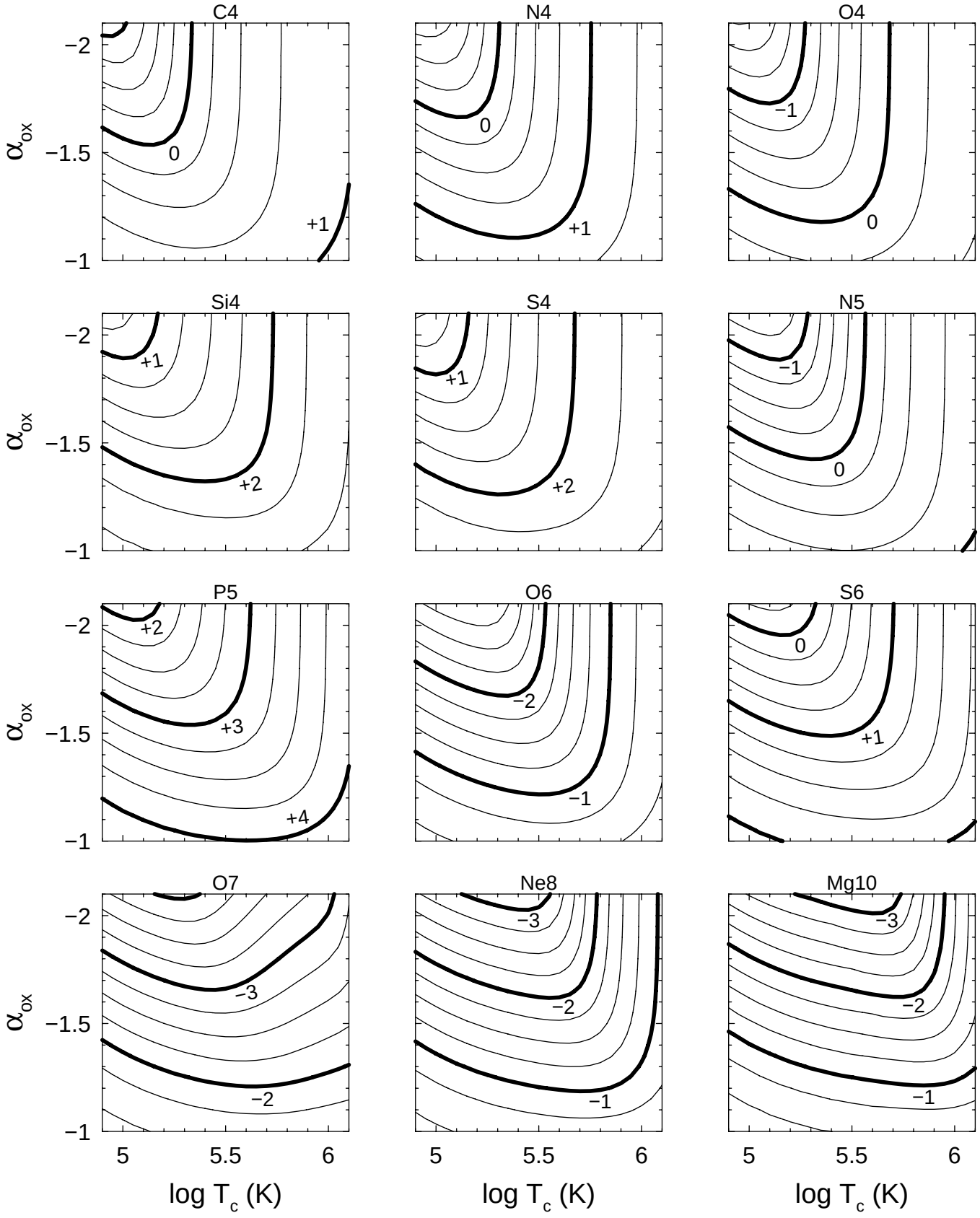
C4
N4
O4
Si4
S4
N5
P5
O6
S6
O7
Ne8
Mg10
α_ox
−2
−1.5
−1
5
5.5
6
log T_c (K)
0
+1
−1
+2
+3
+4
−2
−3

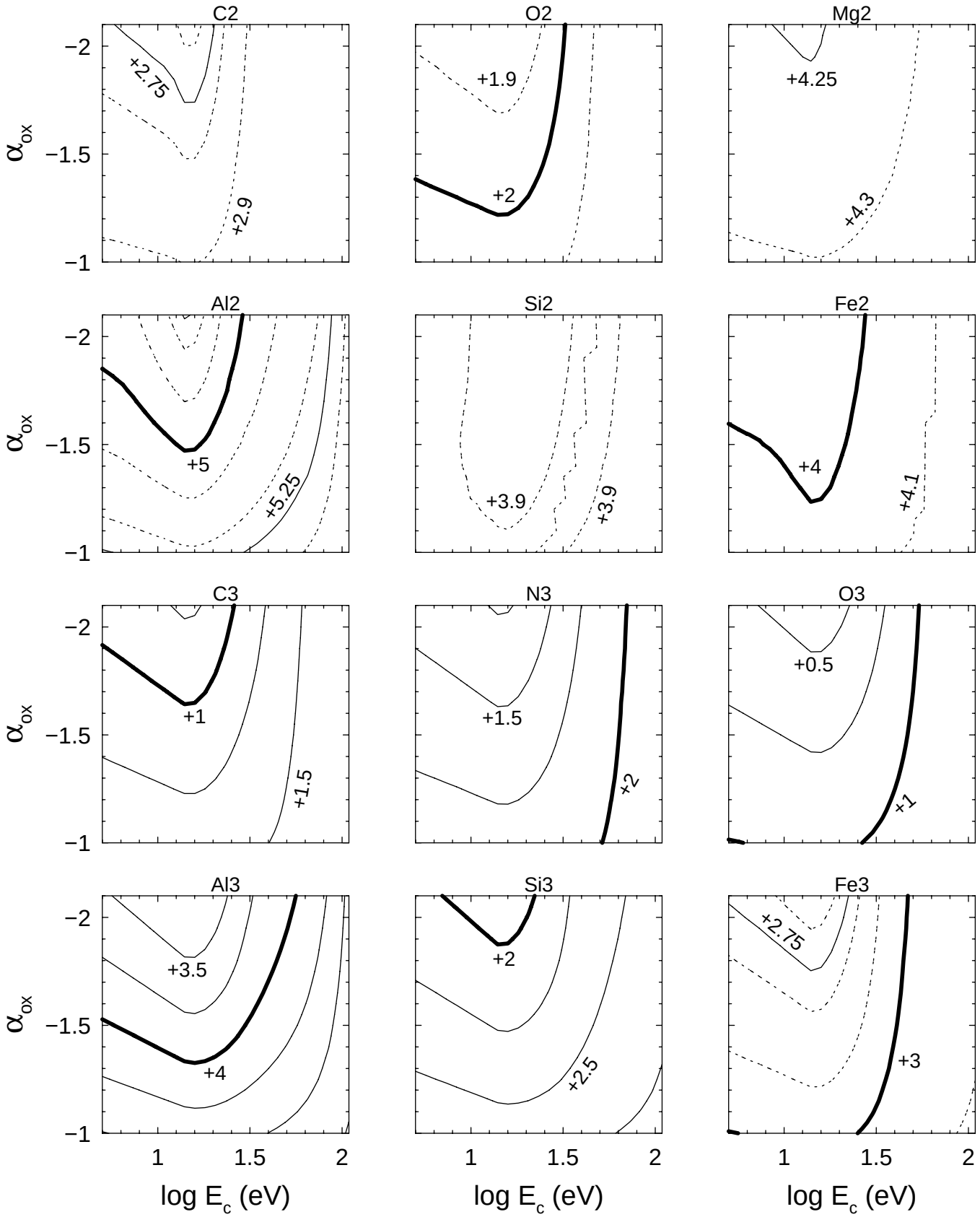
C2
+2.75
+2.9
O2
+1.9
+2
Mg2
+4.25
+4.3
Al2
+5
+5.25
Si2
+3.9
+3.9
Fe2
+4
+4.1
C3
+1
+1.5
N3
+1.5
+2
O3
+0.5
+1
Al3
+3.5
+4
Si3
+2
+2.5
Fe3
+2.75
+3
−2
−1.5
−1
1
1.5
2
α_{ox}
log E_c (eV)

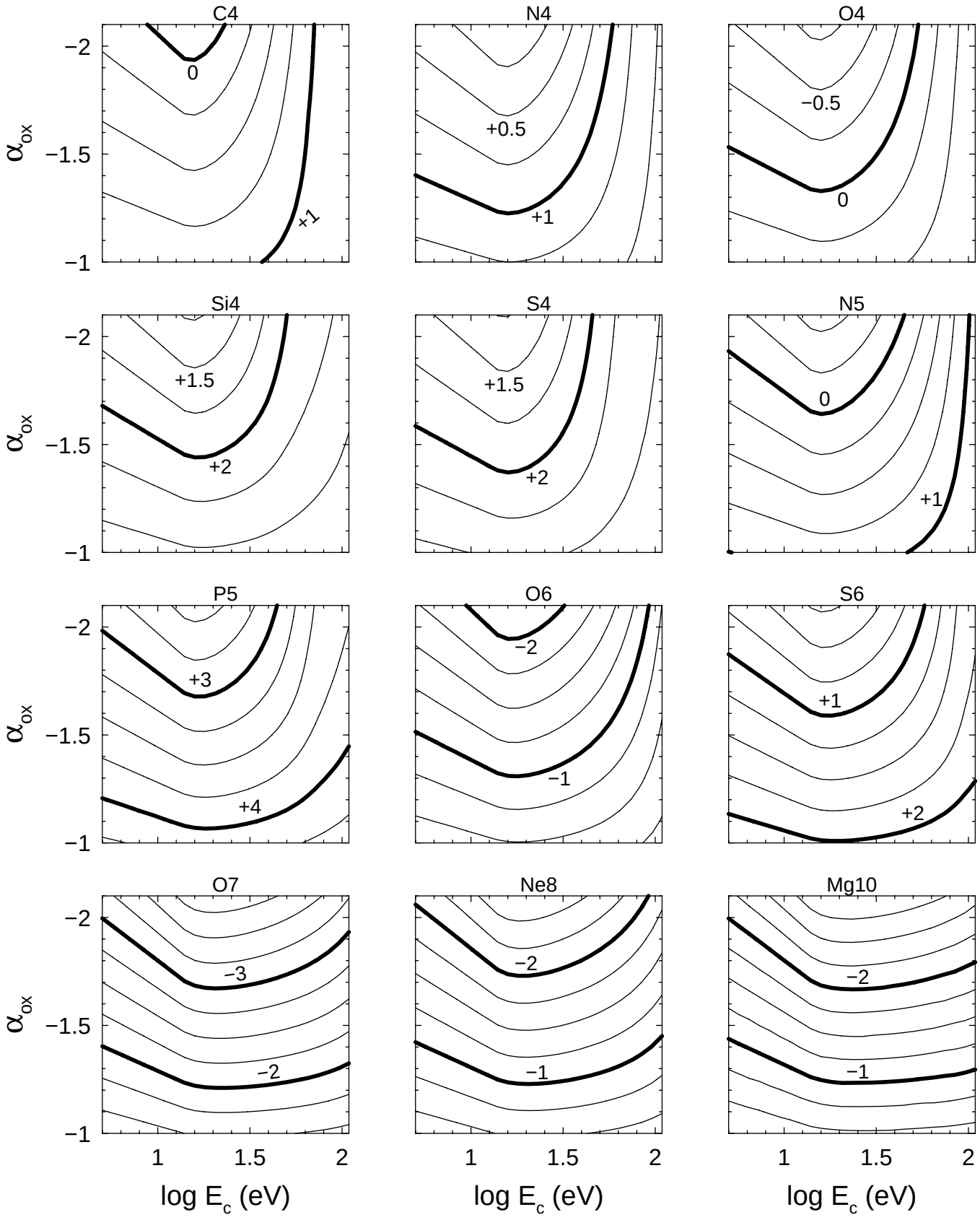
C4
N4
O4
Si4
S4
N5
P5
O6
S6
O7
Ne8
Mg10
0
+0.5
−0.5
+1
+1.5
+2
+3
+4
−1
−2
−3
α_ox
−2
−1.5
−1
1
1.5
2
log E_c (eV)

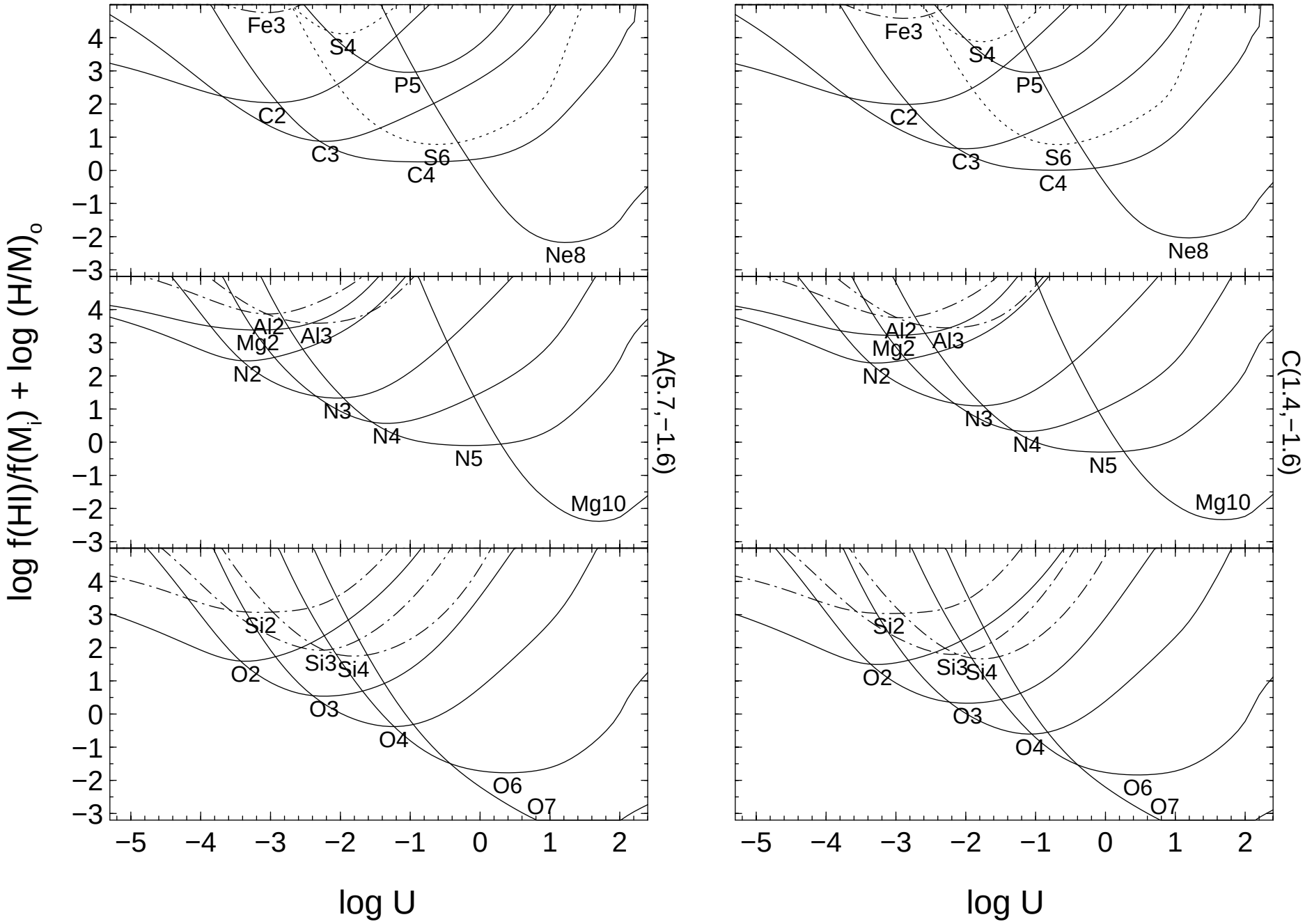
log f(HI)/f(M_i) + log (H/M)_o
log U
log U
A(5.7,−1.6)
C(1.4,−1.6)
Fe3
S4
P5
C2
C3
S6
C4
Ne8
Al2
Mg2
Al3
N2
N3
N4
N5
Mg10
Si2
Si3
Si4
O2
O3
O4
O6
O7

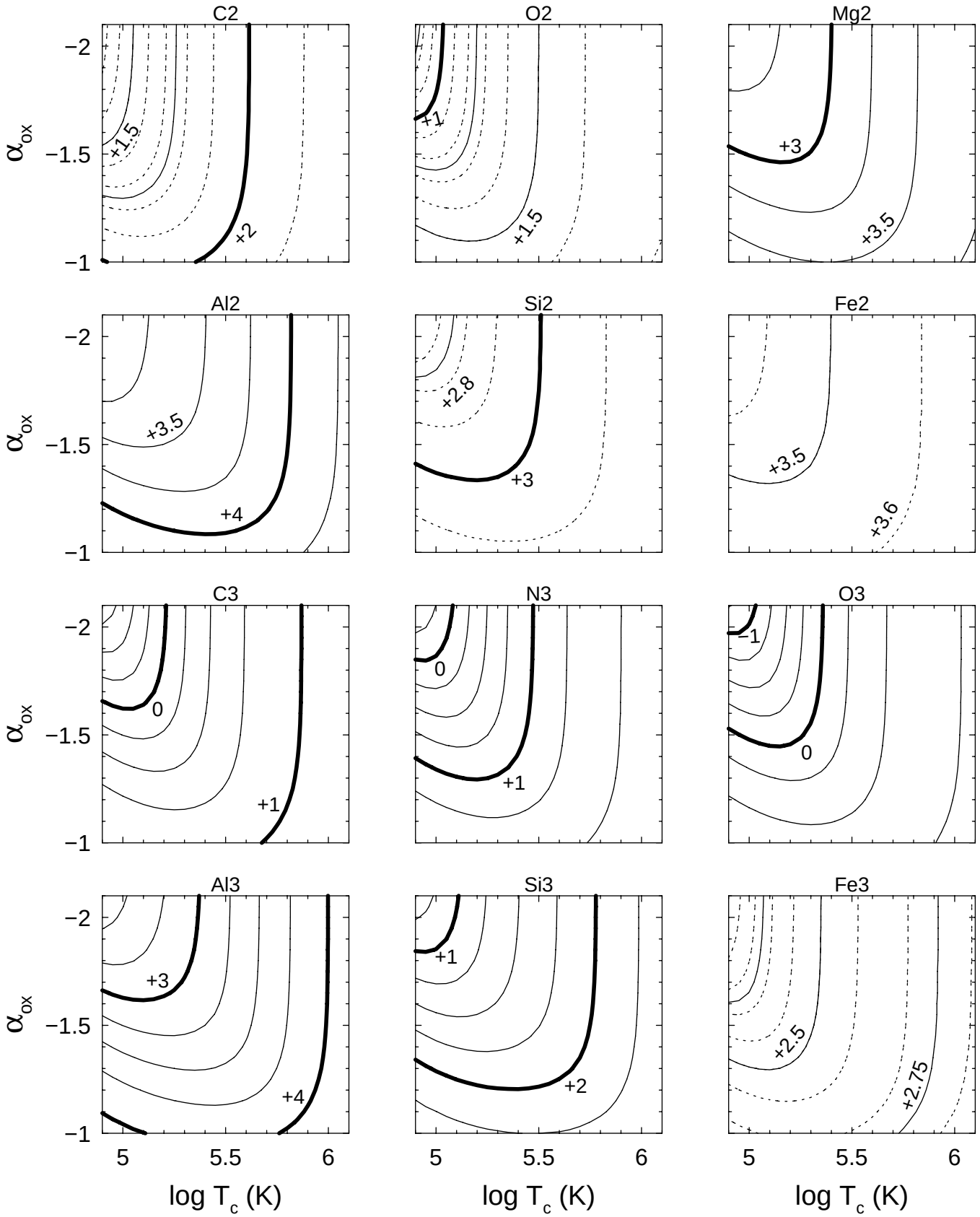
C2
+1.5
+2
O2
+1
+1.5
Mg2
+3
+3.5
Al2
+3.5
+4
Si2
+2.8
+3
Fe2
+3.5
+3.6
C3
0
+1
N3
0
+1
O3
−1
0
Al3
+3
+4
Si3
+1
+2
Fe3
+2.5
+2.75
−2
−1.5
−1
α_{ox}
5
5.5
6
log T_c (K)

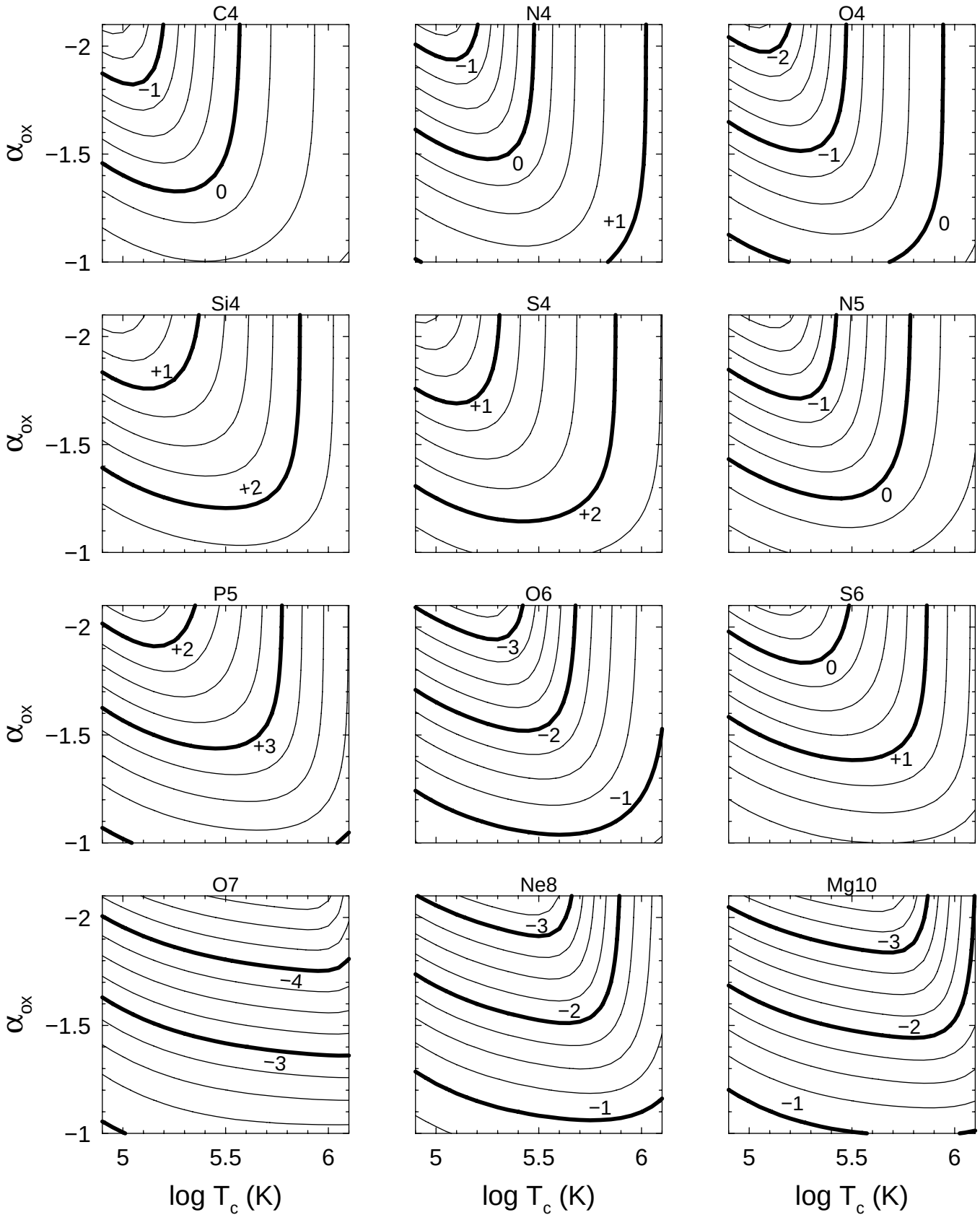
C4
N4
O4
Si4
S4
N5
P5
O6
S6
O7
Ne8
Mg10
α_ox
−2
−1.5
−1
5
5.5
6
log T_c (K)
−1
0
+1
+2
+3
−4
−3
−2

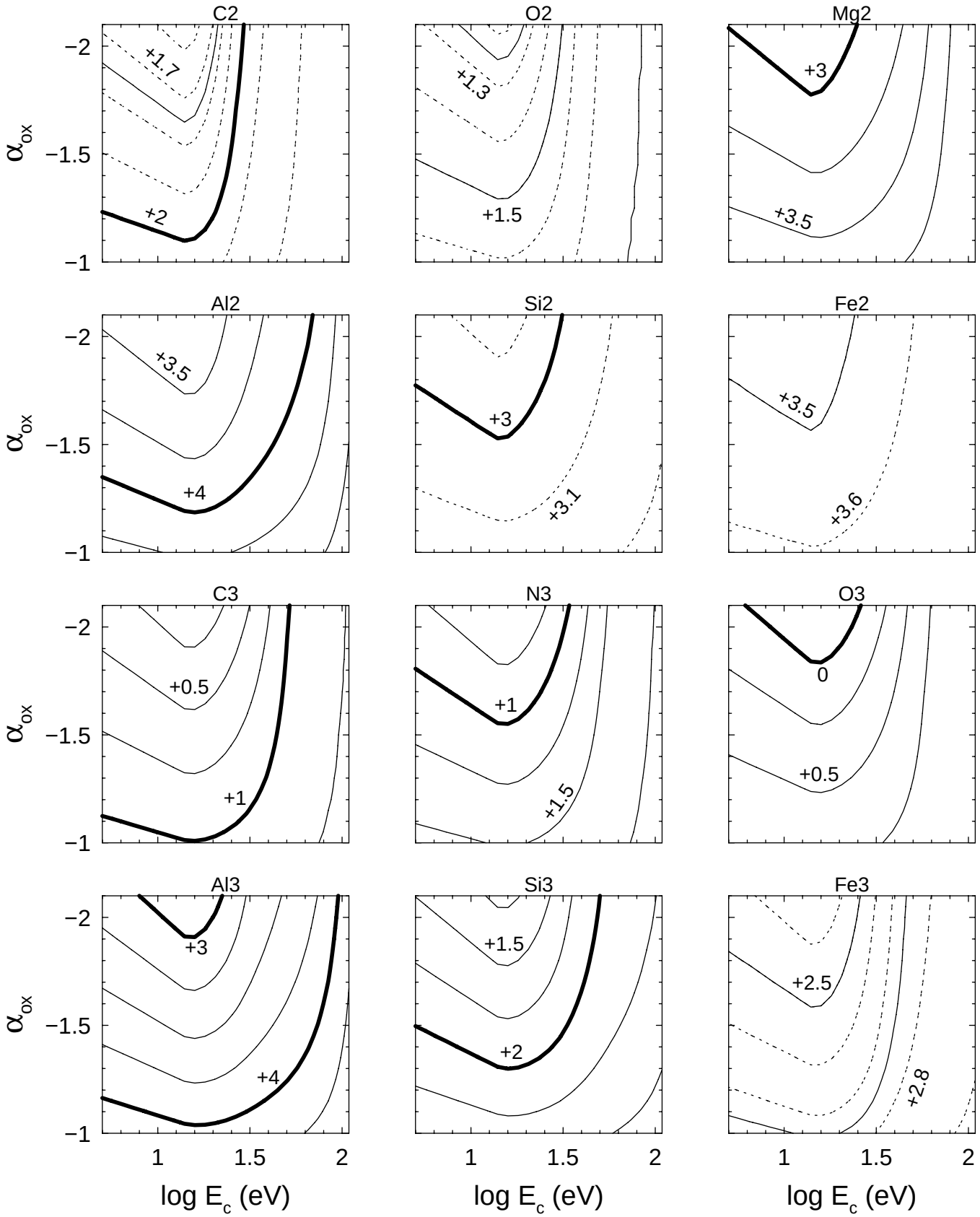
C2
+1.7
+2
O2
+1.3
+1.5
Mg2
+3
+3.5
Al2
+3.5
+4
Si2
+3
+3.1
Fe2
+3.5
+3.6
C3
+0.5
+1
N3
+1
+1.5
O3
0
+0.5
Al3
+3
+4
Si3
+1.5
+2
Fe3
+2.5
+2.8
α_{ox}
−2
−1.5
−1
1
1.5
2
log E_c (eV)

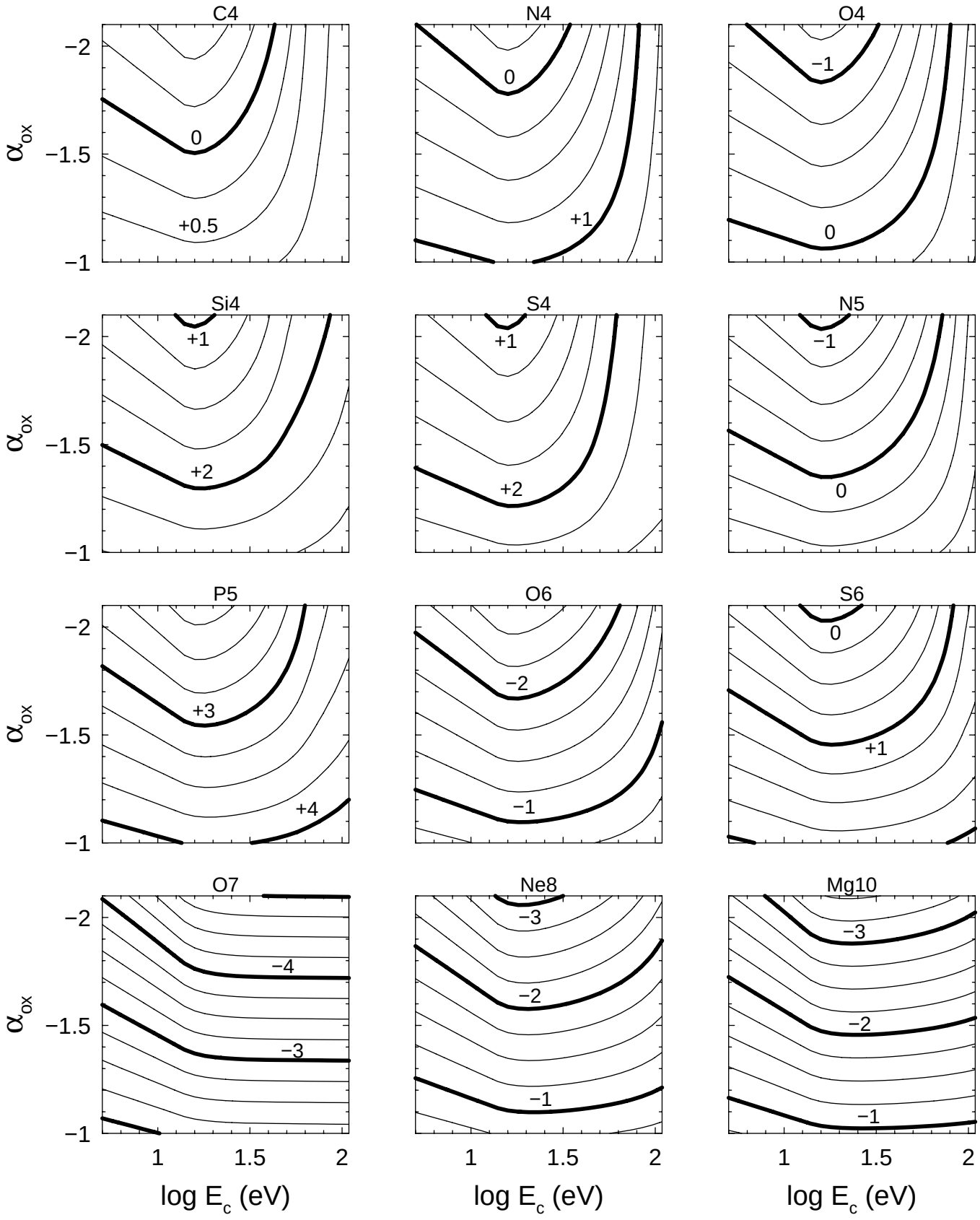
C4
N4
O4
Si4
S4
N5
P5
O6
S6
O7
Ne8
Mg10
α_ox
log E_c (eV)
−2
−1.5
−1
1
1.5
2
0
+0.5
+1
−1
+2
−2
+3
+4
−3
−4

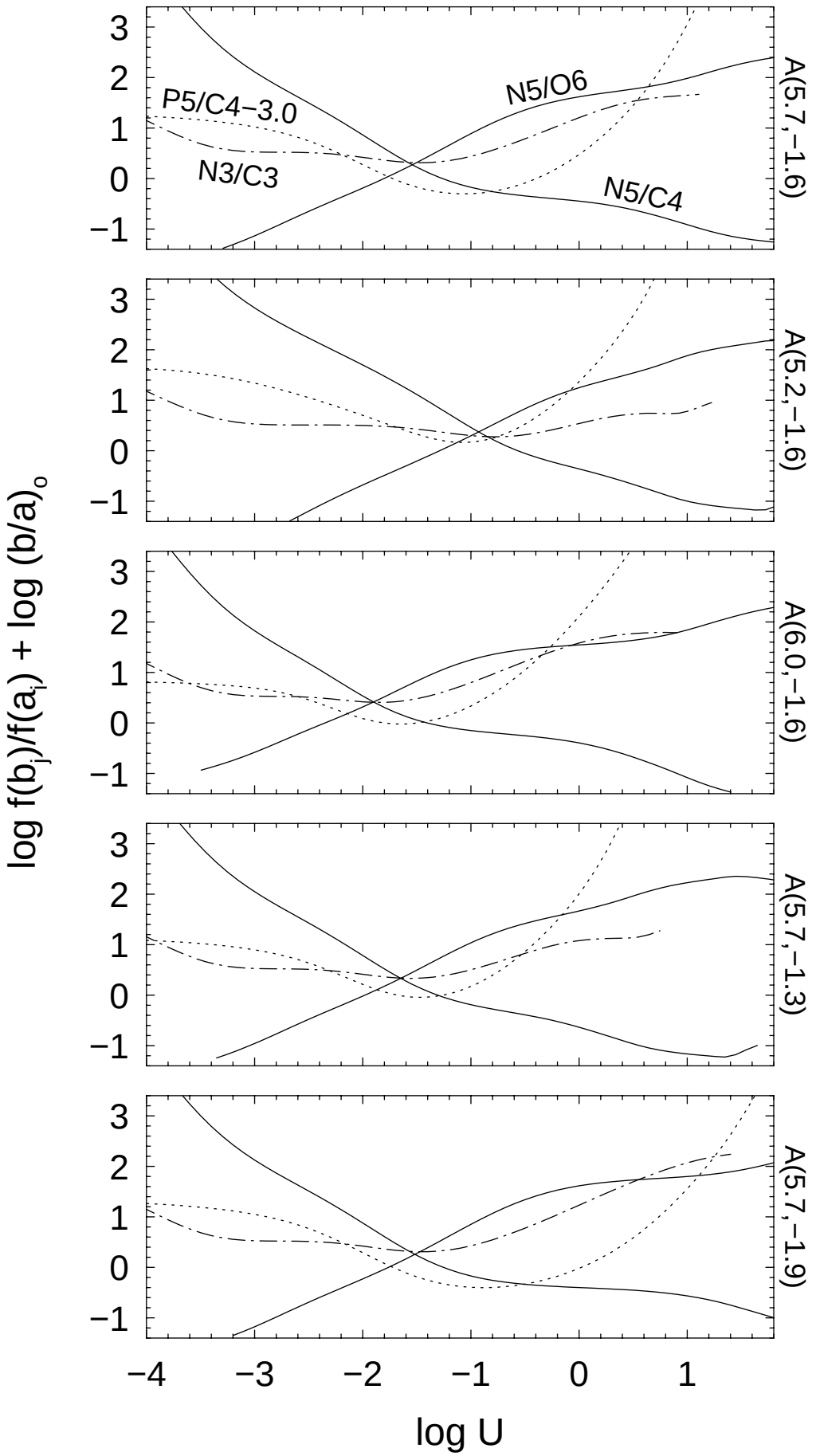
log f(b_j)/f(a_i) + log (b/a)_o
log U
P5/C4−3.0
N3/C3
N5/O6
N5/C4
A(5.7,−1.6)
A(5.2,−1.6)
A(6.0,−1.6)
A(5.7,−1.3)
A(5.7,−1.9)

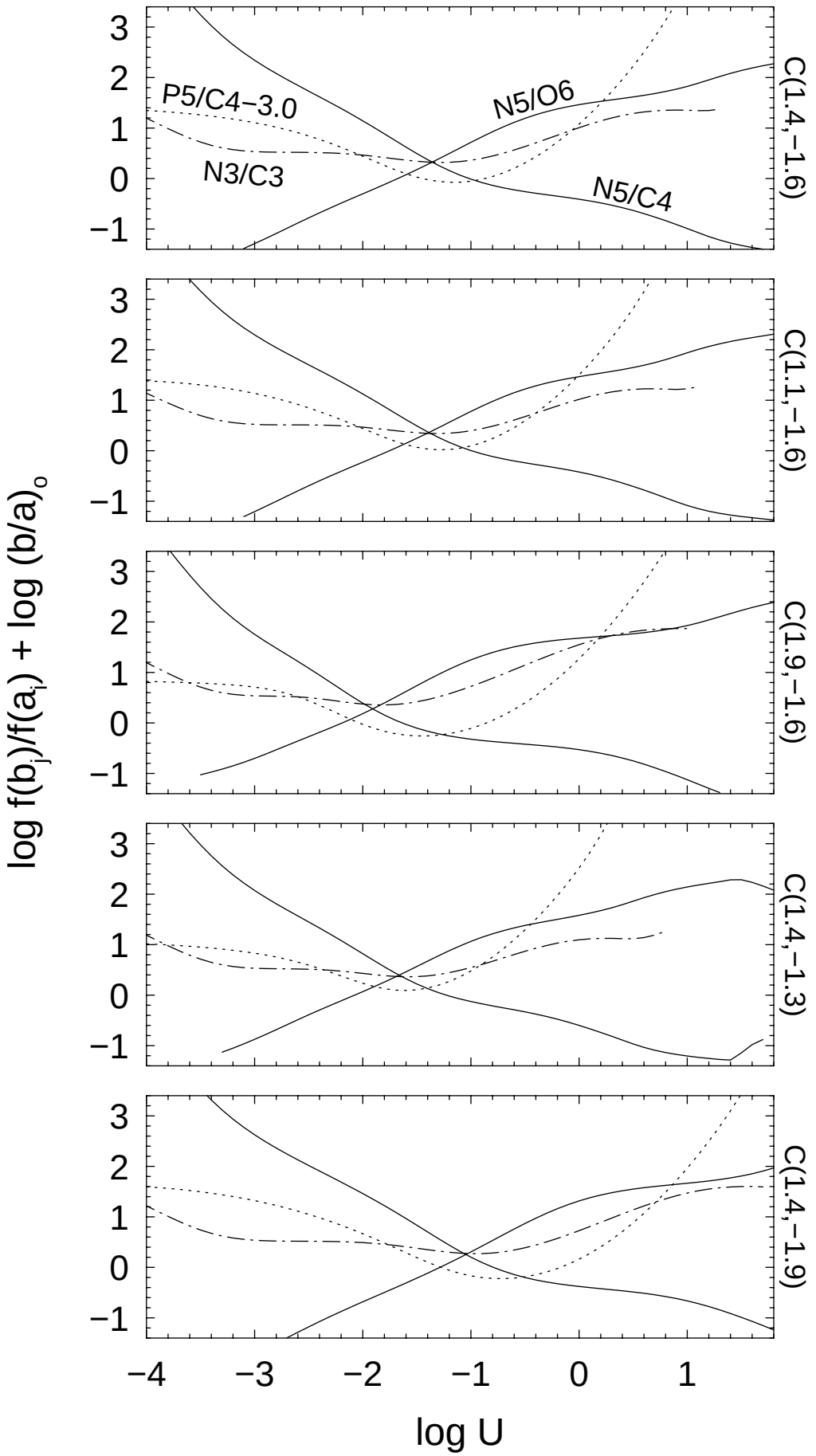
P5/C4−3.0
N5/O6
N3/C3
N5/C4
C(1.4,−1.6)
C(1.1,−1.6)
C(1.9,−1.6)
C(1.4,−1.3)
C(1.4,−1.9)
log f(b_j)/f(a_i) + log (b/a)_o
log U
3
2
1
0
−1
−4
−3
−2
−1
0
1

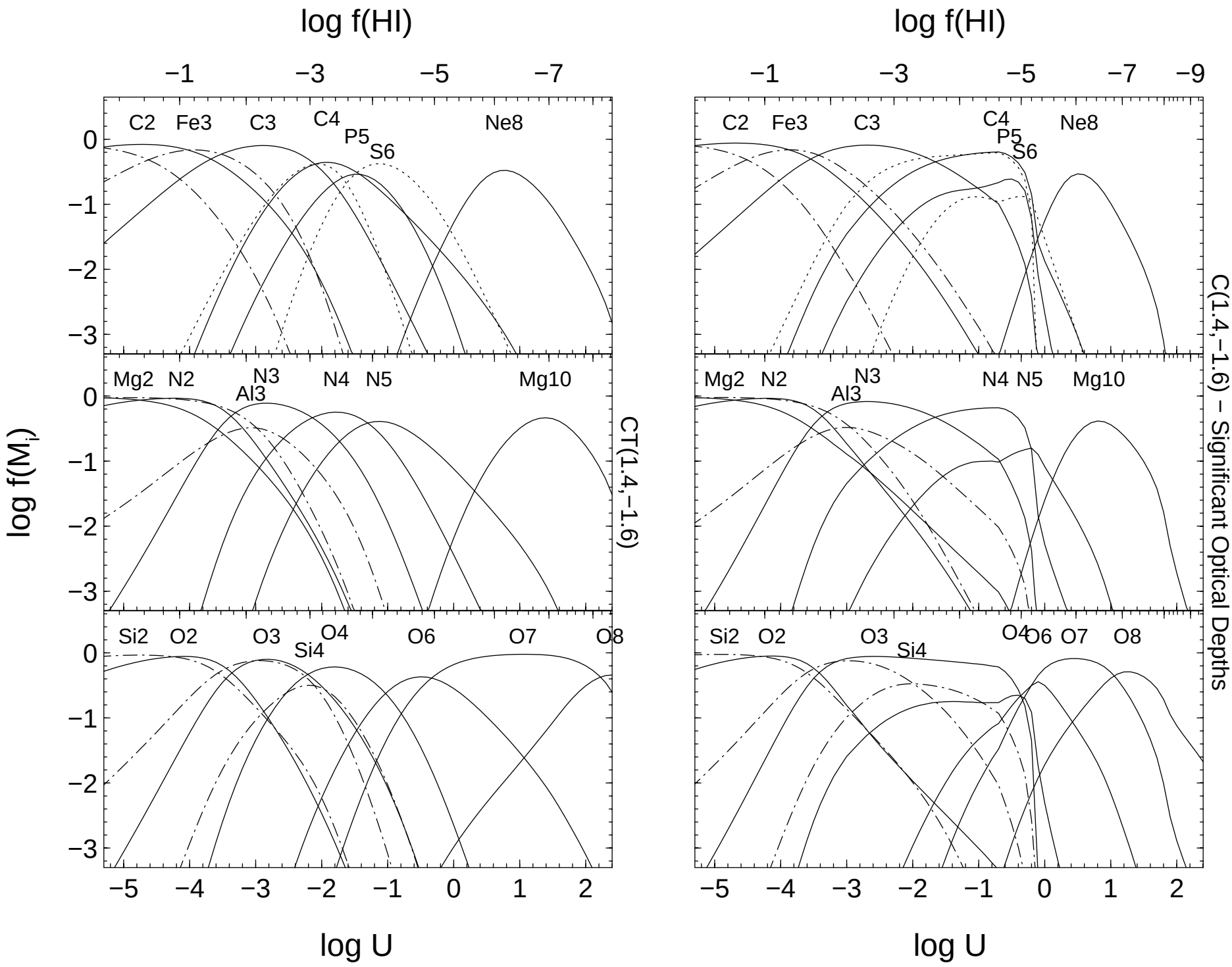
log f(HI)
−1
−3
−5
−7
−9
C2
Fe3
C3
C4
P5
S6
Ne8
Mg2
N2
N3
Al3
N4
N5
Mg10
Si2
O2
O3
Si4
O4
O6
O7
O8
log f(M_i)
CT(1.4,−1.6)
C(1.4,−1.6) − Significant Optical Depths
log U
0
−1
−2
−3
−4
1
2

TABLE 3

Derived Metal Abundances

			Continuum A		Continuum C			
Ion	log N	peak?	[M/H]	log U	[M/H]	log U	[M/H]$_{min}$	log U_{min}
Q 0000−263 ($z_a = 4.0606$, $\Delta v = -2960$)					log N(HI) = $15.2^{+0.8}_{-0.2}$			
C2	<13.3		–	–	–	–	–	–
C4	$13.1^{+0.2}_{-0.0}$	p	$-2.2^{+1.0}_{-0.7}$	$-1.5^{-0.7}_{+0.7}$	$-2.0^{+0.9}_{-0.1}$	$-1.6^{-0.7}_{+0.1}$	$-2.5^{+1.1}_{-0.1}$	$-0.3^{-0.7}_{+0.1}$
N5	<13.1		–	–	–	–	–	–
Si2	<12.7		–	–	–	–	–	–
Si3	<12.6		–	–	–	–	–	–
Si4	<12.9		–	–	–	–	–	–
Q 0000−263 ($z_a = 4.0617$, $\Delta v = -2890$)					log N(HI) = $15.1^{+0.9}_{-0.1}$			
C2	<13.5		–	–	–	–	–	–
C4	$13.7^{+0.2}_{-0.2}$	p	$-1.5^{+1.0}_{-0.7}$	$-1.5^{-0.7}_{+0.7}$	$-1.3^{+0.9}_{-0.1}$	$-1.6^{-0.7}_{+0.1}$	$-1.8^{+1.1}_{-0.1}$	$-0.3^{-0.7}_{+0.1}$
N5	<13.1		–	–	–	–	–	–
Q 0000−263 ($z_a = 4.0688$, $\Delta v = -2480$)					log N(HI) = $15.0^{+1.7}_{-0.5}$			
C2	<13.2		–	–	–	–	–	–
C4	$13.5^{+0.1}_{-0.0}$	p	$-1.6^{+1.0}_{-0.7}$	$-1.5^{-0.7}_{+0.7}$	$-1.4^{+0.9}_{-0.1}$	$-1.6^{-0.7}_{+0.1}$	$-1.9^{+1.1}_{-0.1}$	$-0.3^{-0.7}_{+0.1}$
N5	<13.0		–	–	–	–	–	–
Q 0000−263 ($z_a = 4.1010$, $\Delta v = -590$)					log N(HI) = $14.4^{+1.4}_{-0.1}$			
C2	<13.7		–	–	–	–	–	–
C4	$13.5^{+0.0}_{-0.2}$	p	$-1.0^{+1.0}_{-0.7}$	$-1.5^{-0.7}_{+0.7}$	$-0.8^{+0.9}_{-0.1}$	$-1.6^{-0.7}_{+0.1}$	$-1.3^{+1.1}_{-0.1}$	$-0.3^{-0.7}_{+0.1}$
N5	<13.1		–	–	–	–	–	–
Si2	<12.7		–	–	–	–	–	–
Si3	<13.2		–	–	–	–	–	–
Si4	$13.0^{+0.1}_{-0.0}$	p	$-0.1^{+1.1}_{-0.4}$	$-1.8^{-0.8}_{+0.4}$	$+0.1^{+0.7}_{-0.1}$	$-1.9^{-0.5}_{+0.1}$	$-0.2^{+0.9}_{-0.1}$	$-1.4^{-0.6}_{+0.1}$
Q 0000−263 ($z_a = 4.1260$, $\Delta v = +880$)					log N(HI) = $13.8^{+0.1}_{-0.2}$			
C2	<13.5		–	–	–	–	–	–
C4	$13.6^{+0.1}_{-0.0}$	p	$-0.3^{+1.0}_{-0.7}$	$-1.5^{-0.7}_{+0.7}$	$-0.1^{+0.9}_{-0.1}$	$-1.6^{-0.7}_{+0.1}$	$-0.6^{+1.1}_{-0.1}$	$-0.3^{-0.7}_{+0.1}$
N5	<13.2		–	–	–	–	–	–
Si2	<12.8		–	–	–	–	–	–
Si3	$12.4^{+0.2}_{-0.2}$	p	$+0.6^{+0.6}_{-0.3}$	$-2.7^{-0.3}_{+0.2}$	$+0.6^{+0.6}_{-0.1}$	$-2.8^{-0.2}_{+0.1}$	$+0.1^{+0.7}_{-0.1}$	$-1.9^{-0.5}_{+0.1}$
Si4	<12.9		–	–	–	–	–	–

TABLE 3 (*cont.*)

			Continuum A		Continuum C			
Ion	log N	peak?	[M/H]	log U	[M/H]	log U	[M/H]$_{min}$	log U_{min}
Q 0000−263 ($z_a = 4.1270$, $\Delta v = +940$)					log N(HI) = $12.7^{+0.4}_{-0.2}$			
C2	<13.7		–	–	–	–	–	–
C4	$13.3^{+0.1}_{-0.1}$	p	$+0.5^{+1.0}_{-0.7}$	$-1.5^{-0.7}_{+0.7}$	$+0.7^{+0.9}_{-0.1}$	$-1.6^{-0.7}_{+0.1}$	$+0.2^{+1.1}_{-0.1}$	$-0.3^{-0.7}_{+0.1}$
N5	<13.2		–	–	–	–	–	–
Si2	<12.8		–	–	–	–	–	–
Si3	<13.7		–	–	–	–	–	–
Si4	<12.9		–	–	–	–	–	–
Q 0000−263 ($z_a = 4.1297$, $\Delta v = +1100$)					log N(HI) = $14.6^{+0.7}_{-0.3}$			
C2	<13.5		–	–	–	–	–	–
C4	$13.5^{+0.4}_{-0.2}$	p	$-1.2^{+1.0}_{-0.7}$	$-1.5^{-0.7}_{+0.7}$	$-1.0^{+0.9}_{-0.1}$	$-1.6^{-0.7}_{+0.1}$	$-1.5^{+1.1}_{-0.1}$	$-0.3^{-0.7}_{+0.1}$
N5	<13.0		–	–	–	–	–	–
O6	$14.1^{+0.1}_{-0.1}$	p	$-2.9^{+1.7}_{-0.3}$	$+0.4^{-1.5}_{+0.2}$	$-2.4^{+0.9}_{-0.1}$	$-0.2^{-0.7}_{+0.2}$	$-2.8^{+0.8}_{-0.2}$	$+0.8^{-0.4}_{+0.4}$
Si2	<12.8		–	–	–	–	–	–
Si3	<12.3		–	–	–	–	–	–
Si4	<12.8		–	–	–	–	–	–
Q 0000−263 ($z_a = 4.1310$, $\Delta v = +1170$)[a]					log N(HI) < 14.5			
C2	<13.5		–	–	–	–	–	–
C4	$14.3^{+1.7}_{-0.3}$	p	$-0.3^{+1.0}_{-0.7}$	$-1.5^{-0.7}_{+0.7}$	$-0.1^{+0.9}_{-0.1}$	$-1.6^{-0.7}_{+0.1}$	$-0.6^{+1.1}_{-0.1}$	$-0.3^{-0.7}_{+0.1}$
N5	$13.1^{+0.2}_{-0.1}$	p	$-2.2^{+1.6}_{-0.3}$	$-0.4^{-1.2}_{+0.4}$	$-1.7^{+1.0}_{-0.1}$	$-0.8^{-0.8}_{+0.1}$	$-2.2^{+1.0}_{-0.2}$	$+0.4^{-0.4}_{+0.1}$
Si2	<12.8		–	–	–	–	–	–
Si3	<13.4		–	–	–	–	–	–
Si4	$12.9^{+0.1}_{-0.1}$	p	$-0.3^{+1.1}_{-0.4}$	$-1.8^{-0.8}_{+0.4}$	$-0.1^{+0.7}_{-0.1}$	$-1.9^{-0.5}_{+0.1}$	$-0.4^{+0.9}_{-0.1}$	$-1.4^{-0.6}_{+0.1}$
Q 0000−263 ($z_a = 4.1323$, $\Delta v = +1250$)[a]					log N(HI) < 14.9			
C2	<13.5		–	–	–	–	–	–
C4	$14.5^{+0.4}_{-0.3}$	p	$-0.5^{+1.0}_{-0.7}$	$-1.5^{-0.7}_{+0.7}$	$-0.3^{+0.9}_{-0.1}$	$-1.6^{-0.7}_{+0.1}$	$-0.8^{+1.1}_{-0.1}$	$-0.3^{-0.7}_{+0.1}$
N5	$13.2^{+0.1}_{-0.2}$	p	$-2.5^{+1.6}_{-0.3}$	$-0.4^{-1.2}_{+0.4}$	$-2.0^{+1.0}_{-0.1}$	$-0.8^{-0.8}_{+0.1}$	$-2.5^{+1.0}_{-0.2}$	$+0.4^{-0.4}_{+0.1}$
Si2	<12.8		–	–	–	–	–	–
Si3	$12.2^{+0.3}_{-0.2}$	p	$-0.7^{+0.6}_{-0.3}$	$-2.7^{-0.3}_{+0.2}$	$-0.7^{+0.6}_{-0.1}$	$-2.8^{-0.2}_{+0.1}$	$-1.2^{+0.7}_{-0.1}$	$-1.9^{-0.5}_{+0.1}$
Si4	<12.8		–	–	–	–	–	–

TABLE 3 (*cont.*)

Ion	log N	peak?	Continuum A [M/H]	Continuum A log U	Continuum C [M/H]	Continuum C log U	Continuum C [M/H]$_{min}$	Continuum C log U_{min}
Q 0000−263 ($z_a = 4.1334$, $\Delta v = +1310$)[a]	log N(HI) < 14.0							
C2	<13.5		–	–	–	–	–	–
C4	$14.0^{+1.5}_{-0.3}$		$+0.0^{+1.1}_{-0.4}$	$-1.5^{-0.7}_{+0.4}$	$+0.0^{+1.0}_{-0.0}$	$-1.5^{-0.5}_{+0.0}$	$-0.4^{+1.1}_{-0.1}$	$-0.3^{-0.7}_{+0.1}$
N5	$13.1^{+0.2}_{-0.1}$		$+0.5^{+0.3}_{-0.5}$	"	$+0.1^{+0.5}_{-0.0}$	"	$-1.7^{+1.0}_{-0.2}$	$+0.4^{-0.4}_{+0.1}$
Si2	<12.8		–	–	–	–	–	–
Si3	$12.5^{+0.0}_{-0.2}$		$+0.1^{+1.0}_{-0.5}$	"	$+0.1^{+0.9}_{-0.0}$	"	$+0.0^{+0.7}_{-0.1}$	$-1.9^{-0.5}_{+0.1}$
Si4	$12.8^{+0.2}_{-0.0}$		$+0.0^{+1.1}_{-0.4}$	"	$+0.1^{+0.9}_{-0.0}$	"	$+0.0^{+0.9}_{-0.1}$	$-1.4^{-0.6}_{+0.1}$
Q 0000−263 ($z_a = 4.1342$, $\Delta v = +1360$)	log N(HI) = $15.0^{+0.2}_{-0.2}$							
C2	<13.5		–	–	–	–	–	–
C4	$14.7^{+1.3}_{-0.4}$		$-0.3^{+1.1}_{-0.4}$	$-1.5^{-0.7}_{+0.4}$	$-0.3^{+1.0}_{-0.0}$	$-1.5^{-0.5}_{+0.0}$	$-0.7^{+1.1}_{-0.1}$	$-0.3^{-0.7}_{+0.1}$
N5	$13.3^{+0.3}_{-0.0}$		$-0.3^{+0.3}_{-0.5}$	"	$-0.7^{+0.5}_{-0.0}$	"	$-2.5^{+1.0}_{-0.2}$	$+0.4^{-0.4}_{+0.1}$
Si2	<12.8		–	–	–	–	–	–
Si3	$12.5^{+0.0}_{-0.5}$		$-0.9^{+1.0}_{-0.5}$	"	$-0.9^{+0.9}_{-0.0}$	"	$-1.0^{+0.7}_{-0.1}$	$-1.9^{-0.5}_{+0.1}$
Si4	$12.9^{+0.1}_{-0.1}$		$-0.9^{+1.1}_{-0.4}$	"	$-0.8^{+0.9}_{-0.0}$	"	$-0.9^{+0.9}_{-0.1}$	$-1.4^{-0.6}_{+0.1}$
UM 675 ($z_a = 2.134$, $\Delta v = -1240$)	log N(HI) = 14.8							
C3	13.8	p	$+0.1^{+0.4}_{-0.3}$	$-2.8^{-0.2}_{+0.1}$	$+0.1^{+0.5}_{-0.2}$	$-2.8^{-0.3}_{+0.2}$	$-0.5^{+0.7}_{-0.2}$	$-1.8^{-0.6}_{+0.2}$
C4	14.6	p	$+0.0^{+0.7}_{-0.6}$	$-1.7^{-0.6}_{+0.4}$	$+0.1^{+0.7}_{-0.3}$	$-1.8^{-0.5}_{+0.2}$	$-0.4^{+0.9}_{-0.3}$	$-0.5^{-0.7}_{+0.2}$
N3	14.2	p	$+1.0^{+0.4}_{-0.3}$	$-2.8^{-0.2}_{+0.2}$	$+1.0^{+0.5}_{-0.2}$	$-2.8^{-0.2}_{+0.2}$	$+0.4^{+0.7}_{-0.3}$	$-1.7^{-0.7}_{+0.2}$
N5	14.8	p	$-0.4^{+1.2}_{-0.6}$	$-0.7^{-1.0}_{+0.6}$	$+0.0^{+0.8}_{-0.4}$	$-1.0^{-0.7}_{+0.1}$	$-0.5^{+0.9}_{-0.3}$	$+0.1^{-0.5}_{+0.3}$
O6	15.2	p	$-1.6^{+1.3}_{-0.5}$	$+0.0^{-1.1}_{+0.5}$	$-1.2^{+0.8}_{-0.3}$	$-0.4^{-0.6}_{+0.3}$	$-1.7^{+0.8}_{-0.3}$	$+0.7^{-0.5}_{+0.3}$
Ne8	15.4	p	$-1.6^{+1.0}_{-0.5}$	$+1.0^{-0.9}_{+0.5}$	$-1.4^{+0.7}_{-0.4}$	$+0.8^{-0.5}_{+0.3}$	$-1.7^{+0.7}_{-0.4}$	$+1.3^{-0.3}_{+0.4}$
PKS 0424−131 ($z_a = 2.100$, $\Delta v = -6160$)[a]	log N(HI) < 15.3							
C2	13.5	p	$+1.1^{+0.1}_{-0.1}$	$-4.7^{+0.0}_{-0.0}$	$+1.1^{+0.1}_{-0.1}$	$-4.7^{+0.0}_{-0.0}$	$+0.2^{+0.2}_{-0.2}$	$-2.9^{+0.1}_{-0.2}$
C4	13.7	p	$-0.9^{+0.2}_{-0.9}$	$-2.1^{-0.2}_{+0.7}$	$-1.1^{+0.6}_{-0.3}$	$-1.9^{-0.4}_{+0.1}$	$-1.6^{+0.7}_{-0.3}$	$-0.7^{-0.5}_{+0.1}$
N5	<12.7		–	–	–	–	–	–
O1	<13.1		–	–	–	–	–	–
Si2	12.7	p	$+1.2^{+0.0}_{-0.0}$	$-4.6^{-0.1}_{+0.0}$	$+1.2^{+0.0}_{-0.0}$	$-4.6^{-0.1}_{+0.1}$	$+0.4^{+0.1}_{-0.1}$	$-3.0^{-0.1}_{+0.1}$
Si3	12.8	p	$-0.1^{+0.2}_{-0.4}$	$-2.9^{-0.1}_{+0.2}$	$-0.2^{+0.3}_{-0.2}$	$-2.9^{-0.1}_{+0.1}$	$-0.6^{+0.4}_{-0.3}$	$-2.2^{-0.3}_{+0.2}$
Si4	12.9	p	$-0.4^{+0.4}_{-0.6}$	$-2.3^{-0.3}_{+0.5}$	$-0.5^{+0.5}_{-0.2}$	$-2.2^{-0.3}_{+0.2}$	$-0.7^{+0.5}_{-0.3}$	$-1.7^{-0.5}_{+0.1}$

TABLE 3 (*cont.*)

			Continuum A		Continuum C			
Ion	log N	peak?	[M/H]	log U	[M/H]	log U	[M/H]$_{min}$	log U_{min}
PKS 0424−131 ($z_a = 2.133$, $\Delta v = -3033$)					log N(HI) = 14.5			
C4	13.8	p	$+0.0^{+0.2}_{-0.9}$	$-2.1^{-0.2}_{+0.7}$	$-0.2^{+0.6}_{-0.3}$	$-1.9^{-0.4}_{+0.1}$	$-0.7^{+0.7}_{-0.3}$	$-0.7^{-0.5}_{+0.1}$
N5	14.3	p	$+0.2^{+0.4}_{-1.0}$	$-1.3^{-0.4}_{+0.8}$	$0.0^{+0.6}_{-0.3}$	$-1.1^{-0.6}_{+0.1}$	$-0.5^{+0.7}_{-0.2}$	$+0.0^{-0.4}_{+0.1}$
PKS 0424−131 ($z_a = 2.173$, $\Delta v = +760$)					log N(HI) = 14.9			
C2	<12.6		–	–	–	–	–	–
C4	14.2		$-0.3^{+0.2}_{-0.6}$	$-1.5^{-0.3}_{+0.3}$	$-0.4^{+0.4}_{-0.3}$	$-1.4^{-0.4}_{+0.1}$	$-0.7^{+0.7}_{-0.3}$	$-0.7^{-0.5}_{+0.1}$
N5	>13.3		–	–	–	–	–	–
Si3	12.0		$-0.2^{+0.5}_{-0.4}$	"	$-0.3^{+0.1}_{-0.3}$	"	$-1.1^{+0.4}_{-0.3}$	$-2.2^{-0.3}_{+0.2}$
Si4	12.7		$-0.3^{+0.5}_{-0.3}$	"	$-0.2^{+0.2}_{-0.3}$	"	$-0.5^{+0.5}_{-0.3}$	$-1.7^{-0.5}_{+0.1}$
Q 0450−131 ($z_a = 2.1050$, $\Delta v = -13{,}600$)[a]					log N(HI) < 15.2			
C2	13.3		$+0.3^{+0.1}_{-0.4}$	$-2.5^{-0.2}_{+0.3}$	$+0.2^{+0.3}_{-0.1}$	$-2.5^{-0.2}_{+0.0}$	$+0.1^{+0.2}_{-0.3}$	$-2.8^{-0.2}_{+0.2}$
C4	13.8		$+0.0^{+0.4}_{-0.2}$	"	$+0.2^{+0.1}_{-0.2}$	"	$-1.5^{+0.8}_{-0.4}$	$-0.6^{-0.6}_{+0.3}$
N5	<12.5		–	–	–	–	–	–
O1	<12.8		–	–	–	–	–	–
Si2	12.2:		$+0.1^{+0.2}_{-0.2}$	"	$+0.1^{+0.2}_{-0.0}$	"	$+0.0^{+0.1}_{-0.1}$	$-2.9^{-0.2}_{+0.3}$
Si4	13.1		$+0.3^{+0.3}_{-0.3}$	"	$+0.4^{+0.2}_{-0.2}$	"	$-0.5^{+0.6}_{-0.4}$	$-1.6^{-0.6}_{+0.3}$
Q 0450−131 ($z_a = 2.2302$, $\Delta v = +2100$)[a]					log N(HI) < 14.7			
C2	<12.9		–	–	–	–	–	–
C4	13.7		$-0.7^{+0.4}_{-1.0}$	$-1.1^{-0.4}_{+0.5}$	$-1.0^{+0.9}_{-0.3}$	$-1.0^{-0.4}_{+0.3}$	$-1.1^{+0.8}_{-0.4}$	$-0.6^{-0.6}_{+0.3}$
N5	14.1		$-0.4^{+0.6}_{-0.3}$	"	$-0.5^{+0.7}_{-0.4}$	"	$-1.0^{+0.8}_{-0.4}$	$+0.2^{-0.6}_{+0.2}$
O1	<12.8		–	–	–	–	–	–
Si2	<12.4		–	–	–	–	–	–
Si3	12.2		$+0.7^{+0.7}_{-1.0}$	"	$+0.5^{+1.2}_{-0.1}$	"	$-0.7^{+0.5}_{-0.4}$	$-2.1^{-0.4}_{+0.3}$
Si4	13.3		$+0.7^{+0.8}_{-1.0}$	"	$+0.5^{+1.0}_{-0.3}$	"	$+0.2^{+0.6}_{-0.4}$	$-1.6^{-0.6}_{+0.3}$
HS 1946+7658 ($z_a = 3.03841$, $\Delta v = -930$)					log N(HI) = 14.4			
C4	13.2	p	$-0.5^{+0.2}_{-1.1}$	$-2.1^{-0.1}_{+0.8}$	$-1.0^{+0.8}_{-0.2}$	$-1.7^{-0.6}_{+0.2}$	$-1.5^{+1.0}_{-0.3}$	$-0.2^{-0.8}_{+0.1}$

TABLE 3 (*cont.*)

			Continuum A		Continuum C			
Ion	log N	peak?	[M/H]	log U	[M/H]	log U	[M/H]$_{min}$	log U_{min}
HS 1946+7658 ($z_a = 3.0496$, $\Delta v = -100$)[a]					log N(HI) < 16.5			
C2	13.6		$-0.3^{+0.0}_{-0.6}$	$-2.1^{-0.2}_{+0.3}$	$-0.6^{+0.7}_{-0.3}$	$-1.9^{-0.3}_{+0.0}$	$-1.0^{+0.3}_{-0.3}$	$-2.8^{-0.2}_{+0.2}$
C4	>15.0		$-0.7^{+0.3}_{-0.3}$	"	$-0.9^{+0.4}_{-0.2}$	"	$-1.8^{+1.0}_{-0.3}$	$-0.2^{-0.7}_{+0.1}$
N5	13.6		$-1.7^{+1.3}_{-0.0}$	"	$-0.8^{+0.3}_{-0.3}$	"	$-3.6^{+1.0}_{-0.3}$	$+0.5^{-0.5}_{+0.1}$
O1	<13.6		–	–	–	–	–	–
Al2	11.7		$-0.2^{+0.7}_{-0.7}$	"	$-0.6^{+0.8}_{-0.1}$	"	$-1.1^{+0.5}_{-0.3}$	$-2.8^{-0.4}_{+0.1}$
Al3	12.6		$-0.2^{+0.7}_{-0.7}$	"	$-0.6^{+0.8}_{-0.1}$	"	$-0.6^{+0.7}_{-0.3}$	$-1.9^{-0.6}_{+0.1}$
Si2	12.7		$-0.4^{+0.4}_{-0.4}$	"	$-0.6^{+0.5}_{-0.1}$	"	$-0.8^{+0.2}_{-0.1}$	$-2.7^{-0.4}_{+0.2}$
Si3	>13.7		$-0.8^{+0.6}_{-0.6}$	"	$-1.1^{+0.6}_{-0.2}$	"	$-2.2^{+0.6}_{-0.2}$	$-1.9^{-0.5}_{+0.2}$
Si4	>14.3		$-0.3^{+0.5}_{-0.4}$	"	$-0.5^{+0.5}_{-0.2}$	"	$-0.9^{+0.8}_{-0.3}$	$-1.3^{-0.7}_{+0.1}$
Q 2116−358 ($z_a = 2.306062$, $\Delta v = -3140$)					log N(HI) = 12.0			
C4	12.7	p	$+1.4^{+0.2}_{-1.1}$	$-2.1^{-0.2}_{+0.8}$	$+1.1^{+0.6}_{-0.4}$	$-1.8^{-0.5}_{+0.2}$	$+0.6^{+0.8}_{-0.4}$	$-0.6^{-0.6}_{+0.3}$
N5	13.3	p	$+1.6^{+0.5}_{-1.3}$	$-1.3^{-0.4}_{+1.2}$	$+1.3^{+0.8}_{-0.4}$	$-1.0^{-0.7}_{+0.2}$	$+0.9^{+0.8}_{-0.4}$	$+0.2^{-0.6}_{+0.2}$
Q 2116−358 ($z_a = 2.306251$, $\Delta v = -3120$)					log N(HI) = 13.6			
C4	13.8	p	$+0.9^{+0.2}_{-1.1}$	$-2.1^{-0.2}_{+0.8}$	$+0.6^{+0.6}_{-0.4}$	$-1.8^{-0.5}_{+0.2}$	$+0.1^{+0.8}_{-0.4}$	$-0.6^{-0.6}_{+0.3}$
N5	13.3	p	$+0.0^{+0.5}_{-1.3}$	$-1.3^{-0.4}_{+1.2}$	$-0.3^{+0.8}_{-0.4}$	$-1.0^{-0.7}_{+0.2}$	$-0.7^{+0.8}_{-0.4}$	$+0.2^{-0.6}_{+0.2}$
Q 2116−358 ($z_a = 2.306571$, $\Delta v = -3090$)					log N(HI) = 13.3			
C4	13.2	p	$+0.6^{+0.2}_{-1.1}$	$-2.1^{-0.2}_{+0.8}$	$+0.3^{+0.6}_{-0.4}$	$-1.8^{-0.5}_{+0.2}$	$-0.2^{+0.8}_{-0.4}$	$-0.6^{-0.6}_{+0.3}$
N5	13.5	p	$+0.5^{+0.5}_{-1.3}$	$-1.3^{-0.4}_{+1.2}$	$+0.2^{+0.8}_{-0.4}$	$-1.0^{-0.7}_{+0.2}$	$-0.2^{+0.8}_{-0.4}$	$+0.2^{-0.6}_{+0.2}$
Q 2116−358 ($z_a = 2.306802$, $\Delta v = -3070$)					log N(HI) = 13.3			
C4	14.3	p	$+1.7^{+0.2}_{-1.1}$	$-2.1^{-0.2}_{+0.8}$	$+1.4^{+0.6}_{-0.4}$	$-1.8^{-0.5}_{+0.2}$	$+0.9^{+0.8}_{-0.4}$	$-0.6^{-0.6}_{+0.3}$
N5	14.6	p	$+1.6^{+0.5}_{-1.3}$	$-1.3^{-0.4}_{+1.2}$	$+1.3^{+0.8}_{-0.4}$	$-1.0^{-0.7}_{+0.2}$	$+0.9^{+0.8}_{-0.4}$	$+0.2^{-0.6}_{+0.2}$
Q 2116−358 ($z_a = 2.307090$, $\Delta v = -3040$)					log N(HI) = 13.7			
C4	13.9	p	$+0.9^{+0.2}_{-1.1}$	$-2.1^{-0.2}_{+0.8}$	$+0.6^{+0.6}_{-0.4}$	$-1.8^{-0.5}_{+0.2}$	$+0.1^{+0.8}_{-0.4}$	$-0.6^{-0.6}_{+0.3}$
N5	13.5	p	$+0.1^{+0.5}_{-1.3}$	$-1.3^{-0.4}_{+1.2}$	$-0.2^{+0.8}_{-0.4}$	$-1.0^{-0.7}_{+0.2}$	$-0.6^{+0.8}_{-0.4}$	$+0.2^{-0.6}_{+0.2}$

TABLE 3 (*cont.*)

			Continuum A		Continuum C			
Ion	log N	peak?	[M/H]	log U	[M/H]	log U	[M/H]$_{min}$	log U_{min}
Q 2116−358 (z_a = 2.317019, Δv = −2150)					log N(HI) = 13.9			
C2	13.0	p	$+2.0^{+0.1}_{-0.1}$	$-4.7^{-0.0}_{+0.0}$	$+2.0^{+0.1}_{-0.2}$	$-4.7^{-0.0}_{+0.0}$	$+1.1^{+0.2}_{-0.3}$	$-2.8^{-0.3}_{+0.2}$
C4	13.7	p	$+0.5^{+0.2}_{-1.1}$	$-2.1^{-0.2}_{+0.8}$	$+0.2^{+0.6}_{-0.4}$	$-1.8^{-0.5}_{+0.2}$	$-0.3^{+0.8}_{-0.4}$	$-0.6^{-0.6}_{+0.3}$
N5	13.3	p	$-0.3^{+0.5}_{-1.3}$	$-1.3^{-0.4}_{+1.2}$	$-0.6^{+0.8}_{-0.4}$	$-1.0^{-0.7}_{+0.2}$	$-1.0^{+0.8}_{-0.4}$	$+0.2^{-0.6}_{+0.2}$
Si3	12.3	p	$+0.8^{+0.2}_{-0.5}$	$-2.9^{-0.1}_{+0.2}$	$+0.6^{+0.4}_{-0.2}$	$-2.8^{-0.2}_{+0.1}$	$+0.2^{+0.5}_{-0.4}$	$-2.1^{-0.4}_{+0.3}$
Si4	13.0	p	$+1.1^{+0.4}_{-0.9}$	$-2.2^{-0.4}_{+0.6}$	$+0.9^{+0.6}_{-0.4}$	$-2.1^{-0.4}_{+0.2}$	$+0.7^{+0.6}_{-0.5}$	$-1.6^{-0.6}_{+0.3}$
Q 2116−358 (z_a = 2.317685, Δv = −2190)					log N(HI) = 14.2			
C2	13.4	p	$+2.1^{+0.1}_{-0.1}$	$-4.7^{-0.0}_{+0.0}$	$+2.1^{+0.1}_{-0.2}$	$-4.7^{-0.0}_{+0.0}$	$+1.2^{+0.2}_{-0.3}$	$-2.8^{-0.3}_{+0.2}$
C4	14.1	p	$+0.6^{+0.2}_{-1.1}$	$-2.1^{-0.2}_{+0.8}$	$+0.3^{+0.6}_{-0.4}$	$-1.8^{-0.5}_{+0.2}$	$-0.2^{+0.8}_{-0.4}$	$-0.6^{-0.6}_{+0.3}$
N5	13.5	p	$-0.4^{+0.5}_{-1.3}$	$-1.3^{-0.4}_{+1.2}$	$-0.7^{+0.8}_{-0.4}$	$-1.0^{-0.7}_{+0.2}$	$-1.1^{+0.8}_{-0.4}$	$+0.2^{-0.6}_{+0.2}$
Si2	12.6	p	$+2.2^{+0.0}_{-0.0}$	$-4.6^{+0.0}_{-0.1}$	$+2.2^{+0.0}_{-0.0}$	$-4.6^{+0.1}_{-0.1}$	$+1.4^{+0.1}_{-0.2}$	$-2.9^{-0.2}_{+0.3}$
Si3	13.0	p	$+1.2^{+0.2}_{-0.5}$	$-2.9^{-0.1}_{+0.2}$	$+1.0^{+0.4}_{-0.2}$	$-2.8^{-0.2}_{+0.1}$	$+0.6^{+0.5}_{-0.4}$	$-2.1^{-0.4}_{+0.3}$
Si4	12.7	p	$+0.5^{+0.4}_{-0.9}$	$-2.2^{-0.4}_{+0.6}$	$+0.3^{+0.6}_{-0.4}$	$-2.1^{-0.4}_{+0.2}$	$+0.1^{+0.6}_{-0.5}$	$-1.6^{-0.6}_{+0.3}$
Q 2116−358 (z_a = 2.318129, Δv = −2050)					log N(HI) = 14.7			
C2	14.2	p	$+2.4^{+0.1}_{-0.1}$	$-4.7^{-0.0}_{+0.0}$	$+2.4^{+0.1}_{-0.2}$	$-4.7^{-0.0}_{+0.0}$	$+1.5^{+0.2}_{-0.3}$	$-2.8^{-0.3}_{+0.2}$
C4	14.0	p	$+0.0^{+0.2}_{-1.1}$	$-2.1^{-0.2}_{+0.8}$	$-0.3^{+0.6}_{-0.4}$	$-1.8^{-0.5}_{+0.2}$	$-0.8^{+0.8}_{-0.4}$	$-0.6^{-0.6}_{+0.3}$
N5	13.0	p	$-1.4^{+0.5}_{-1.3}$	$-1.3^{-0.4}_{+1.2}$	$-1.7^{+0.8}_{-0.4}$	$-1.0^{-0.7}_{+0.2}$	$-2.1^{+0.8}_{-0.4}$	$+0.2^{-0.6}_{+0.2}$
Al2	11.8	p	$+2.2^{+0.1}_{-0.2}$	$-5.0^{-0.1}_{+0.0}$	$+2.1^{+0.2}_{-0.1}$	$-4.9^{-0.2}_{+0.0}$	$+0.8^{+0.5}_{-0.3}$	$-2.9^{-0.4}_{+0.2}$
Si2	13.0	p	$+2.1^{+0.0}_{-0.0}$	$-4.6^{+0.0}_{-0.1}$	$+2.1^{+0.0}_{-0.0}$	$-4.6^{+0.1}_{-0.1}$	$+1.3^{+0.1}_{-0.2}$	$-2.9^{-0.2}_{+0.3}$
Si3	13.0	p	$+0.7^{+0.2}_{-0.5}$	$-2.9^{-0.1}_{+0.2}$	$+0.5^{+0.4}_{-0.2}$	$-2.8^{-0.2}_{+0.1}$	$+0.1^{+0.5}_{-0.4}$	$-2.1^{-0.4}_{+0.3}$
Si4	13.3	p	$+0.6^{+0.4}_{-0.9}$	$-2.2^{-0.4}_{+0.6}$	$+0.4^{+0.6}_{-0.4}$	$-2.1^{-0.4}_{+0.2}$	$+0.2^{+0.6}_{-0.5}$	$-1.6^{-0.6}_{+0.3}$
Q 2116−358 (z_a = 2.318795, Δv = −1990)					log N(HI) = 14.2			
C2	13.9	p	$+2.6^{+0.1}_{-0.1}$	$-4.7^{-0.0}_{+0.0}$	$+2.6^{+0.1}_{-0.2}$	$-4.7^{-0.0}_{+0.0}$	$+1.7^{+0.2}_{-0.3}$	$-2.8^{-0.3}_{+0.2}$
C4	15.0	p	$+1.5^{+0.2}_{-1.1}$	$-2.1^{-0.2}_{+0.8}$	$+1.2^{+0.6}_{-0.4}$	$-1.8^{-0.5}_{+0.2}$	$+0.7^{+0.8}_{-0.4}$	$-0.6^{-0.6}_{+0.3}$
N5	12.9	p	$-1.0^{+0.5}_{-1.3}$	$-1.3^{-0.4}_{+1.2}$	$-1.3^{+0.8}_{-0.4}$	$-1.0^{-0.7}_{+0.2}$	$-1.7^{+0.8}_{-0.4}$	$+0.2^{-0.6}_{+0.2}$
Al2	11.7	p	$+2.6^{+0.1}_{-0.2}$	$-5.0^{-0.1}_{+0.0}$	$+2.5^{+0.2}_{-0.1}$	$-4.9^{-0.2}_{+0.0}$	$+1.2^{+0.5}_{-0.3}$	$-2.9^{-0.4}_{+0.2}$
Al3	12.4	p	$+2.2^{+0.4}_{-0.7}$	$-3.1^{-0.3}_{+0.4}$	$+2.0^{+0.6}_{-0.3}$	$-3.0^{-0.4}_{+0.2}$	$+1.7^{+0.6}_{-0.4}$	$-2.2^{-0.5}_{+0.3}$
Si2	13.2	p	$+2.8^{+0.0}_{-0.0}$	$-4.6^{+0.0}_{-0.1}$	$+2.8^{+0.0}_{-0.0}$	$-4.6^{+0.1}_{-0.1}$	$+2.0^{+0.1}_{-0.2}$	$-2.9^{-0.2}_{+0.3}$
Si3	13.0	p	$+1.2^{+0.2}_{-0.5}$	$-2.9^{-0.1}_{+0.2}$	$+1.0^{+0.4}_{-0.2}$	$-2.8^{-0.2}_{+0.1}$	$+0.6^{+0.5}_{-0.4}$	$-2.1^{-0.4}_{+0.3}$
Si4	13.8	p	$+1.6^{+0.4}_{-0.9}$	$-2.2^{-0.4}_{+0.6}$	$+1.4^{+0.6}_{-0.4}$	$-2.1^{-0.4}_{+0.2}$	$+1.2^{+0.6}_{-0.5}$	$-1.6^{-0.6}_{+0.3}$

TABLE 3 (*cont.*)

			Continuum A		Continuum C			
Ion	log N	peak?	[M/H]	log U	[M/H]	log U	[M/H]$_{min}$	log U_{min}
PG 2302+029 ($z_a = 0.702$, $\Delta v = -56{,}000$)[a]			log N(HI) < 14.6					
C4	14.8	p	$+0.4^{+0.7}_{-0.6}$	$-1.7^{-0.6}_{+0.4}$	$+0.5^{+0.7}_{-0.3}$	$-1.8^{-0.5}_{+0.2}$	$+0.0^{+0.9}_{-0.3}$	$-0.5^{-0.7}_{+0.2}$
N5	15.0	p	$+0.0^{+1.2}_{-0.6}$	$-0.7^{-1.0}_{+0.6}$	$+0.4^{+0.8}_{-0.4}$	$-1.0^{-0.7}_{+0.1}$	$-0.1^{+0.9}_{-0.3}$	$+0.1^{-0.5}_{+0.3}$
O6	15.6	p	$-1.0^{+1.3}_{-0.5}$	$+0.0^{-1.1}_{+0.5}$	$-0.6^{+0.8}_{-0.3}$	$-0.4^{-0.6}_{+0.3}$	$-1.1^{+0.8}_{-0.3}$	$+0.7^{-0.5}_{+0.3}$
Q 0226−104 (BAL)			log N(HI) = 15.8 ± 0.1					
C3	15.6 ± 0.2	p	$+0.9^{+0.4}_{-0.3}$	$-2.8^{-0.2}_{+0.1}$	$+0.9^{+0.5}_{-0.2}$	$-2.8^{-0.3}_{+0.2}$	$+0.3^{+0.7}_{-0.2}$	$-1.8^{-0.6}_{+0.2}$
C4	16.20 ± 0.05	p	$+0.6^{+0.7}_{-0.6}$	$-1.7^{-0.6}_{+0.4}$	$+0.7^{+0.7}_{-0.3}$	$-1.8^{-0.5}_{+0.2}$	$+0.2^{+0.9}_{-0.3}$	$-0.5^{-0.7}_{+0.2}$
N3	16.3 ± 0.2	p	$+2.1^{+0.4}_{-0.3}$	$-2.8^{-0.2}_{+0.2}$	$+2.1^{+0.5}_{-0.2}$	$-2.8^{-0.2}_{+0.2}$	$+1.5^{+0.7}_{-0.3}$	$-1.7^{-0.7}_{+0.2}$
N5	16.3 ± 0.1	p	$+0.1^{+1.2}_{-0.6}$	$-0.7^{-1.0}_{+0.6}$	$+0.5^{+0.8}_{-0.4}$	$-1.0^{-0.7}_{+0.1}$	$+0.0^{+0.9}_{-0.3}$	$+0.1^{-0.5}_{+0.3}$
O3	16.7 ± 0.2	p	$+1.6^{+0.4}_{-0.3}$	$-2.8^{-0.2}_{+0.3}$	$+1.6^{+0.5}_{-0.2}$	$-2.8^{-0.2}_{+0.1}$	$+1.1^{+0.7}_{-0.2}$	$-1.8^{-0.7}_{+0.2}$
O4	16.7 ± 0.2	p	$+0.4^{+0.9}_{-0.6}$	$-1.6^{-0.6}_{+0.6}$	$+0.6^{+0.8}_{-0.3}$	$-1.7^{-0.5}_{+0.2}$	$+0.2^{+0.9}_{-0.3}$	$-0.9^{-0.7}_{+0.2}$
O6	16.5 ± 0.1	p	$-1.3^{+1.3}_{-0.5}$	$+0.0^{-1.1}_{+0.5}$	$-0.9^{+0.8}_{-0.3}$	$-0.4^{-0.6}_{+0.3}$	$-1.4^{+0.8}_{-0.3}$	$+0.7^{-0.5}_{+0.3}$
Si4	15.3 ± 0.1	p	$+1.0^{+0.9}_{-0.4}$	$-1.9^{-0.7}_{+0.3}$	$+1.2^{+0.7}_{-0.3}$	$-2.0^{-0.5}_{+0.2}$	$+1.0^{+0.7}_{-0.3}$	$-1.6^{-0.6}_{+0.3}$
S4	14.7 ± 0.1	p	$+0.6^{+0.7}_{-0.5}$	$-1.8^{+0.3}_{-0.6}$	$+0.6^{+0.8}_{-0.2}$	$-1.9^{-0.5}_{+0.2}$	$+0.4^{+0.8}_{-0.3}$	$-1.4^{+0.2}_{-0.7}$
S6	15.9 ± 0.2	p	$+0.7^{+1.1}_{-0.4}$	$-0.8^{-1.1}_{+0.4}$	$+1.0^{+0.8}_{-0.4}$	$-1.0^{-0.7}_{+0.2}$	$+0.7^{+0.8}_{-0.3}$	$-0.6^{-0.4}_{+0.4}$
Q 1246−057 (BAL)			log N(HI) = 15.5					
C4	15.8	p	$+1.0^{+0.2}_{-1.1}$	$-2.1^{-0.2}_{+0.8}$	$+0.7^{+0.7}_{-0.4}$	$-1.8^{-0.5}_{+0.2}$	$+0.2^{+0.8}_{-0.4}$	$-0.6^{-0.6}_{+0.3}$
N5	16.0	p	$+0.7^{+0.5}_{-1.3}$	$-1.3^{-0.4}_{+1.2}$	$+0.4^{+0.8}_{-0.4}$	$-1.0^{-0.7}_{+0.2}$	$+0.2^{+0.8}_{-0.4}$	$+0.2^{-0.6}_{+0.2}$
Si4	15.0	p	$+1.5^{+0.4}_{-0.9}$	$-2.2^{-0.4}_{+0.6}$	$+1.3^{+0.6}_{-0.4}$	$-2.1^{-0.4}_{+0.2}$	$+1.1^{+0.6}_{-0.4}$	$-1.6^{-0.6}_{+0.3}$
RS 23 (BAL)			log N(HI) = 15.3					
C4	15.8	p	$+1.2^{+0.2}_{-1.1}$	$-2.1^{-0.2}_{+0.8}$	$+0.9^{+0.7}_{-0.4}$	$-1.8^{-0.5}_{+0.2}$	$+0.4^{+0.8}_{-0.4}$	$-0.6^{-0.6}_{+0.3}$
N5	15.5	p	$+0.5^{+0.5}_{-1.3}$	$-1.3^{-0.4}_{+1.2}$	$+0.2^{+0.8}_{-0.4}$	$-1.0^{-0.7}_{+0.2}$	$+0.0^{+0.8}_{-0.4}$	$+0.2^{-0.6}_{+0.2}$
Si4	15.3	p	$+2.0^{+0.4}_{-0.9}$	$-2.2^{-0.4}_{+0.6}$	$+1.8^{+0.6}_{-0.4}$	$-2.1^{-0.4}_{+0.2}$	$+1.6^{+0.6}_{-0.4}$	$-1.6^{-0.6}_{+0.3}$

TABLE 3 (*cont.*)

			Continuum A		Continuum C			
Ion	log N	peak?	[M/H]	log U	[M/H]	log U	[M/H]$_{min}$	log U_{min}
Mean BALQSO			log N(HI) = 15.4					
C4	16.0	p	$+1.3^{+0.2}_{-1.1}$	$-2.1^{-0.2}_{+0.8}$	$+1.0^{+0.7}_{-0.4}$	$-1.8^{-0.5}_{+0.2}$	$+0.5^{+0.8}_{-0.4}$	$-0.6^{-0.6}_{+0.3}$
N5	16.1	p	$+1.0^{+0.5}_{-1.3}$	$-1.3^{-0.4}_{+1.2}$	$+0.7^{+0.8}_{-0.4}$	$-1.0^{-0.7}_{+0.2}$	$+0.5^{+0.8}_{-0.4}$	$+0.2^{-0.6}_{+0.2}$
O6	16.3	p	$-0.5^{+0.7}_{-1.1}$	$-0.6^{-0.5}_{+1.1}$	$-0.6^{+0.7}_{-0.3}$	$-0.4^{-0.6}_{+0.3}$	$-1.1^{+0.7}_{-0.4}$	$+0.7^{+0.3}_{-0.5}$
Si4	15.2:	p	$+1.8^{+0.4}_{-0.9}$	$-2.2^{-0.4}_{+0.6}$	$+1.6^{+0.6}_{-0.4}$	$-2.1^{-0.4}_{+0.2}$	$+1.4^{+0.6}_{-0.4}$	$-1.6^{-0.6}_{+0.3}$

[a] All [M/H] results for these systems are lower limits because N(HI) is an upper limit.